CDF/THESIS/EXOTIC/PUBLIC/5212
IEKP-KA/99-23

Suche nach Supersymmetrie mit Verletzung der R-Parität im 4–Leptonen–Kanal bei CDF

Zur Erlangung des akademischen Grades eines

DOKTORS DER NATURWISSENSCHAFTEN

von der Fakultät für Physik der Universität (TH) Karlsruhe

genehmigte

DISSERTATION

von

Armin Köngeter
aus Birkesdorf, jetzt Düren

Tag der mündlichen Prüfung : 5. November 1999

Referent: Herr Prof. Dr. Th. Müller
Korreferent: Herr Prof. Dr. J. Hauser

Abstract

In this Thesis a search for R-parity violating SUSY in the multi lepton channel in CDF run IB data is presented . This is the first search in this channel performed at a hadron collider.

We assume the existence of a coupling violating R-parity and lepton number conservation. If the coupling is small, the cascade decays of squarks, gluinos and bosinos to the lightest neutralino will only be changed slightly by this new coupling. These decays then can be handled within the R-parity conserving mSUGRA. In addition to the processes from the R-parity conserving mSUGRA, we consider the R-parity violating decay of the lightest neutralino into two charged leptons and one neutrino.

Finding 1 event in 87.5 pb^{-1} all scenarios yielding 5.1 or more events are excluded, limiting R_P violating minimal SUGRA models with a non-zero coupling λ_{121} to $M_{1/2} \gtrsim 130$ GeV. This corresponds to a mass of the lightest neutralino of $\gtrsim 55$ GeV, while the masses of the second lightest neutralino and the lightest chargino are excluded up to 118 GeV/c^2. The squarks and gluinos are excluded up to squark (gluino) masses of $\gtrsim 360$ GeV ($\gtrsim 380$ GeV).

0 Suche nach R-paritätsverletzenden Zerfällen von Neutralinos mit CDF (Eine Zusammenfassung)

In der vorliegenden Arbeit wird die erste Suche nach R-paritätsverletzenden Zerfällen der leichtesten Neutralinos im vier Leptonen Kanal an einem Hadronenbeschleuniger beschrieben. Die Suche wurde anhand von 87.5 pb^{-1} Daten, die in den Jahren 1994 bis 1996 (Run Ib) mit dem CDF–Experiment genommen wurden, durchgeführt.

Der Suche zugrunde liegt die Theorie der Supersymmetrie (SUSY). Angewandt auf das Gebiet der Elementarteilchenphysik besagt diese Theorie, daß es zu jedem der aus dem Standardmodell (SM) der Elementarteilchenphysik bekannten Fermionen einen bosonischen Partner gibt und umgekehrt. Diese Partnerteilchen werden auch Superpartner oder SUSY–Teilchen genannt. Die Partnerteilchen der SM–Fermionen tragen die Namen der Fermionen mit einem vorangestellten "S". Die Partnerteilchen der SM–Bosonen werden durch eine angehängt Endung "-ino" gekennzeichnet. Die Partnerteilchen der SM–Bosonen mischen und nur die Masseneigenzustände sind beobachtbar. Die beiden geladenen Masseneigenzustände werden als Charginos, die vier neutralen als Neutralinos bezeichnet. In Formeln wird für die SUSY–Teilchen das Symbol der entsprechenden SM–Teilchen mit einer Tilde verwendet. Das Zeichen für die Charginos ist $\tilde{\chi}_i^{\pm}$, dasjenige für die Neutralinos ist $\tilde{\chi}_i^0$. Hierbei läuft i von 1 bis 2 für Charginos und von 1 bis 4 für Neutralinos, wobei per Definition für das leichteste Teilchen $i = 1$ gilt.

Bisher hat man keine supersymmetrischen Elementarteilchen nachweisen können. Dies kann dadurch erklärt werden, daß die Theorie und die Lagrange–Funktion zwar supersymmetrisch sind, der Grundzustand diese Symmetrie allerdings nicht aufweist. Ein solches Verhalten wird spontane Symmetriebrechung genannt. Ein ähnlicher Effekt führt im SM zur Brechung der elektroschwachen Symmetrie durch das Higgs–Boson. Als Folge der spontanen Symmetriebrechung erhalten die Superpartner andere Massen als die SM–Teilchen. Die exakten Werte der Massen hängen von der genauen Art und Weise ab, in der die Symmetriebrechung vonstatten geht. Im allgemeinen führt die spontane Symmetriebrechung eine große Zahl von neuen Parametern in die Theorie ein. Wenn man die Brechung der Supersymmetrie im Rahmen einer weitergehenden Theorie erklärt, kann man die Zahl der neu einzuführenden Parameter deutlich reduzieren. In der vorliegenden Arbeit wurde als grundlegende Theorie die sogenannte Supergravitation verwendet. Diese Theorie erklärt die Symmetriebrechung durch die Kopplung des beobachtbaren Teilchenspektrums an einen verborgenen Sektor. Im verborgenen Sektor existiert ein Feld mit einem sehr großen Vakuumerwartungswert, das durch Gravitation mit dem sichtbaren Sektor wechselwirkt. Beschränkt man sich auf Supergravitation auf den minimalem, mit dem SM vereinbarbaren Teilcheninhalt (mSUGRA), so benötigt man zur vollständigen Beschreibung des Teilchen– und Zerfallsspektrums zusätzlich zu den freien Parametern des SM noch vier zusätzliche Parameter und ein Vorzeichen:

- M_0, die universelle Fermionenmasse,

- $M_{1/2}$, die universelle Bosonenmasse,
- A_0, der Skalierungsfaktor für den kubischen Anteil des Superpotentials
- $\tan(\beta) = v_2/v_1$, das Verhältnis der Vakuumerwartungswerte der beiden Higgsdubletts,
- SGN(μ), das Vorzeichen des Higgs–Massenparameters.

Einige der Wechselwirkungen, die mit den aus dem SM bekannten Eich–Symmetrien und SUSY vereinbar sind, führen zu einem Zerfall des Protons. Die Lebensdauer des Protons wäre aufgrund dieser Prozesse deutlich kleiner als die experimentell bestimmte untere Grenze.

Die Theorie muß dergestalt modifiziert werden, daß die betreffenden Prozesse unterdrückt sind. Von einem theoretischen Standpunkt aus wäre es unbefriedigend die Wechselwirkungen einfach wegzulassen, ohne eine tiefergehende Begründung dafür zu haben. Das gesamte SM und seine supersymmetrischen Erweiterungen sind auf Symmetrieüberlegungen aufgebaut. Daher ist es naheliegend, eine neue Symmetrie einzuführen, die bestimmte Kopplungen verbietet. Meist wird die Erhaltung der sognannten R–Parität (R_P) gefordert. Diese multiplikative Quantenzahl ist definiert als

$$R_P \equiv (-1)^{3B+L+2S},$$

wobei B die Baryonenzahl, L die Leptonenzahl und S der Spin des betreffenden Teilchens ist. Alle SM–Teilchen haben R-Parität 1, während für ihre Superpartner $R_P = -1$ gilt. Ist R_P erhalten, so unterliegt das Superpotential und damit die Lagrange–Dichte einer weiteren Symmetrie. Diese neue Symmetrie führt dazu, daß Superpartner nur paarweise erzeugt werden können und daß bei dem Zerfall eines Superpartners wieder eine ungerade Anzahl von Teilchen mit negativer R–Parität entstehen muß. Dies wiederum hat zur Folge, daß das leichteste Supersymmetrische Teilchen (LSP) stabil ist.

Die Einführung der R-Paritätserhaltung verbietet folgende Terme im Superpotential

$$W_R = \lambda_{ijk} L_i L_j E^c_k + \lambda'_{ijk} L_i Q_j D^c_k + \lambda''_{ijk} U^c_i D^c_j D^c_k + \kappa_i H_2 L_i.$$

Hierbei sind λ, λ' und λ'' Kopplungskonstanten, i, j und k sind Generationenindizes und κ_i sind Massenfaktoren. L und Q sind die linkshändigen Lepton– und Quark–Superfelder, U, D und E sind die Superfelder der rechtshändigen up–Quarks, down–Quarks und des rechthändigen Leptons. H_2 ist ein Higgs–Superfeld. Alle vier Terme führen zur Verletzung der R_P. Der letzte Term beschreibt die Mischung zwischen den Higgs–Bosonen und den Leptonen. Durch geeignete Definition vom H_1 und L_i kann der Term wegrotiert werden [20]. Im Weiteren werden alle κ_i–Terme ignoriert. Die drei übrigen Terme beschreiben Kopplungen zwischen Fermionen und ihren Superpartnern.

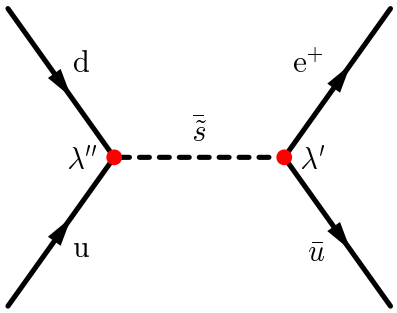

Abbildung 0.1: *Der Zerfall des Protons durch die Kopplungen λ' und λ''. Die R_P-verletzenden Kopplungen sind durch Punkte markiert. Das dritte Quark des Protons ist nicht gezeigt.*

Der λ''–Term beschreibt die Wechselwirkung von drei Quark–Superfeldern unter Verletzung der Baryonenzahl. Falls eines der beteiligten Superfeldern zur dritten Quarks–Generation gehört, kann diese Kopplung zu Änderungen der Zerfallsraten des top–Quarks oder zur Produktion von einzelnen top–Squarks an Hadron–Beschleunigern führen. Anderenfalls wären die Effekte einer von Null verschiedenen Kopplung λ'' an Hadron–Beschleunigern wegen des hohen QCD–Untergrundes nur schwer zu erkennen. λ' koppelt ein Lepton–Superfeld mit zwei Quark–Superfeldern unter Verletzung der Leptonenzahl. Diese Wechselwirkung führt dazu, daß Squarks sowohl an Leptonen als auch an Quarks koppeln und wurde als Erklärung für den bei Hera gefundenen Überschuß von Ereignissen mit hohem Impulsübertrag vorgeschlagen [21]. Die CDF–Kollaboration hat nach durch eine Kopplung λ'_{121} hervorgerufenen Ereignissen gesucht, aber kein entsprechendes Signal gemessen [22]. Zur Zeit werden andere Aspekte einer von Null verschiedenen Kopplung λ' untersucht. Eine Kopplung λ führt zu einer Wechselwirkung zwischen zwei Leptonen und einem Slepton unter Verletzung der Leptonenzahl. Die Matrix der λ–Elemente ist antisymmetrisch unter Vertauschung der ersten beiden Indizes. Daher sind alle Diagonalelemente Null und es verbleiben 9 unabhängige Terme.

Das simultane Vorhandensein von Kopplungen λ' und λ'' führt über Diagramme, wie das in Abbildung 0.1 gezeigte, zu schnellem Protonenzerfall.

Fordert man R–Paritätserhaltung, so werden nicht nur diejenigen Terme verboten, die zum Protonenzerfall beitragen, sondern auch alle übrigen Kopplungen, welche die R–Parität verletzen. Dies ist unbefriedigend, weil es keine physikalischen Gründe gibt, die gegen das Vorhandensein der übrigen Terme sprechen und weil R_P nur eine von vielen möglichen Symmetrien ist, die den Protonenzerfall verhindern würden. Fordert man die Erhaltung einer der anderen Symmetrien, sind meist nur bestimmte Kombinationen von λ, λ' und λ'' verboten, aber im Allgemeinen nicht alle drei Kopplungen.

Eine Kopplung λ alleine kann nicht zu einem Zerfall des Protons führen, weil diese Wechselwirkung nur die Leptonenzahl verletzt. Zum Zerfall des Protons ist aber eine zusätzliche Verletzung der Baryonenzahl erforderlich.

In dieser Arbeit wurde nach Signalen für eine von Null verschiedene Kopplung λ_{121} am Tevatron Beschleuniger gesucht. Eine solche Kopplung wird die Erzeugung von SUSY–Teilchen am Tevatron nicht beeinflussen, weil der Ausgangszustand rein hadronisch ist und die neue Wechselwirkung nur Leptonen und ihre Superpartner miteinander koppelt. Die Zerfälle der SUSY–Teilchen werden ebenfalls von der neuen Wechselwirkung nur unwesentlich beeinflußt, weil diese deutlich schwächer ist als die übrigen Kopplungen. Daher ist der einzige Effekt, der durch das Vorhandensein einer Kopplung λ_{121} auftreten würde der Zerfall des LSPs. Weil im größten Teil des mSUGRA Parameterraumes das leichteste Neutralino das LSP ist, wurden nur die Zerfälle dieses Teilchens untersucht. Die Feynman Diagramme, die den Zerfall des $\tilde{\chi}_1^0$ beschreiben, sind in Abbildung 0.2 gezeigt. Der Zerfall erfolgt stets über ein virtuelles Slepton, das dann unter Verletzung der R–Parität in zwei Leptonen zerfällt. Ein näheres Studium der Zerfälle zeigt, daß man folgende Teilchen als Zerfallsprodukte mit gleicher Wahrscheinlichkeit erwartet

$$\mu\bar{e}\nu_e, \quad \bar{\mu}e\bar{\nu}_e, \quad e\bar{e}\nu_\mu, \quad e\bar{e}\bar{\nu}_\mu.$$

In dem hier verwendeten Modell werden SUSY–Teilchen paarweise erzeugt und zerfallen dann in ein LSP pro SUSY–Teilchen. Weil diese Zerfälle meistens über mehrere Stufen ablaufen, werden sie häufig auch Kaskade–Zerfälle genannt. Nach den Kaskade–Zerfällen verbleiben noch zwei LSPs pro Ereignis, die unter Verletzung der R-Parität in jeweils zwei geladene Leptonen und ein Neutrino zerfallen. Deshalb erwartet man im Endzustand vier geladene Leptonen[1]. Weitere Leptonen können durch den Zerfall von massiven SUSY–Teilchen in LSPs erzeugt werden.

Die Produktion von SUSY–Teilchen an Hadronen–Beschleunigern kann über diverse Kanäle erfolgen. Die meisten dieser Kanäle sind analog den Erzeugungsprozessen der SM–Partner der jeweiligen Teilchen. Zusätzlich sind Prozesse möglich, bei denen SUSY–Teilchen im t– oder im u–Kanal ausgetauscht werden. In der Region, in der die vorliegende Analyse sensitiv ist, dominiert die Erzeugung von Charginos, Neutralinos und Sleptonen. Die Haupt–Erzeugungsprozesse für diese Teilchen sind der Zerfall von virtuellen Photonen, Z– oder W–Bosonen im s–Kanal. Im t– und im u–Kanal ist nur die Erzeugung von Charginos und Neutralinos möglich. Hierbei tauschen zwei Quarks ein Squark aus, wobei jedes Quark ein Chargino oder Neutralino abstrahlt.

Das Tevatron ist der zur Zeit höchstenergetische Proton–Antiproton Beschleuniger. Bis 1995 betrug die Schwerpunktsenergie 1.8 TeV. Momentan werden sowohl der Beschleuniger als auch die beiden Detektoren "Collider Detector at Fermilab" (CDF) und D0 umgebaut. Nach Beendigung des Umbaus im Frühjahr 2000 wird die Schwerpunktsenergie bei 2.0 TeV liegen.

Die Protonen und Antiprotonen, die im Tevatron kollidieren, werden über einen mehrstufigen Beschleunigungsprozeß auf die notwendige Energie gebracht. Die Proto-

[1] Die untersuchte Kopplung erlaubt nur Zerfälle der LSPs in Elektronen oder Myonen. Taus können durch den Zerfall von schwereren SUSY–Teilchen entstehen, wobei die hier dargestellte Analyse nur auf die aus leptonischen Tau–Zerfällen stammenden Elektronen und Myonen sensitiv ist. Im Weiteren bezeichnet der Begriff Leptonen Elektronen und Myonen, aber keine Taus.

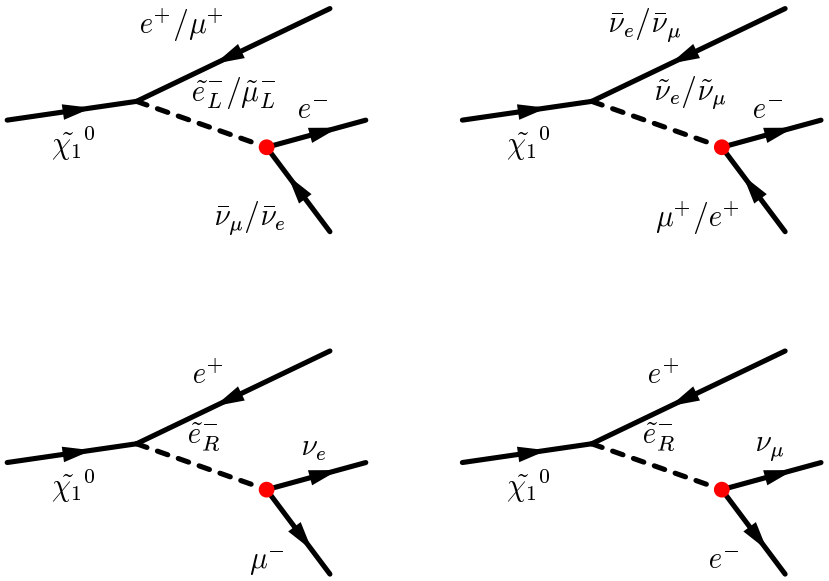

Abbildung 0.2: *Die Zerfallskanäle des leichtesten Neutralinos für den Fall einer von Null verschiedenen Kopplung λ_{121}. Der Vertices, an denen die R_P–verletzende Kopplung auftritt, sind durch Punkte markiert.*

nen werden aus molekularem Wasserstoff gewonnen und über mehrere Beschleunigerstufen bis auf eine Energie von zunächst 8 GeV beschleunigt. Nach Erreichen dieser Energie werden die meisten Protonen in das Tevatron eingespeist, während ein kleiner Teil zur Erzeugung von Antiprotonen auf einen Wolfram–Block geleitet wird. Die dabei entstehenden Antiprotonen werden von den übrigen Teilchen separiert, fokussiert und stochastisch gekühlt. Im sogenannten Accumulator werden die Antiprotonen solange angereichert, bis Ihre Zahl für die gewünschte Luminosität ausreicht. Analog zu den Protonen werden die Antiprotonen nun beschleunigt und in das Tevatron eingespeist. Jeweils sechs Pakete Protonen und Antiprotonen laufen in entgegengesetzten Richtungen im Tevatron um und werden an zwei definierten Wechselwirkungspunkten zur Kollision gebracht.

Während des Zeitraumes in dem die Datennahme für diese Analyse stattfand, bestand ein Paket aus typischerweise $22.5 \cdot 10^{10}$ Protonen bzw. $6.5 \cdot 10^{10}$ Antiprotonen. Die integrierte Luminosität betrug 87.5 pbarn^{-1} für den verwendeten Datensatz.

An jedem der zwei Wechselwirkungspunkte befindet sich ein Universaldetektor, der die in den Kollisionen entstehenden Teilchen mißt. Für die vorliegende Analyse wurden Daten verwendet, die während der Zeit von 1994-1996 mit dem CDF–Detektor aufgezeichnet wurden. Der Detektor besteht aus einem schalenförmig aufgebauten System von Unterdetektoren, die jeweils für eine bestimmte Aufgabe optimiert sind. Die innerste Lage bilden die Spur–Detektoren, die die Bahn der vom Wechselwirkungspunkt kommenden Teilchen vermessen und damit Aufschluß über den Impuls der Teilchen ge-

	3 Leptonen	≥ 4 Leptonen
bb	47.02 ± 2.61	0.28 ± 0.14
Drell-Yan	18.71 ± 1.4	$0 \pm^{0.10}_{0.0}$
$t\bar{t}$	1.21 ± 0.10	0.08 ± 0.02
ZZ, ZW, WW	0.53 ± 0.08	0.02 ± 0.01
Summe MC	67.5 ± 3.0	$0.37 \pm^{0.17}_{0.14}$
Fehlidentifizierte Jets	$154 \pm 2 \pm^{268}_{39}$	$1.19 \pm 0.08 \pm^{2.08}_{0.3}$
MC und Fehlidentifizierte Jets	$221.5 \pm 4 \pm^{268}_{39}$	$1.56 \pm^{0.19}_{0.16} \pm^{2.08}_{0.3}$
GEMESSEN	185	1

Tabelle 0.1 : *Die Anzahl der erwarteten Ereignisse mit drei und vier Leptonen im Vergleich zur Anzahl der in den Daten identifizierten Ereignisse.*

ben. Außerdem wird bestimmt, ob die Teilchen vom Wechselwirkungspunkt stammen, oder ob sie erst durch den Zerfall langlebiger Teilchen wie der b–Quarks entstanden sind. Die Spur–Detektoren befinden sich in einem 1.4 T starken Magnetfeld, das von einem direkt außerhalb der Spurkammern befindlichen Solenoiden erzeugt wird. Die zweite Unterdetektorlage bilden die Kalorimeter. In den elektro–magnetischen Kalorimetern entwickeln Elektronen und Photonen durch Bremsstrahlung und Paarproduktion von Elektronen elektro–magnetische Schauer. Die Energie der Schauern und damit auch die der einfallenden Teilchen wird mit Hilfe von Szintillatoren und Driftkammern gemessen. Die hadronischen Kalorimeter befinden sich (in Flugrichtung der Teilchen) hinter den elektro–magnetischen Kalorimetern und messen die Energie der hadronischen Schauern, die durch wiederholte Wechselwirkungen der Hadronen mit dem Absorbermaterial entstehen. Außerhalb der Kalorimeter befinden sich die Myon–Kammern, in denen die Spuren aller Teilchen, die die Kalorimeter wieder verlassen, nochmals gemessen werden. Aufgrund ihrer hohen Masse werden Myonen in den Kalorimetern nicht gestoppt.

Die CDF–Kollaboration verwendet ein vierstufiges Triggersystem zur Auswahl der physikalisch interessantesten Ereignisse aus den vom Detektor gemessenen Daten. Der für dies Arbeit verwendete Datensatz wurde mit Hilfe des Run IB Dilepton–Trigger aufgezeichnet. Dieser Trigger wählt alle Ereignisse aus, die in der letzten Trigger–Stufe zwei Leptonen enthalten. Für die vorliegende Analyse werden die Selektionskriterien für die Leptonen gegenüber den Kriterien des Triggers verschärft. Zusätzlich werden nur Ereignisse ausgewählt, die zwei weitere Leptonen enthalten. Die verwendeten Selektionskriterien entsprechen den Standard–Kriterien der CDF SUSY–Arbeitsgruppe zur Identifikation von Elektronen und Myonen. Falls das erste Lepton ein Elektron ist muß seine Energie über 12 GeV liegen, bei Myonen gilt entsprechendes für den Impuls. Die drei übrigen Leptonen müssen eine Energie über 5 GeV haben, falls es sich um Elektronen handelt, Myonen müssen entsprechend einen Impuls über 5 GeV/c haben. Da im Signal sowohl Elektronen als auch Myonen erwartet werden, darf jedes der vier Leptonen entweder eine Elektron oder ein Myon sein.

Der von SM–Prozessen herrührende Untergrund setzt sich aus zwei Komponenten zusammen, Ereignissen mit vier echten Leptonen und Ereignissen mit drei echten Leptonen und einem hadronischen Jet, der fälschlicherweise als Lepton identifiziert wurde. Zur Abschätzung des SM–Untergrundes mit vier echten Leptonen wurden Monte Carlo (MC) Simulationen von $b\bar{b}$–Erzeugung, top–Quark–Paarerzeugung, Drell–Yan Produktion von Leptonen und der Produktion von Paaren schwerer Bosonen (ZZ, ZW, WW) untersucht. Der SM–Untergrund aus Ereignissen mit vier echten Leptonen wurde zu

$$0.37\pm^{0.17}_{0.14}$$

ermittelt. Die Anzahl der Ereignisse, die einen misidentifizierten Jet enthalten , wurde mit verschiedenen Methoden abgeschätzt, die alle im Wesentlichen dieselben Ergebnisse liefern. Die für die hier präsentierten Ergebnisse verwendete Methode basiert auf der Berechnung einer Fehlidentifizierungswahrscheinlichkeit pro im Detektor gefundener Spur. Dazu wird in einem Datensatz, in dem keine echten Leptonen vorhanden sind, nach Objekten gesucht, die die Selektionskriterien für Leptonen erfüllen. Die Anzahl dieser Objekte wird durch die Zahl der in dem Datensatz vorhandenen Spuren dividiert, um die Wahrscheinlichkeit zu erhalten, daß eine Spur als Lepton identifiziert wird. Aus dem Dileptonen–Datensatz werden diejenigen Ereignisse extrahiert, die zwei oder drei Leptonen gemäß den in der vorliegenden Analyse verwendeten Kriterien enthalten. Um die Anzahl der erwarteten Ereignisse mit fehlidentifizierten Leptonen zu berechnen, wurde die Zahl der zusätzlich zu den bereits identifizierten Leptonen vorhandenen Spuren mit der im vorhergehenden Schritt ermittelten Wahrscheinlichkeit multipliziert. Man erwartet

$$1.19 \pm 0.08\pm^{2.08}_{0.3}$$

Ereignisse mit drei echten und einem fehlidentifizierten Lepton aus dieser Quelle. Die Gesamtzahl der vom SM erwarteten Ereignisse mit vier oder mehr Leptonen ist damit

$$1.56 \pm^{0.19}_{0.16} \pm^{2.08}_{0.3}.$$

Die Anzahl der erwarteten Ereignisse ist zusammen mit der Zahl der in den Daten gefundenen Ereignissen in Tabelle 0.1 gezeigt. Der Anteil von Signal–Ereignissen mit drei Leptonen ist zu gering, als daß er gegenüber dem Untergrund erkennbar wäre. Der Datensatz mit drei Leptonen dient als Kontrollprobe, während ein Signal sich durch eine erhöhte Anzahl von Ereignissen im vier–Leptonen Kanal bemerkbar machen würde.

Ein Test der Zuverlässigkeit der Untergrund–Abschätzung ist in Abbildung 0.3 gezeigt. Das Spektrum der invarianten Massen der beiden höchstenergetischen Leptonen im drei–Lepton–Datensatz wird mit dem Spektrum des vom SM erwarteten Untergrundes verglichen. Die Massenverteilungen für die MC–Beiträge wurde den Resultaten der Detektorsimulation entnommen, wobei nur die Beiträge von $b\bar{b}$ und Drell–Yan berücksichtigt wurden. Zur Ermittlung des Spektrums für die Ereignisse mit einem misidentifizierten Jet wurde angenommen, daß der misidentifizierte Jet eine kleinere Energie hat als die beiden echten Leptonen und man daher nach entsprechender Skalierung das

Massenspektrum der Leptonen aus dem Dilepton–Datensatz verwenden darf. Für die Leptonen mit gleicher Ladung ist die Übereinstimmung zwischen dem erwarteten und dem beobachteten Spektrum sehr gut. Im Falle der Leptonen mit entgegengesetzter Ladung ist die Übereinstimmung immer noch gut, allerdings erwartet man im Bereich der Z–Masse mehr Ereignisse als man tatsächlich findet. Eine mögliche Erklärung für diese Diskrepanz ist in der Annahme zu sehen, daß der misidentifizierte Jet immer eine kleinere Energie hat als die beiden echten Leptonen. Wenn diese Annahme nicht zutrifft und der misidentifizierte Jet das erste oder zweite identifizierte Lepton ist, wird die invariante Masse der beiden höchstenergetischen Leptonen nicht mehr derjenigen der beiden echten Leptonen entsprechen. Dadurch wird die Überhöhung der Z–Resonanz in Massenspektrum nicht mehr so deutlich zu sehen sein wie im Fall der Ereignisse mit 2 Leptonen.

In dem untersuchten Datensatz wurde ein Ereignis mit exakt vier Leptonen gefunden. Dieses Ereignis enthält zwei Elektronen und drei hadronische Cluster. Zwei der hadronische Cluster enthalten jeweils ein Myon. b–Quark Paarerzeugung ist der dominierende SM Produktionsprozeß sowohl für Ereignisse mit vier echten Leptonen als auch für Ereignisse mit drei Leptonen und einem misidentifizierten Jet. Daher ist es naheliegend zu untersuchen, ob sich in dem Vier–Lepton–Ereignis Hinweise auf b–Quarks ergeben. Mit einer Standard–b–Identifizierung, dem sogenannten "Secondary Vertex Tagging", wird einer der hadronischen Cluster, die ein Myon enthalten, als Kandidat für einen b–Jet identifiziert.

Das gefundene Ereignis ist konsistent mit den Erwartungen aus dem SM. Die Existenz einer von Null verschiedenen Kopplung λ_{121} ist deshalb für einen großen Bereich des mSUGRA Parameterraumes ausgeschlossen. Um einen konservativen Grenzwert zu erhalten wird angenommen, daß es sich bei dem gefundenen Ereignis um ein Signal für $\not{R}_P$–SUSY handelt und der Bereich des Parameterraumes aus, in dem signifikant mehr als ein Ereignis erwartet wird, ausgeschlossen. Der mit einem Vertrauensintervall von 95% ausgeschlossene Bereich in Abhängigkeit von dem beiden Parametern M_0 und $M_{1/2}$ ist in Abbildung 0.4 gezeigt. Die übrigen Parameter wurden auf feste Werte gesetzt

$$A_0 = 0, \quad \tan(\beta) = 2, \quad \mathrm{SGN}(\mu) = -1.$$

Der Parameter A_0 beeinflußt nur die Mischung der top–Squarks, die in der vorliegenden Analyse nicht berücksichtigt wurden. Deshalb wurde der Wert für A_0 willkürlich auf Null gesetzt. Der Wert des Vorzeichens von μ wurde negativ gewählt, konsistent mit früheren CDF–Analysen. $\tan\beta$ wurde wie in den bisherigen CDF–Analysen auf den Wert 2 gelegt. Werte vom $M_{1/2}$ größer als 130 GeV sind für alle untersuchten Werte von M_0 ausgeschlossen. Für kleine Werte von M_0 ist der ausgeschlossene Bereich größer und erreicht $M_{1/2}$–Werte bis 150 GeV. Das Abfallen und schnelle Wiederansteigen des Grenzwertes bei $M_{1/2}$–Werten von ungefähr 90 GeV wird durch drastische Änderungen des leptonischen Verzweigungsverhältnisses in den Kaskade–Zerfällen von schweren SUSY–Teilchen hervorgerufen. Wie anhand von Abbildung 7.4 zu erkennen ist, übersteigen bei ansteigenden Werten von M_0 die Massen des linkshändigen Sleptons, des

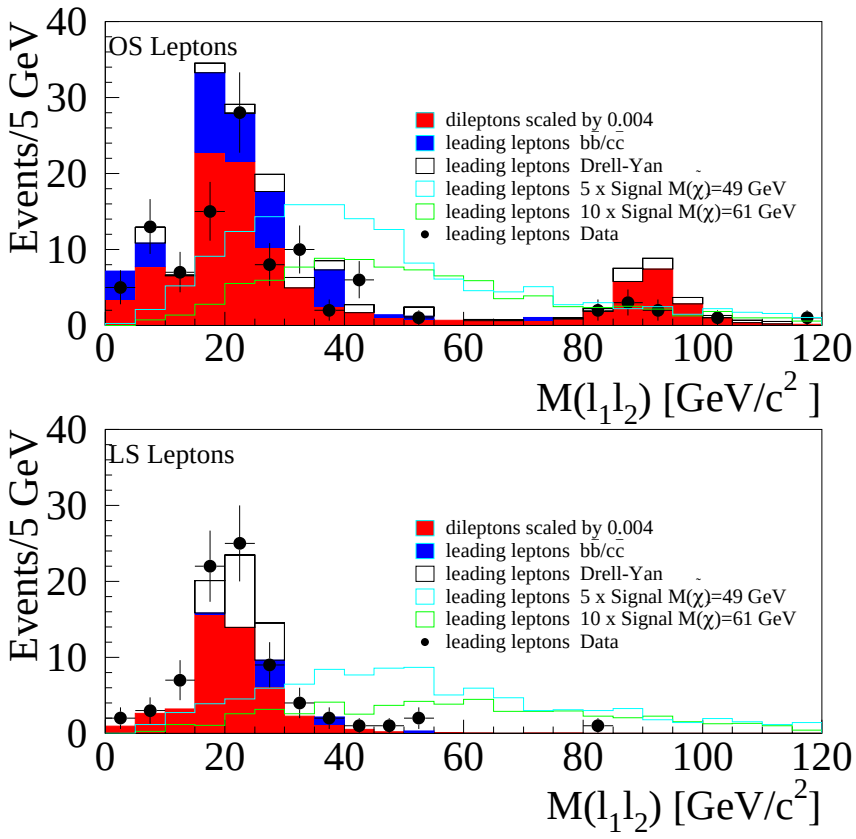

Abbildung 0.3: *Das Massenspektrum der beiden höchstenergetischen Leptonen im drei–Leptonen Datensatz im Vergleich zu den Vorhersagen von MC und misidentifizierten Jets. Die obere Abbildung zeigt das Spektrum für Leptonen mit entgegengesetzter Ladung, während die untere das entsprechende Spektrum für Leptonen mit gleicher Ladung zeigt. Zum Vergleich wurde die Anzahl der Ereignisse, die von zwei Signal–Szenarien erwartet werden, eingezeichnet. Um diese Szenarien sichtbar zu machen, wurde die Anzahl der Ereignisse mit Faktoren 5 und 10 multipliziert.*

Sneutrinos und des rechtshändigen Sleptons nacheinander die Masse des zweitleichtesten Neutralinos und des leichtesten Charginos, deren Massen fast entartet sind. Der Zerfall der Charginos und Neutralinos in das LSP durch das rechtshändige Slepton ist unterdrückt. In dem M_0–Bereich, in dem das linkshändige Slepton schwerer als das zweitleichteste Neutralino und das leichteste Chargino ist, während das Sneutrino leichter als beide ist, hat das leptonische Verzweigungsverhältnis für Kaskadezerfälle ein Minimum. Da ein nicht–verschwindender Anteil der Leptonen, die in der Analyse identifiziert werden, aus ebendiesen Zerfällen stammt, nimmt die Akzeptanz für

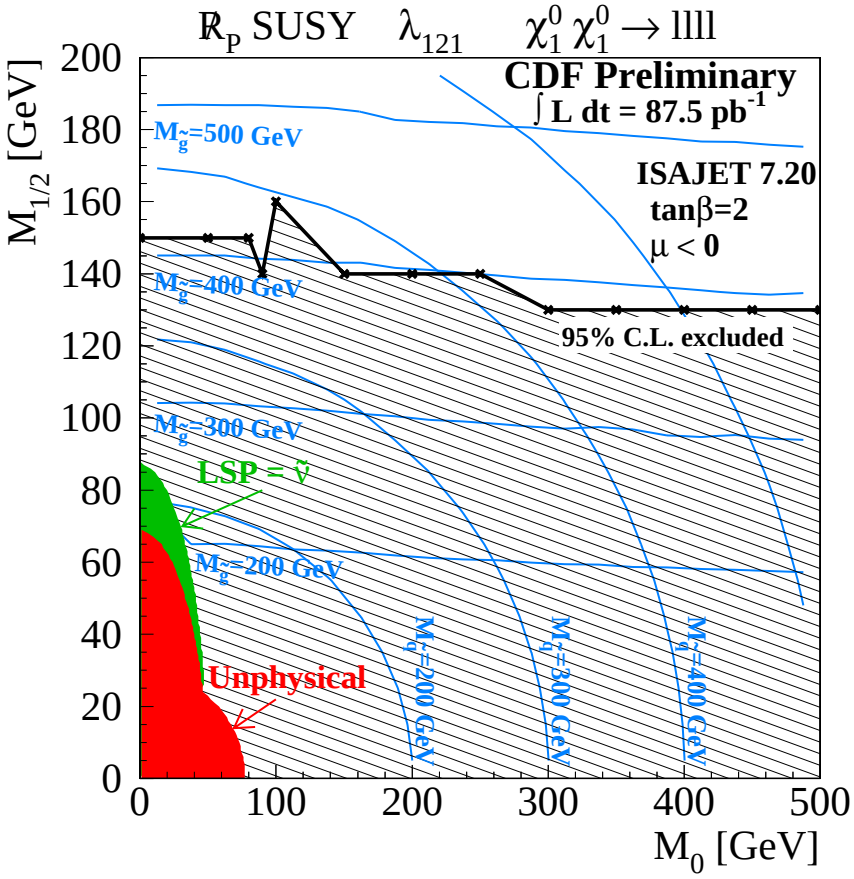

Abbildung 0.4: *Der ausgeschlossene Bereich in der $M_{1/2}$–M_0 Ebene. Die Massen von Gluino und Squark sind als Konturen eingezeichnet. Der dunkle Bereich unten links ist unphysikalisch, weil dort keine elektroschwache Symmetriebrechung stattfindet oder tachionische Teilchen existieren. In der etwas helleren Region ist nicht das leichteste Neutralino, sondern das Sneutrino das LSP. In diesem Bereich erwartet man eine andere Signatur als die hier untersuchte.*

Signal–Ereignisse stark ab. Sobald das Sneutrino schwerer als das zweitleichteste Neutralino und das leichteste Chargino ist, steigt das leptonische Verzweigungsverhältnis sprunghaft an, weil jetzt der Zerfall in das rechtshändige Slepton dominiert.

Die ausgeschlossenen Bereiche in der M_0–$M_{1/2}$–Ebene können in untere Grenzen für die Massen der verschiedenen SUSY–Teilchen umgerechnet werden. Damit sind alle Szenarien, bei denen die Masse des leichtesten Neutralinos unter 55 GeV/c^2 liegt, ausgeschlossen. Hierbei ist das Limit auf die Masse des leichtesten Neutralinos ein direktes Limit, anders als im Fall der R_P–Erhaltung, in dem das leichteste Neutralino unsichtbar ist und nur indirekte Grenzwerte bestimmt werden können. Ebenso ausgeschlossen sind

Szenarien mit einer Charginomasse unter 118 GeV/c^2. Im Rahmen der Supergravitation sind die Massen aller SUSY–Teilchen miteinander korreliert. Dadurch erhält man ein indirektes Limit aus die Masse der Gluinos und Squarks von ungefähr 400 GeV/c^2 für den Fall, daß beide Teilchen die selbe Masse haben.

CDF/THESIS/EXOTIC/PUBLIC/5212
IEKP-KA/99-23

Search for R-Parity violating SUSY in the CDF Multi-Lepton channel

Zur Erlangung des akademischen Grades eines

DOKTORS DER NATURWISSENSCHAFTEN

von der Fakultät für Physik der Universität (TH) Karlsruhe

genehmigte

DISSERTATION

von

Armin Köngeter
aus Birkesdorf, jetzt Düren

Tag der mündlichen Prüfung : 5. November 1999

Referent: Herr Prof. Dr. Th. Müller
Korreferent: Herr Prof. Dr. J. Hauser

Abstract

In this Thesis a search for R-parity violating SUSY in the multi lepton channel in CDF run IB data is presented . This is the first search in this channel performed at a hadron collider.

We assume the existence of a coupling violating R-parity and lepton number conservation. If the coupling is small, the cascade decays of squarks, gluinos and bosinos to the lightest neutralino will only be changed slightly by this new coupling. These decays then can be handled within the R-parity conserving mSUGRA. In addition to the processes from the R-parity conserving mSUGRA, we consider the R-parity violating decay of the lightest neutralino into two charged leptons and one neutrino.

Finding 1 event in 87.5 pb^{-1} all scenarios yielding 5.1 or more events are excluded, limiting R_P violating minimal SUGRA models with a non-zero coupling λ_{121} to $M_{1/2} \gtrsim 130$ GeV. This corresponds to a mass of the lightest neutralino of $\gtrsim 55$ GeV, while the masses of the second lightest neutralino and the lightest chargino are excluded up to 118 GeV/c^2. The squarks and gluinos are excluded up to squark (gluino) masses of $\gtrsim 360$ GeV ($\gtrsim 380$ GeV).

Contents

List of Figures

List of Tables

1 Introduction

In the field of particle physics the so called Standard Model (SM) describes all known particles and their interactions. The SM combines the two theories of Quantum Chromo Dynamics (QCD) and the Glashow–Salam–Weinberg (GSW) model of the electroweak interaction. In a multitude of high-precision experiments performed in the last years no significant deviations from SM predictions were found[2] All particles predicted by the model except the Higgs boson have been found. From an experimental view the SM is thus the best tested and most reliable models in physics. Still, the model has several theoretical deficiencies which should not occur in a fundamental theory (see page 6). If the SM is not fundamental then there must exist an extension or addition which eliminates the deficiencies of the SM.

The extension to the SM favoured by many physicists is the introduction of supersymmetry (SUSY) into the Standard Model. SUSY describes a symmetry between fermions (particles with half-integer spin) and bosons (particles with integer spin). In its simplest form this theory predicts the existence of superpartners for each SM particle. The spin of the superpartners differs from the spin of its SM partner by half a unit. The only other difference between the partner particles is their mass. This mass difference is a consequence of the breaking of SUSY. Theoretical considerations predict the mass of the lightest supersymmetric particle (LSP) below 1 TeV. SUSY still has several shortcomings from a theoretical point (see page 15). Nevertheless it may be next necessary step on the way of finding the fundamental theory of everything.

The theoretical model used in this dissertation is based on supergravity. Supergravity is a SUSY model in which SUSY is broken due to gravitational effect. In addition, the unification of all couplings at a high energy scale M_{GUT} is assumed. The specific model used in this thesis also assumes the existence of a coupling which violates R-parity and lepton-number. This coupling will lead to LSP decays into two charged and one neutral lepton. The signature expected is four leptons, because in the scenario under study sparticles are pair–produced and decay dominantly through R-parity conserving channels. Only the decays of the LSPs violate R-parity.

The data used for this search were taken with the collider detector at Fermilab during the years 1994-1995. The integrated luminosity of the data used is 87.5 pb^{-1}.

[2]The only unexpected effect found are neutrino oscillations. These can be explained by introducing massed for all neutrinos, but require no major additions or changes to the SM.

2 The Standard Model of Particle Physics

The Standard Model of particle physics is the extremely successful model used to describe elementary particles and the interactions between them. The model is described in various textbooks like [1].

Elementary particles are divided into two classes according to their internal angular momentum, the so-called spin. Particles with integer spin are called bosons, particles with half integer spin are called fermions. Depending on the spin the behaviour of the particles is different. E.g. macroscopic matter consists of electrons and protons which both are fermions with spin 1/2. On the other hand the electro-magnetic force between charged particles is mediated by photons, which have spin 1 and thus are bosons. In generalisation of this interactions between fermions can be described by the exchange of bosons.

The fermions in the SM are further classified into three generations according to their mass. The first generation consists of the electron e^-, the electron-neutrino ν_e, the up-quark u, the down-quark d and their anti-particles. The particles of the second and third generation have identical properties except for their higher masses. The second generation leptons (fermions which like the electron and the neutrino do not take part in the strong interaction) are the muon μ^- and the muon neutrino ν_μ. The other two particles belonging to the second generation are the strange quark s and the charm quark c. The third generation consists of the tau lepton τ, its neutrino ν_τ and the bottom and top quarks b and t. The fermions of the SM are listed in table 2.1. As the exact classification of the fermions is important for the construction of the SM, I will go into some more detail here.

The first description of fermions as quantum-mechanical objects goes back to P. Dirac (1927). In this description fermions are particles solving the Dirac equation. There are four independent solutions to this equations, two of which have negative energies. Dirac interpreted the two solutions with positive energy as the two spin-states of the electron e^-. The states with negative energy were interpreted as the two spin states of the positron e^+, a particle with positive charge which in all other respects is identical to the electron. With the discovery of the positron in 1933 Dirac's interpretation was verified. Another popular interpretation of the four states of the solution of the Dirac-equation goes back to Weyl. He found that by applying the projection operator γ_5 to a Dirac-fermion one can define two particles consisting of two states each. For the electron these particles are the left-handed electron with its partner the right-handed positron (e^-_L, e^+_R) and the right-handed electron with its partner the left-handed positron (e^-_R, e^+_L). This interpretation at first seems to be just an accidental feature of relativistic quantum-theory. Still the observation of parity violation in the weak interaction by Wu (1957) [2] proved that the Weyl-interpretation has a deeper meaning. The weak interaction couples only to the left-handed projections of the fermions. This can either be described in Dirac-notation by using the projection-operator. In Weyl-notation the interpretation is easier, as the two projections are different particles and it is natural

	Leptons	Quarks
1st Generation	e, ν_e	d, u
2nd Generation	μ, ν_μ	s, c
3rd Generation	τ, ν_τ	b, t

Tabelle 2.1 : *The three fermion generations of the Standard Model.*

that some interactions will not involve some of these particles.

All massive right-handed fermions can be transformed into left-handed ones and vice versa by a Lorentz-transformation. This can be interpreted as "overtaking" the particles and will only work for massive particles. Massless particles move at the speed of light and thus there is no possible Lorentz-transformation which reverses the direction of the particles. This introduces a peculiar effect for neutrinos. If neutrinos are massless then the right-handed neutrinos (and the left-handed anti-neutrinos) would only interact through gravitation like photons, which can accelerated and slowed down in gravitational fields. Still there is no way to measure this interaction and the neutrinos can not be transformed into left-handed neutrinos by a Lorentz-transformation. Thus there no way of detecting such particles. As a consequence right-handed neutrinos are usually considered non-existent. Measurements of solar neutrinos [3] indicate neutrino mixing and thus a non-zero mass for the neutrinos. More evidence for neutrino oscillations [4] comes from LSND[3], one of two experiments studying neutrinos produced in pion decay. The LSND measurements are not confirmed [5] by Karmen[4], which studies the same channel. The strongest evidence for neutrino masses yet comes from recent measurements of atmospheric neutrinos by the Superkamiokande collaboration [6]. If these measurements are further confirmed they might force the interpretation of the neutrino-sector of the SM to be modified.

At the present four different bosons and their interactions are known: the photon γ, the Z^0, the $W^\pm$ and the gluon g. There are eight different colour charge states of the gluon.

For a theoretical description it has proven reasonable to construct a Lagrange density similar to the Lagrange function in classical physics. One starts with a density for fermions without interactions between them. The interactions and bosons are then introduced by requiring the Lagrangian to be invariant under certain groups of gauge transformations. The additional terms introduced to obtain this invariance describe the bosons and the coupling of fermions and bosons.

All known interactions in particle physics can be deducted by requiring local gauge-invariance with respect to the groups U(1), SU(2) and SU(3)(see e.g. [1]). This formalism is known from classical electro–dynamics, where the existence of the electro–magnetic potential and the vector–potential are derived from the local gauge–invariance

[3]Liquid Scintillator Neutrino Detector

[4]Karlsruhe Rutherford Medium Energy Neutrino Experiment

of the Theory. In Quantum–Field–Theories one starts with the Lagrangian for non–interacting fermions and demand that the wave–functions of the fermions are invariant under local gauge transformations. This is achieved by adding a new term to the Lagrangian, which describes a bosonic field mediating an interaction between the fermions.

Local gauge invariance implies the conservation of an additive quantum number. A simple example for such a quantum number is the electrical charge, which is conserved because of the U(1) gauge invariance of QED. Analogous to the electrical charge quantum numbers conserved as a consequence of gauge invariance are called charges. The ways in which the charges add and couple to the gauge fields are determined by the associated symmetry group.

The construction of a Lagrangian of the desired form is possible without complication as long as the fermions are all massless. One finds the neutral B^0 boson, three W-bosons with the charges -1, 0 and 1 as well as eight charge states of the gluon. Like the fermions all bosons are massless in this model.

The charge states of the gluon can be represented as an SU(3)-octet. The associated charge is called colour charge. The elementary values (colours) of this charge are red, green and blue with the anti-colours $\overline{\text{red}}$, $\overline{\text{green}}$, $\overline{\text{blue}}$. Gluons carry two colour charges, one colour and one anti-colour. Quarks have either a colour or an anti-colour. All other particles are colourless, which means that they don't participate in this interaction. The properties of the gluons predicted by this form of the theory agree well with their observed properties. The strong interaction, which is carried by the gluons, is described adequately.

The properties of the other bosons are not described correctly by this form of the theory. The B^0 is not identical to the photon or the Z^0 and the W^0 is not seen in experiment. As the $W^\pm$ and Z^0 bosons have rather high masses it is valid to assume that the differences will disappear if masses are introduced.

The simplest way to consider masses is to introduce mass-terms into the Lagrangian. Doing this will lead to non-renormalisable divergences, which would make the theory useless. A much more elegant method to create masses is the introduction of a so-called higgs-field. This field has four independent degrees of freedom and can be represented as a complex vector

$$\phi(x) = \begin{pmatrix} \phi^+ \\ \phi^0 \end{pmatrix} = \begin{pmatrix} \phi_1(x) + i\phi_2(x) \\ \phi_3(x) + i\phi_3(x) \end{pmatrix}.$$

The Lagrangian is

$$\mathcal{L}_{\text{Higgs}} = (D_\mu\phi)^\dagger(D^\mu\phi) - V(\phi),$$

where the potential $V(\phi)$ is given by

$$V(\phi) = \mu^2\phi^\dagger\phi + \lambda(\phi^\dagger\phi)^2.$$

Terms of higher order in ϕ are not allowed because they will lead to unrenormalisable divergencies. The lowest energetic state corresponds to fields which are constant in space

Interaction	Boson	Symmetry Group
Electro-Weak	Photon γ, $W^{\pm}$, Z^0,	U(1)×SU(2)
Strong	Gluons g	SU(3)
–	Higgs h	–

Tabelle 2.2 : *The interactions of the SM together with the bosons mediating the interactions and the symmetry groups associated with the interactions.*

and time. The vacuum expectation values are given by the minimum of the potential V. For $\mu^2 \geq 0$ the potential has a trivial minimum at $\phi = 0$, which reflects the symmetry of the potential. For $\mu^2 < 0$ the minima lie on a circle of radius $v = \sqrt{-2\mu/\lambda}$. In the lowest energetic state the system has spontaneously chosen one special value for the vacuum expectation value. This value then no longer reflects the symmetry of the potential. The phenomenon is called spontaneous symmetry breaking. It is similar to the spontaneous ordering of electron spins in ferromagnetic metals.

For $\mu^2 < 0$ the higgs field can be parametrised such that exactly one of its components has a vacuum expectation value (VEV) different from zero. Then the Lagrangian can be transformed in a way that yields mass terms for fermions and bosons. The non-zero term from the higgs-field gives an additional scalar boson with non-zero mass. This particle is called the higgs-boson. The components of the higgs-field with VEVs of zero are absorbed into the fermions and bosons.

The B^0 and W bosons were introduced in order to preserve invariance under the $U(1)_Y \times SU(2)_L$ symmetry transformations. Y is the weak hypercharge, a quantum number similar to the electrical charge. The L in the SU(2)-group means that the interaction affects only left-handed fermions. The charge belonging to this interaction is the third component of the weak isospin T_3, which is similar to the spin. The particles interacting with the $W^{\pm}$ bosons are arranged in isospin-doublets. Particles not taking part in this interaction have isospin 0.

After the introduction of the higgs-boson the $U(1)_Y \times SU(2)_L$ symmetry of the ground-state is broken and the B^0 and the W^0 boson mix. The mixed states are called the mass-eigenstates as they describe the physical particles one can detect. The states before mixing are called the weak eigenstates, as they are the states produced in the weak interaction. It is possible to choose the mixing in a way that gives a massless and a massive boson, which have the properties observed in the photon and the Z^0. The bosons of the SM are shown in table 2.2.

The accuracy of the model described above was shown by many experiments during the last years. All particles predicted by the SM except for the higgs boson have been found[5]. The measured properties of the particles and their interactions agree well with the predictions of the SM. Thus from the experimental point of view the SM is a complete and accurate description of elementary particle physics. From the theoretical

[5]There is only indirect evidence for the existence of the third generation neutrino (ν_τ).

point of view there are still some insufficiencies in the SM. These insufficiencies should not exist in a fundamental theory.

Some of the weak points of the SM are:

1. The SM has a large number of parameters which are not predicted by the theory, but have to be determined by experiments.

2. The charges of quarks and leptons differ by simple factors, although in the SM their charges are not correlated. A fundamental theory would have to introduce such a correlation, probably by introducing a symmetry between quarks and leptons.

3. The SM includes the classical theory of gravity. A fundamental theory must include a quantum theory of gravity for energies higher than the Planck scale.

4. The electro-magnetic interaction is not asymptotically free, thus it will not give the correct results at very high energies. The energy scale at which this effect becomes important is higher than the Planck scale and thus effects from quantum gravity may be important. The theory at these energies will be significantly different from the quantum electro dynamics (QED) seen at low energies. Thus also the SM has to be modified at high energies.

5. The higgs boson couples to all massive particles, including itself. This causes corrections to the higgs-mass which diverge quadratically. Such behaviour indicates that the SM is only valid below a certain energy scale and has to be replaced by a different model at higher energies.

The first three problems mentioned above can be solved by requiring the three couplings to unify at high energies. Such theories are called grand unified theories (GUTs). In this theory all interactions will be unified into one single interaction following a single symmetry group at energies above the unification scale. At lower energies this symmetry will be broken to $U(1) \times SU(2) \times SU(3)$ yielding the SM.

GUTs reduce the number of free parameters and couple quarks and leptons directly thus explaining the ratio of their charges. The interactions coupling quarks and leptons are mediated by new heavy bosons, which are the remnants of the GUT symmetry group.

Still the divergences in the higgs masses remain and there are other difficulties in connection with these models. E.g. the unification of the coupling constants of the three interactions is not perfect. Extrapolating the couplings measured at the energies accessible by todays machines to high energies, one would expect that all couplings have the same values at the unification scale. In GUT theories based solely on the SM the extrapolation shows that the coupling constants do not meet at a single point, so that there have to be several stages of unification or other processes which finally lead to a unification of all forces.

A rather simple form of a GUT, the assumption of a SU(5) symmetry at high energies, has already been disproved by experiment. In this special theory the probability for proton decays is higher than the measured value. Also the SU(5) GUT predicts a value for the weak mixing angle at the Z^0–mass of $\sin\theta_w = 0.2$, while the global average of measurements is 0.2260 ± 0.0039 [7]. These values disagree by several standard deviations. As a consequence one has to use other, more complex groups if one insists on constructing a GUT solely on the SM.

An addition to the SM, which can solve the problem of the higgs self-coupling and can be combined with GUTs is supersymmetry, which will be discussed in the next chapter.

3 Supersymmetry

Supersymmetry (SUSY) is a fundamental symmetry between fermions and bosons. This symmetry has been successfully applied to many problems in quantum mechanics and other fields of physics. As SUSY is so successful in solving physical problems it is reasonable to apply the concepts and tools of SUSY to particle physics. One then can study the consequences of SUSY in this field and investigate if there are any proofs that it is realized here.

In this chapter a short introduction to SUSY will be given. The chapter begins with a short description of SUSY in general and about its application to quantum mechanics. Then the applications of SUSY to particle physics and its consequences will be discussed. The discussion follows closely [8].

3.1 The Concept of Supersymmetry

SUSY introduces two new quantum mechanical operators which transfer a fermionic state to a bosonic state and vice versa. Using destructor and creator notation these two operators can be written as

$$Q_+ = b^- f^+; \qquad Q_- = b^+ f^-,$$

where $b^\pm$ ($f^\pm$) are the boson (fermion) creator and destructor operators. The operator Q_+ (Q_-) decreases (increases) the number of bosons by one while increasing (decreasing) the number of fermions by one. The operators Q_+ and Q_- are non-hermitian. Often it is more convenient to use instead the linear combinations

$$Q_1 = Q_+ + Q_- \qquad \text{and} \qquad Q_2 = -i(Q_+ - Q_-),$$

which are hermitian.

In general one can have an infinite number of bosons in any quantum mechanical system, while one may only have zero or one fermions. In SUSY every state has a fermionic quantum number (either 0 or 1) associated with it. The states where the fermionic quantum number is 0 are called bosonic states, the ones with a fermionic quantum number of 1 are called fermionic states. As a consequence of SUSY states with the same bosonic quantum numbers but different fermionic quantum numbers always appear in pairs. The pair of bosonic and fermionic states are related in such a way that many of the divergencies occurring in quantum-mechanics are weakened or solved.

3.1.1 The Hydrogen Atom

In this section the energy states of the hydrogen atom are calculated using the tools and methods of SUSY. The results obtained with this method do not differ from the results obtained with the standard methods. Still, the way they are calculated is very

elegant. The method demonstrated in this example can be applied to a multitude of physical problems. The example given in this subsection was adapted from [8].

The effective potential for the hydrogen atom is composed from the Coulomb potential and the contribution due to the angular momentum. It has the form

$$V_{\text{eff}} = -\frac{e^2}{r} + \frac{l(l+1)\hbar^2}{2mr^2}. \tag{1}$$

Here m, e and l are the reduced mass, the charge and the angular momentum of the electron and r is the distance between electron and proton. From eqn. (1) one sees that the radial part of the Schrödinger equation is

$$\left[-\frac{\hbar^2}{2m}\frac{d^2}{dr^2} - \frac{e^2}{r} + \frac{l(l+1)\hbar^2}{2mr^2}\right]\psi_{nl}(r) = E\psi_{nl}(r),$$

here the quantum number n counts the nodes in the wave function. The ground state wave function has no nodes, the first excited state one node and so on. The solution of the problem starts with finding an ansatz for the ground state wave function. Looking at the asymptotic behaviour of the function one finds

$$\psi(r) \approx \exp(-\alpha r^2) \quad \text{for large values of} \quad r,$$

with a positive constant α. To avoid unphysical behaviour for small values of r one has to add a factor r^γ with $\gamma \geq 1$ to the ansatz obtaining

$$\psi_0(r) = Cr^\gamma e^{-\alpha r}.$$

The values of the constants α and γ are obtained by inserting the ansatz into the Schrödinger equation

$$-\gamma(\gamma-1)r^{\gamma-2} + 2\alpha\gamma r^{\gamma-1} - \alpha^2 r^\gamma - \frac{2me^2}{\hbar^2}r^{\gamma-1} + l(l+1)r^{\gamma-2} = \frac{2mE}{\hbar^2}r^\gamma.$$

Comparing the coefficients gives

$$\gamma = l+1 \qquad \text{and} \qquad \alpha = \frac{me^2}{(l+1)\hbar^2}.$$

In addition the energy of the ground state can be determined to be

$$E_0 = -\frac{me^4}{2\hbar^2(l+1)^2}.$$

So far only standard quantum mechanical techniques have been used to find the ground state of the problem and its energy. SUSY can now be used to calculate all higher states and their energies from the known ground state.

A quantum mechanical problem can be solved using SUSY if the Schrödinger equation can be written as

$$-\frac{\hbar^2}{2m}\psi'' + \frac{1}{2}\left(W^2 - \frac{\hbar}{\sqrt{m}}W'\right)\psi = 0.$$

The function W is called the superpotential and has the dimension of $[\text{energy}]^{1/2}$.

Inserting the known ground state wave function ψ_0 one obtains:

$$\frac{\psi_0''}{\psi_0} = \left(\frac{\sqrt{m}}{\hbar}W\right)^2 - \left(\frac{\sqrt{m}}{\hbar}W\right)'.$$

Using

$$\left(\frac{\psi_0'}{\psi_0}\right)' = \frac{\psi_0''}{\psi_0} - \left(\frac{\psi_0'}{\psi_0}\right)^2$$

one finds

$$\left(\frac{\psi_0'}{\psi_0}\right)^2 + \left(\frac{\psi_0'}{\psi_0}\right)' = \left(\frac{\sqrt{m}}{\hbar}W\right)^2 - \left(\frac{\sqrt{m}}{\hbar}W\right)'.$$

And thus the superpotential can be calculated from the ground state wave function

$$W = -\frac{\hbar}{\sqrt{m}}\frac{\psi_0'}{\psi_0} = -\frac{\hbar}{\sqrt{m}}\frac{d}{dx}\log\psi_0.$$

For the Coulomb potential the superpotential becomes

$$W(r;l) = \frac{\hbar}{\sqrt{m}}\left[\alpha - \frac{\gamma}{r}\right] = \frac{\hbar}{\sqrt{m}}\left[\frac{me^2}{(l+1)\hbar} - \frac{l+1}{r}\right].$$

The superpotential determines two partner potentials through the relation:

$$V_1 = \frac{1}{2}\left[W^2 - \frac{\hbar}{\sqrt{m}}W'\right] \qquad \text{and} \qquad V_2 = \frac{1}{2}\left[W^2 + \frac{\hbar}{\sqrt{m}}W'\right].$$

For the case of the hydrogen atom the partner potentials are

$$V_1(r;l) = \frac{me^4}{2\hbar^2(l+1)^2} - \frac{e^2}{r} + \frac{l(l+1)\hbar^2}{2mr^2}$$

and

$$V_2(r;l) = \frac{me^4}{2\hbar^2(l+1)^2} - \frac{e^2}{r} + \frac{l(l+1)(l+2)\hbar^2}{2mr^2}.$$

V_1 is the effective potential of eqn. (1) minus the energy of the ground state. This construct is necessary because in SUSY the ground state must have the energy $E = 0$. In unbroken SUSY this state is the only one which is non-degenerate. The first excited

state of the potential V_1 is degenerate with the ground state of V_2. The same holds for higher excited states of V_1 and V_2:

$$E^{(1)} = 0 \qquad \text{and} \qquad E_n^{(2)} = E_{n+1}^{(1)}.$$

Thus if one knows the ground state energy $E_1^{(2)}$ of the partner potential V_2 one automatically knows the energy of the first excited state $E_1^{(1)}$ of the original potential V_1.

If the difference between the two potentials $R(a)$ does not depend on x also the potentials $V_1 + R(a) = V_2$ and $V_2 + R(a) \equiv V_3$ are partner potentials. Thus knowing the ground state energy of the V_3 one knows the first excited state of V_2 and also the second excited state of V_1. This construct can be continued to obtain all possible states of V_1. The method of calculating only the ground state of one potential and then obtaining all higher energetic states by finding a general formula for the superpotentials is called SUSY-chains.

Returning to the hydrogen problem the two potentials differ by

$$R(a_1) = V_2(r;l) - V_1(r;l) = \frac{me^4}{2\hbar^2}\left[\frac{1}{(a_1)^2} - \frac{1}{(a_1+1)^2}\right]. \tag{2}$$

Where the parameter $a_1 \equiv l + 1$. $R(a_k)$ does not depend on r, thus it is possible to use a SUSY-chain to determine all states of V_1 and thus of the Coulomb potential. Eqn. (2) can be generalised for arbitrary values of a_k

$$R(a_k) = R(l + k - 1) = \frac{me^4}{2\hbar^2}\left[\frac{1}{(l+k)^2} - \frac{1}{(l+k+1)^2}\right].$$

In order to obtain the energy of a specific excited state E_n of V_1 we have to sum over all $R(a_k)$ with $a_k \leq n$:

$$E_n^{(1)} = \sum_{l=0}^{n} R(l) =$$
$$\frac{me^4}{2\hbar^2}\left[\frac{1}{(l+1)^2} - \frac{1}{(l+2)^2} + \frac{1}{(l+2)^2} + \cdots - \frac{1}{(l+n)^2} + \frac{1}{(l+n)^2} - \frac{1}{(l+n+1)^2}\right].$$

In the sum all terms except for the first and the last cancel, thus the energy is

$$E_n^{(1)} = \frac{me^4}{2\hbar^2}\left[\frac{1}{(l+1)^2} - \frac{1}{(l+n+1)^2}\right].$$

Finally the energy for the Coulomb potential is obtained adding the ground state energy to $E_n^{(1)}$:

$$E_{nl} = E_M^{(1)} + E_0 = -\frac{me^4}{2\hbar^2}\frac{1}{(l+n+1)^2}.$$

In this section I have used a rather simple example to demonstrate the power SUSY has in solving physical problems. The concept of the superpotential and the idea of two states closely connected by supersymmetry have been introduced. In the following sections the consequences of applying SUSY to field theoretic models will be discussed.

3.2 Supersymmetry in Particle Physics

In this section the concept of SUSY will be applied to particle physics and the consequences will be studied. I will not go into the details of constructing a supersymmetric Lagrangian, but instead will describe the most important features of a supersymmetric field theory. For an introduction into supersymmetry in particle physics see e.g. [9] and references therein, for a review see e.g. [10]. Experimental results are summarised in [7] and references therein.

The SM of particle physics was described in chapter 2. The SM is a field theory with a SU(3)×SU(2)×U(1) symmetry. Adding SUSY to the SM will introduce new degrees of freedom, which in most cases can be interpreted as new particles[6].

SUSY is introduced into the SM by constructing a Lagrangian which is invariant under SUSY transformations. This is achieved by first constructing a superpotential W, from which then the Lagrange density is calculated. The superpotential must be invariant under gauge and SUSY transformations and analytic in the scalar fields. As the fermion mass terms in the Lagrangian are derivatives of the superpotential the Lagrangian must be analytic in the scalar fields as well. A direct consequence is that unlike in the SM one may not use the complex conjugate of the Higgs field in the Lagrangian. Thus in SUSY one needs at least a second Higgs doublet in order to give masses to both types of quarks. The second doublet also avoids anomalies arising from fermionic triangle loops.

As a consequence of introducing a second Higgs boson one gets two scalar neutral Higgs bosons (h^0) and (H^0) as well as a pseudoscalar neutral Higgs (A^0) and a pair of charged scalar Higgses ($H^\pm$).

The model described in the remainder of this section is based on the SM. It introduces the minimal number of new particles necessary to build a field theory invariant unter SUSY transformations. Thus the model is called the Minimal Supersymmetric Standard Model (MSSM)

The particles in a supersymmetric field theory can be classified into supermultiplets. Such a multiplet consists of a bosonic and a fermionic state, which can be transfered into each other by an operator containing only Q, $Q^\dagger$ and a simple spacetime rotation. The simplest form of a supermultiplet is the chiral supermultiplet containing a single Weyl fermion (with two helicity states) and two real scalars. As stated in chapter 2 SM fermions can be described as Weyl fermions and the SM Higgs bosons are described by scalars. Thus both types of particles will naturally be members of chiral multiplets.

The superpartners of fermions are denoted by putting an "sïn front of the fermion name. Thus the partner of the electron is called "selectron". The superpartners of bosons are denoted by appending "-inoät the end of the boson name. E.g. the partner of the Higgs is called Higgsino. In both cases the symbol of the SM particle with a tilde

[6]The interpretation of the new degrees of freedom as particles is valid for linear SUSY only. There are models of nonlinear SUSY, in which the only differences to the SM are changes in the Higgs masses (See e.g. [12]). Nonlinear SUSY is thus often called hidden SUSY.

($\sim$) on top is used. Thus the symbol for the smuon is $\tilde{\mu}$. The same naming conventions are used for groups of particles in a similar way. E.g. the partners of the quarks are called "squarks".

To distinguish between SM particles and their superpartners one defines a multiplicative quantum number called R-parity as [16]

$$R_P \equiv (-1)^{3B+L+2S},$$

where B and L are the baryon and lepton number of the particle and S is its spin. Following this definition all SM particles have R-parity $+1$, whereas their superpartners have R-parity -1.

Usually one assumes that R-parity is conserved. As a direct consequence superpartners can only be produced in pairs and the Lightest Supersymmetric Particle (LSP) is stable.

As all sleptons are scalar particles they do not have a defined handedness. The subscripts L and R and the notation "right-handed" or "left-handed" will still be used to indicate that the particles are the superpartners of the right– and left–handed leptons.

Table 3.1 shows the SM fermions and the two Higgs doublets necessary in SUSY with their respective superpartners. For each supermultiplet a symbol is defined and the particle content is given. The first part of table 3.1 gives the supermultiplets for the three lepton generations. The left–handed supermultiplets are as the particles $\mathrm{SU}_L(2)$–doublets. The right handed superfields are $\mathrm{SU}_L(2)$–singlets. For the construction of supersymmetric Lagrangians it has proven useful to use only left–handed Weyl–spinors. One obtains left–handed superfields from the right–handed one by complex conjugation of the SM–particles and hermitian conjugation of the superpartners. Thus in Table 3.1 the complex–conjugate of the right–handed Fermions and the hermitian conjugate of the right–handed sfermions are used to define the left–handed supermultiplets. The second part of Table 3.1 shows the supermultiplets for the three generations of quark–superfields. The last part of table 3.1 gives the higgs–superfields. The SM–higgs fields are $\mathrm{SU}_L(2)$–doublets and form superfields with the higgsinos.

Both the SM fermions and the SM Higgs boson are members of chiral multiplets. Thus it has been suggested that the SM Higgs boson could be the superpartner of the neutrino and would then be identical to the sneutrino. However closer investigation has shown that such a construct would lead to lepton number violation in excess of the current limits. Therefore one concludes that table 3.1 gives the correct classification of SM particles into supermultiplets.

The chiral supermultiplets can not contain any particles with spin 1. As the SM gauge bosons are spin 1 particles they have to be part of a different form of supermultiplet. These so-called gauge multiplets contain a massless vector boson and a massless spin-1/2 Weyl spinor. As in the SM all masses of the vector bosons and their superpartners are created by electro-weak symmetry breaking. Table 3.2 shows the particle content of the gauge multiplets corresponding to the SM.

Instead of using spin 1/2 Weyl spinors as the superpartners of the vector bosons

Multiplet	Leptons	Sleptons
L_1	(e_L, ν_e)	$(\tilde{e}_L, \tilde{\nu_e})$
L_2	(μ_L, ν_μ)	$(\tilde{\mu}_L, \tilde{\nu_\mu})$
L_3	(τ_L, ν_τ)	$(\tilde{\tau}_L, \tilde{\nu_\tau})$
$\bar{e}_1$	e_R^*	$\tilde{e}_R^\dagger$
$\bar{e}_2$	μ_R^*	$\tilde{\mu}_R^\dagger$
$\bar{e}_3$	τ_R^*	$\tilde{\tau}_R^\dagger$

Multiplet	Quarks	Squarks
Q_1	(u_L, d_L)	$(\tilde{\mathrm{u}}_L, \tilde{\mathrm{b}}_L)$
Q_2	(c_L, s_L)	$(\tilde{\mathrm{c}}_L, \tilde{\mathrm{s}}_L)$
Q_3	(t_L, b_L)	$(\tilde{\mathrm{t}}_L, \tilde{\mathrm{b}}_L)$
$\bar{u}_1$	u_R^*	$\tilde{\mathrm{u}}_R^\dagger$
$\bar{u}_2$	c_R^*	$\tilde{\mathrm{c}}_R^\dagger$
$\bar{u}_3$	t_R^*	$\tilde{\mathrm{t}}_R^\dagger$
$\bar{d}_1$	d_R^*	$\tilde{\mathrm{d}}_R^\dagger$
$\bar{d}_2$	s_R^*	$\tilde{\mathrm{s}}_R^\dagger$
$\bar{d}_3$	b_R^*	$\tilde{\mathrm{b}}_R^\dagger$

Multiplet	Higgs–Bosons	Higgsinos
H_u	(H_u^+, H_u^0)	$(\tilde{H}_u^+, \tilde{H}_u^0)$
H_d	(H_d^0, H_d^-)	$(\tilde{H}_d^0, \tilde{H}_d^-)$

Tabelle 3.1 : *The chiral supermultiplets of the MSSM.*

gauge bosons	gauginos
$W^\pm, W^0$	$\tilde{W}^\pm, \tilde{W}^0$
g	$\tilde{g}$
B^0	$\tilde{B}^0$

Tabelle 3.2 : *The gauge multiplets of the MSSM.*

one also could have constructed a supermultiplet using spin 3/2 spinors. However this would make the theory non-renormalisable.

The superpotential describing the MSSM is

$$W_{\mathrm{MSSM}} = \bar{u} y_u Q H_u - \bar{d} y_d Q H_d - \bar{e} y_e L H_d + \mu H_u H_d. \tag{3}$$

All gauge and family indices have been suppressed. Similar to the SM the mass of the Higgs boson is determined by the μ term. The ys are the Yukawa couplings of the superfields.

SUSY avoids the quadratic divergences in the Higgs masses by introducing fermionic loops in addition to the bosonic loops already present in the SM. The fermionic loops have the same value but opposite sign of the bosonic loops. Thus the divergencies cancel out exactly [10] if the superpartners have the same masses as the SM particles. This is the case only in unbroken SUSY.

In the theory stated so far the superpartners have the same masses as the SM particles. Since no superpartners have been observed so far this expectation is wrong. SUSY can not be realized in the form described so far, but has to be broken. This means that there have to be terms in the Lagrangian that lead to different masses for SM-particles and their superpartners. If the mass differences are not too high ($\Delta M < 250$ GeV) and the mass of the lightest supersymmetric particle (LSP) is not too high ($M_{\mathrm{LSP}} < 1$ TeV), the corrections to the Higgs mass remain finite.

The masses of the superpartners are determined by the exact ways in which SUSY is broken. Here it is important that the breaking is "soft", i.e. that the breaking of SUSY does not introduce quadratical divergencies into the theory.

There is no parallel process for SUSY breaking in the SM. This means that it is only possible to describe the consequences of this process by introducing additional parameters.

The model described so far solves many of the theoretical problems appearing in the SM. Still SUSY breaking introduces up to 105 new parameters which describe the SUSY breaking. In addition there are the parameters necessary to describe the particles and couplings of the SM. It would be very unsatisfactory if a fundamental theory describing everything in the universe would have such a huge number of parameters. One assumes that such a theory has only very few free parameters and thus looks for additions to the MSSM that reduce the number of free parameters while giving at the same time a deeper insight into particle physics.

One first reduction can be achieved by unifying the gauge and the Yukawa interactions at high energies. SUSY theories have the interesting feature that the gauge coupling constants meet in a single point, thus making it probable that a unification takes place.

For the MSSM with grand unification and with equal masses for all squarks a choice of parameters describing all superpartners are:

> The masses of the gluino, the squarks, the left-handed and the right-handed sleptons.
> In addition one needs to know the ratio of the VEV of the Higgs doublets
>
> $$\tan(\beta) = v_2/v_1,$$
>
> the value of the Higgs mass parameter μ and of the trilinear coupling A_0, which relates the Yukawa coupling constants $\lambda = A_0 y$.

Here it was assumed that all three generations of sfermions are degenerate in mass as well as the squarks of each generation.

The next natural step after introducing GUTs is to unify the SM couplings with gravity, which generally is neglected in particle physics due to its weakness. Gravity is very different from the other interactions and currently it is not known how it can be included in a GUT. Still it is possible to construct a theory which includes gravity at a higher energy scale than the GUT scale. Such theories are called supergravity and are

treated in the next section.

3.3 Minimal Supergravity

In this section an overview over the model of minimal supergravity (mSUGRA) [11] and its effects are given.

As discussed in the previous section a major shortcoming of the MSSM is the large number of free parameters. Except for the two parameters needed to describe the additional Higgs doublet, these parameters are a consequence not of SUSY but of SUSY breaking. Thus the number of independent parameters as well as their values depend strongly upon the way SUSY is broken.

There are several known mechanisms to break SUSY. One can introduce the SUSY breaking "by handï.e. by just adding soft SUSY breaking terms into the potential. This is just a parametrisation of the unknown mechanism by which SUSY is broken and in the most general form introduces 105 new parameters into the theory. Introducing SUSY breaking by hand can be helpful in some cases, like in phenomenological studies. Still for a better understanding of the fundamental physics one prefers to deduct the SUSY breaking terms from a more fundamental theory, which also tends to give a smaller number of free parameters. At present there are two popular theories of SUSY breaking. In both theories SUSY is broken in a hidden sector in which a field with a high VEV exists. The two models differ in the way the breaking is mediated to the visible sector:

- Gauge mediated SUSY breaking. Here the SUSY breaking is mediated by loop diagrams involving messenger particles. These messengers couple to the MSSM particles via the ordinary electroweak and QCD interaction. On the other hand the messengers couple to the hidden sector and thus mediate SUSY breaking to the visible sector.

- Supergravity (SUGRA) models. In these models SUSY is broken by the new physics, including quantum gravity which has to exist at the Planck scale. In contrast to gauge mediated models one must introduce a new form of interaction, which is called supergravity. This new interaction couples to the hidden and the visible sector and leads to SUSY breaking at low energies. Supergravity is the only form of SUSY which includes quantum gravity in a rudimentary form and thus is expected to be closest to a really fundamental theory. Also supergravity is the only form of SUSY breaking implemented in the generator (ISAJET 7.20) used for this analysis. Thus I will only discuss supergravity in the remainder of the thesis.

SUGRA theories arise naturally if one makes the step from global SUSY to local SUSY. In global SUSY the Lagrangian is invariant under the global SUSY transformation. Looking at a system of a non-interacting chiral multiplet, $(\phi(x),\psi(x))$, the

Lagrangian is

$$\mathcal{L} = -\partial_\mu \phi^\dagger \partial^\mu \phi - \bar{\psi}(-i)\gamma^\mu \partial_\mu \psi,$$

which is invariant under the global SUSY transformation:

$$\delta\phi(x) = \bar{\epsilon}\psi(x); \qquad \delta\psi(x) = -i\gamma^\mu[\partial_\mu \phi(x)]\epsilon.$$

If one goes from a global SUSY transformation ϵ to a local transformation $\epsilon(x)$, new terms have to be added to the Lagrangian in order to keep it invariant under this new transformation. This is similar to replacing the derivative by the covariant derivative in QED.

The invariance under a local SUSY transformation can be obtained by introducing a new supergravity multiplet consisting of two fields with spin 2 and spin 3/2 respectively. The spin 2 field, $g_{\mu\nu}(x)$, describes a graviton, the boson of the gravitational interaction. The spin 3/2 fermion partner of the graviton is called gravitino $\psi^\mu_\alpha(x)$.

After introducing terms that couple the supergravity multiplet to matter, one finds that at low energies supergravity has a behaviour very similar to the MSSM. However in SUGRA the superpotential contains several terms in addition to the ones known from the MSSM. These terms can be arranged in a way such that they break SUSY.

SUGRA is only valid for energies below the Planck scale ($M_{\rm Pl}$). Above this scale one expects quantum gravity effects to become important. For energies below $M_{\rm Pl}$ but above the unification scale (M_G) SUSY remains unbroken with a yet unknown symmetry group G. Below an energy of M_G SUSY and G both are broken. With several assumptions (see e.g. [11]) one can prove that there exists a class of models with an effective superpotential containing only quadratic and cubic terms and an effective potential of

$$V = \left\{ \sum_a \left| \frac{\partial W}{\partial \phi_a} \right|^2 + V_D \right\} + \left\{ M_0^2 \phi_a \phi_a^\dagger + \left(A_0 W^{(3)} + B_0 W^{(2)} + h.c. \right) \right\},$$

and an universal gaugino mass term

$$\mathcal{L}^\lambda_{\rm mass} = -M_{1/2} \overline{\lambda}^\alpha \lambda^\alpha.$$

Here $W^{(3)}$, ($W^{(2)}$) are the cubic (quartic) terms of the superpotential and M_0 is the universal fermion mass at the GUT scale. If the model preserves R-parity, then W has the form

$$W = \mu_0 H_1 H_2 + \left[\lambda^{(u)}_{ij} Q_i H_2 \bar{u}_j + \lambda^{(d)}_{ij} Q_i H_1 \bar{d}_j + \lambda^{(e)}_{ij} L_i H_1 \bar{e}_j \right], \tag{4}$$

where $\lambda^{(u\,de)}_{ij}$ are the Yukawa coupling constants. $H_{1/2}$ are the two higgs superfields, and $\bar{u}$, $\bar{d}$, $\bar{e}$, Q and L are the superfields as defined in Table 3.1. The indices i and j count the Fermion generations. The extensions to the superpotential responsible for R-parity violation will be given later.

In this framework one needs only five parameters, from which all properties of the superpartners are calculated. A choice of parameters is[7]:

- M_0, the universal fermion mass at the GUT scale,
- $M_{1/2}$, the universal boson mass at the GUT scale,
- A_0, the scaling factor for the cubic parts of the superpotential
- $\tan(\beta) = v_2/v_1$, the ratio of the vacuum expectation values of the two Higgs doublets.
- SGN(μ), the sign of the Higgs mass parameter.

At this point one sees the advantage mSUGRA has over the MSSM. The large number of free parameters originating form SUSY breaking has been replaced by only four plus a sign. A similar behaviour is expected from a fundamental theory. Still there is reason to assume that even supergravity is not the final theory of everything (TOE), but that it is a low energy form of another theory. In SUGRA the masses and couplings of all SM particles are still free parameters, which have to be determined by experiment. The TOE should make predictions for all masses and couplings from only a handful of parameters. In addition this theory must be able to describe quantum gravity effects, which are neglected in SUGRA. A candidate for such a theory is superstring theory, which can yield SUSY-like low energy theories. At the present there are no predictions available from superstring theories, thus in this thesis mSUGRA will be used as the theoretical framework.

3.4 Renormalisation

The input parameters determining the masses and couplings of all particles in mSUGRA are usually given at the GUT scale. In order to find the corresponding masses at the lower energies accessible by experiment the renormalisation group equations (RGEs) have to be applied to the couplings and masses in the Lagrangian.

At the GUT scale the input parameters correspond to certain values of the masses and the couplings of the physical particles. The values of these masses and couplings vary with the energy scale at which they are studied. The dependence on the energy scale is described by the RGEs. In this section the RGEs for the evolution of the masses of the superpartners and of all couplings from the GUT scale down to the energies accessible by collider experiments are given.

For mSUGRA there are a total of 26 RGEs to be solved. The equations for the gauge and Yukawa-couplings have the same form as the corresponding equations in

[7] It is possible to use the parameters B_0 and μ_0 instead of $\tan(\beta)$ and SGN(μ). However I use the parameters given here, as they reduce the number of parameters to 4 plus a sign. The same parametrisation is also used in the MC generator I used.

the SM. They are given here in one loop order for the Yukawa couplings and two loop order for the gauge couplings. The equations for the gauge and Yukawa couplings are identical for the SM and the MSSM. The only difference is in the coefficients b_i and b_{ij}, as their values depend on the number of particles. For values of the running mass Q larger than $M_{\rm SUSY}$ the equations for the gauge and Yukawa couplings are [13]

$$\frac{g_i}{dt} = \frac{g_i}{16\pi^2}\left[b_i g_i^2 + \frac{g_i^2}{16\pi^2}\left(\sum_{j=1}^{3} b_{ij}\tilde{g}_j^2 - \sum_{j=\tau,b,t} a_{ij}\lambda_j^2\right)\right]; \qquad i = 1,2,3, \tag{5}$$

$$\frac{\lambda_\tau}{dt} = \frac{\lambda_\tau}{16\pi^2}\left(-\sum_i c_i^\tau g_i^2 + 3\lambda_b^2 + 4\lambda_\tau^2\right), \tag{6}$$

$$\frac{\lambda_b}{dt} = \frac{\lambda_b}{16\pi^2}\left(-\sum_i c_i^b g_i^2 + \lambda_t^2 + 6\lambda_b^2 + \lambda_\tau^2\right), \tag{7}$$

$$\frac{\lambda_t}{dt} = \frac{\lambda_t}{16\pi^2}\left(-\sum_i c_i^t g_i^2 + 6\lambda_t^2 + \lambda_b^2\right). \tag{8}$$

The variable t is defined as $t = \ln(Q/M_G)$, where M_G is the GUT unification scale. I give the equations for the couplings themselves, as these are the equations that are actually solved by the Monte Carlo generator (ISAJET version 7.20 see [14]). There are equivalent equations for the squares of the couplings, which are also often found in literature.

The coefficients used for b_i and $c_i^{\tau,b,t}$ are given in appendix A. The coefficients a_{ij} and b_{ij} are

$$a_{ij} = \begin{pmatrix} a_{11} & a_{12} & a_{13} \\ a_{21} & a_{22} & a_{23} \\ a_{31} & a_{32} & a_{33} \end{pmatrix} = \begin{pmatrix} 5.2 & 2.8 & 3.6 \\ 6.0 & 6.0 & 2.0 \\ 4.0 & 4.0 & 0.0 \end{pmatrix},$$

$$b_{ij} = \begin{pmatrix} b_{11} & b_{12} & b_{13} \\ b_{21} & b_{22} & b_{23} \\ b_{31} & b_{32} & b_{33} \end{pmatrix} = \begin{pmatrix} 7.96 & 5.40 & 17.60 \\ 1.80 & 25.00 & 24.00 \\ 2.20 & 9.00 & 14.00 \end{pmatrix}.$$

For values of Q less than $M_{\rm SUSY}$ the form of the equations for the gauge couplings (5) stays unchanged, but the coefficients are changed to

$$a_{ij} = \begin{pmatrix} 1.7 & 0.5 & 1.5 \\ 1.5 & 1.5 & 0.5 \\ 2.0 & 2.0 & 0.0 \end{pmatrix}$$

$$b_{ij} = \begin{pmatrix} 3.980 & 2.700 & 8.800 \\ 0.900 & 5.833 & 12.000 \\ 1.100 & 4.500 & -26.000 \end{pmatrix}.$$

In the equations for the Yukawa couplings (6)-(8) in addition to the change in the coefficients additional terms appear for $Q < M_{\rm SUSY}$. Also the Yukawa couplings have

to be matched to the SM couplings.

$$\begin{aligned} g_i(M^-_{\rm SUSY}) &= g_i(M^+_{\rm SUSY}), \\ \lambda_\tau(M^-_{\rm SUSY}) &= \lambda_\tau(M^+_{\rm SUSY})\cos\beta, \\ \lambda_b(M^-_{\rm SUSY}) &= \lambda_b(M^+_{\rm SUSY})\cos\beta, \\ \lambda_t(M^-_{\rm SUSY}) &= \lambda_t(M^+_{\rm SUSY})\sin\beta. \end{aligned}$$

With these changes the RGEs for the Yukawa couplings become

$$\frac{\lambda_\tau}{dt} = \frac{\lambda_\tau}{16\pi^2}\left(-\sum_i c_i^\tau g_i^2 + \frac{5}{2}\lambda_\tau^2\cos^2\beta + 3\lambda_t^2\sin^2\beta + 3\lambda_b^2\cos^2\beta - Y_2(S)\sin^2\beta\right), \quad (9)$$

$$\frac{\lambda_b}{dt} = \frac{\lambda_b}{16\pi^2}\left(-\sum_i c_i^b g_i^2 + \frac{9}{2}\lambda_b^2\cos^2\beta + \frac{3}{2}\lambda_t^2\sin^2\beta + \lambda_\tau^2\cos^2\beta - Y_2(S)\sin^2\beta\right), \quad (10)$$

$$\frac{\lambda_t}{dt} = \frac{\lambda_t}{16\pi^2}\left(-\sum_i c_i^t g_i^2 + \frac{9}{2}\lambda_t^2\sin^2\beta - \frac{3}{2}\lambda_b^2\cos^2\beta + \lambda_\tau^2\cos^2\beta + Y_2(S)\cos^2\beta\right). \quad (11)$$

With the coefficient $Y_2(S)$ given by

$$Y_2(S) = 3\lambda_t^2 - 3\lambda_b^2 - \lambda_\tau^2.$$

The changed values for the coefficients c_i are given in appendix A.

In addition to the six equations (5)-(8) in mSUGRA there are 20 new equations describing the behaviour of the parameters introduced by SUSY breaking. These equations do not exist for the SM. Neglecting the Yukawa couplings the RGEs describing the behaviour of the masses of the superpartners of the first two generations are [15]

$$\frac{d\tilde{m}^2_{L_i}}{dt} = \frac{1}{8\pi^2}\left(-3g_2^2M_2^2 - \frac{3}{5}g_1^2M_1^2\right), \quad (12)$$

$$\frac{d\tilde{m}^2_{E_i}}{dt} = \frac{1}{8\pi^2}\left(-\frac{12}{5}g_1^2M_1^2\right), \quad (13)$$

$$\frac{d\tilde{m}^2_{Q_i}}{dt} = \frac{1}{8\pi^2}\left(-\frac{16}{3}g_3^2M_3^2 - 3g_2^2M_2^2 - \frac{1}{15}g_1^2M_1^2\right), \quad (14)$$

$$\frac{d\tilde{m}^2_{U_i}}{dt} = \frac{1}{8\pi^2}\left(-\frac{16}{3}g_3^2M_3^2 - \frac{16}{15}g_1^2M_1^2\right), \quad (15)$$

$$\frac{d\tilde{m}^2_{D_i}}{dt} = \frac{1}{8\pi^2}\left(-\frac{16}{3}g_3^2M_3^2 - \frac{4}{15}g_1^2M_1^2\right). \quad (16)$$

M_i with $i = 1, 2, 3$ are the gauge boson mass parameters, $\tilde{m}_{L_i}$, $\tilde{m}_{E_i}$, $\tilde{m}_{Q_i}$, $\tilde{m}_{U_i}$ and $\tilde{m}_{D_i}$ are the masses of the left–handed sleptons, right–handed sleptons, left handed squarks and right handed up-type and down-type squarks. For the squarks and sleptons the parameter i denotes the generation and runs from 1 to 2. For the third generation the

Yukawa couplings must be included in the RGEs

$$\frac{d\tilde{m}_{L_3}^2}{dt} = \frac{1}{8\pi^2}\left(-3g_2^2M_2^2 - \frac{3}{5}g_1^2M_1^2 + X_\tau\right), \tag{17}$$

$$\frac{d\tilde{m}_{\tau}^2}{dt} = \frac{1}{8\pi^2}\left(-\frac{12}{5}g_1^2M_1^2 + 2X_\tau\right), \tag{18}$$

$$\frac{d\tilde{m}_{Q_3}^2}{dt} = \frac{1}{8\pi^2}\left(-\frac{16}{3}g_3^2M_3^2 - 3g_2^2M_2^2 - \frac{1}{15}g_1^2M_1^2 + X_b + X_t\right), \tag{19}$$

$$\frac{d\tilde{m}_{t}^2}{dt} = \frac{1}{8\pi^2}\left(-\frac{16}{3}g_3^2M_3^2 - \frac{16}{15}g_1^2M_1^2 + 2X_t\right), \tag{20}$$

$$\frac{d\tilde{m}_{b}^2}{dt} = \frac{1}{8\pi^2}\left(-\frac{16}{3}g_3^2M_3^2 - \frac{4}{15}g_1^2M_1^2 + 2X_b\right). \tag{21}$$

The parameters $X_{\tau,b,t}$ are defined as:

$$\begin{aligned} X_\tau &= \lambda_\tau^2\left(\tilde{m}_{L_3}^2 + \tilde{m}_\tau^2 + m_{H_1}^2 + A_\tau^2M_0^2\right), \\ X_b &= \lambda_b^2\left(\tilde{m}_{Q_3}^2 + \tilde{m}_b^2 + m_{H_1}^2 + A_b^2M_0^2\right), \\ X_t &= \lambda_t^2\left(\tilde{m}_{Q_3}^2 + \tilde{m}_t^2 + m_{H_2}^2 + A_t^2M_0^2\right). \end{aligned}$$

The RGEs for the gaugino masses are:

$$\frac{dM_i}{dt} = b_ig_i^2M_i, \tag{22}$$

with the parameters b_i from appendix A. The calculations start at $M_{\rm GUT}$, where the mass parameters are related by

$$\tilde{m}_{L_i}^2(0) = \tilde{m}_{E_i}^2(0) = \tilde{m}_{Q_i}^2(0) = \tilde{m}_{U_i}^2(0) = \tilde{m}_{D_i}^2(0) \equiv M_0^2,$$

$$M_1(0) = M_2(0) = M_3(0) \equiv M_{1/2}.$$

The equations for the bilinear and trilinear couplings are

$$\frac{dA_t}{dt} = -\frac{1}{8\pi^2}\left(\frac{16}{3}g_3^2\frac{M_3}{M_0} + 3g_2^2\frac{M_2}{M_0} + \frac{13}{15}g_1^2\frac{M_1}{M_0} - 6\lambda_t^2A_t - \lambda_b^2A_b\right), \tag{23}$$

$$\frac{dA_b}{dt} = -\frac{1}{8\pi^2}\left(\frac{16}{3}g_3^2\frac{M_3}{M_0} + 3g_2^2\frac{M_2}{M_0} + \frac{7}{15}g_1^2\frac{M_1}{M_0} - 6\lambda_b^2A_b - \lambda_t^2A_t - \lambda_\tau^2A_\tau\right), \tag{24}$$

$$\frac{dA_\tau}{dt} = -\frac{1}{8\pi^2}\left(3g_2^2\frac{M_2}{M_0} + \frac{9}{5}g_1^2\frac{M_1}{M_0} - 3\lambda_b^2A_b - 4\lambda_\tau^2A_\tau\right), \tag{25}$$

$$\frac{dB}{dt} = \frac{1}{8\pi^2}\left(\frac{3}{5}g_1^2M_1 + 3g_2^2M_2 + 3\lambda_t^2A_t + 3\lambda_b^2A_b + \lambda_\tau^2A_\tau\right). \tag{26}$$

The terms determining the mass parameters of the Higgs sector are calculated using the RGEs

$$\frac{d\mu}{dt} = \frac{\mu}{16\pi^2}\left(-3g_2^2 - \frac{3}{5}g_1^2 + 3\lambda_t^2 + 3\lambda_b^2 + \lambda_\tau^2\right), \tag{27}$$

$$\frac{dm_{H_1}^2}{dt} = \frac{1}{8\pi^2}\left(-3g_2^2 M_2^2 - \frac{3}{5}g_1^2 M_1 + 3X_b + \lambda_\tau^2\right), \tag{28}$$

$$\frac{dm_{H_2}^2}{dt} = \frac{1}{8\pi^2}\left(-3g_2^2 M_2^2 - \frac{3}{5}g_1^2 M_1 + 3X_t\right). \tag{29}$$

$$\tag{30}$$

Here the initial values are

$$\mu(0) \equiv \mu_0 \qquad \text{and} \qquad m_{H_2}(0) = m_{H_1}(0) \equiv M_0.$$

Using the RGEs given here one can derive the weak eigenstates and couplings of all particles existing in mSUGRA numerically. In order to solve these equations one starts at the unification scale by inserting all values in the equations. From this one obtains the derivative of the masses and couplings with respect to t at that point. With the derivative one calculates the values at a slightly smaller scale, at which one again calculates the derivatives. Repeating this process one finally arrives at the values at the scale one is interested in.

Due to the form of the Lagrangian many of the eigenstates mix and the observed mass eigenstates are the result of the mixing. In the following section it will be shown which weak eigenstates mix and how the mass eigenstates can be calculated from the Lagrangian.

3.5 SUSY Particles and their Masses

The particle spectrum of mSUGRA is fixed by five parameters, which determine all masses at the GUT scale. The masses then are evolved from the GUT scale down to the weak scale using the RGEs. These masses are interaction eigenstates. In this section it will be shown how to calculate the mass eigenstates of the SUSY particles.An important issue here is the mixing of weak eigenstates. The mixing creates the mass eigenstates which are the physical particles one can detect.

3.5.1 The Masses of the Charginos

The Lagrange mass-term describing the electrically charged bosinos, which are called charginos is [17]:

$$\mathcal{L}_M^{Ch} = (ig_1/\sqrt{2})\left[v_1 \mathrm{W}^+ \psi_{\mathrm{H}_1}^2 + v_2 \mathrm{W}^- \psi_{\mathrm{H}_2}^1\right] + M_2 \mathrm{W}^+ \mathrm{W}^- - \mu \psi_{\mathrm{H}_1}^2 \psi_{\mathrm{H}_2}^1 + h.c\ , \tag{31}$$

$\mathrm{W}^{\pm}$, $\psi^2_{\mathrm{H}_1}$ and $\psi^1_{\mathrm{H}_2}$ are the Wino and Higgsino superfields. The expression is obviously not diagonal in $\mathrm{W}^{\pm}$, $\psi^2_{\mathrm{H}_1}$ and $\psi^1_{\mathrm{H}_2}$.

Using the definition

$$\psi^+ = (-i\mathrm{W}^+, \psi^1_{\mathrm{H}_2}), \qquad \psi^- = (-i\mathrm{W}^-, \psi^2_{\mathrm{H}_1})$$

one can write equation (31) in the form

$$\mathcal{L}^{Ch}_M = -\frac{1}{2}(\psi^+\psi^-) \begin{pmatrix} 0 & X^T \\ X & 0 \end{pmatrix} \begin{pmatrix} \psi^+ \\ \psi^- \end{pmatrix} + h.c \tag{32}$$

With

$$X = \begin{pmatrix} M_2 & m_{\mathrm{W}}\sqrt{2}\sin\beta \\ m_{\mathrm{W}}\sqrt{2}\cos\beta & \mu \end{pmatrix}. \tag{33}$$

$m_{\mathrm{W}} \equiv 1/4\ g^2(v_1^2 + v_2^2)$ is the mass of the W-boson.

Due to its special form one can diagonalise the mass matrix X by transforming ψ^+ and ψ^- separately. One obtains the mass eigenvectors and eigenstates using

$$\chi^+ = V\psi^+, \qquad \chi^- = V\psi^-, \qquad \text{and} \qquad M_D = U^* X V^{-1},$$

U and V are (2×2) matrices and M_D is the diagonalised form of the matrix X, with the two components M_- and M_+. Now one can rewrite equation (31) as

$$\mathcal{L}^{Ch}_M = -\left(\chi^- M_D \chi^+ + h.c\right). \tag{34}$$

In Dirac–representation this is

$$\mathcal{L}^{Ch}_M = -\left(M_+ \overline{\tilde{\chi}}_1 \tilde{\chi}_1 + M_- \overline{\tilde{\chi}}_2 \tilde{\chi}_2\right), \tag{35}$$

where the Dirac–spinors are defined as

$$\tilde{\chi}_1 = \begin{pmatrix} \chi_1^+ \\ \chi_1^- \end{pmatrix}, \qquad \tilde{\chi}_2 = \begin{pmatrix} \chi_2^+ \\ \chi_2^- \end{pmatrix}. \tag{36}$$

$\chi_i^{\pm}$ with $i = 1, 2$ are the components of the Weyl–spinors $\chi^{\pm}$. From equation (35) one sees that after diagonalising the mass matrix one has two charginos with different masses. One obtains the general formula for the chargino masses

$$\begin{aligned} M^2_{\chi^{\pm}} = \ & \frac{1}{2}\Big[M_2^2 + \mu^2 + 2m_{\mathrm{W}}^2 \\ & \pm\sqrt{\left(M_2^2 - \mu^2\right)^2 + 4m_{\mathrm{W}}^4\cos^2 2\beta + 4m_{\mathrm{W}}^2\left(M_2^2 + \mu^2 + 2M_2\mu\sin 2\beta\right)}\ \Big]. \end{aligned} \tag{37}$$

It is not possible to give the Higgsino and wino content of a chargino, as the contents are generally different for right-handed and left-handed particles.

3.5.2 The Masses of the Neutralinos

The neutralinos are the superpartners of the neutral Higgs bosons, the photon and the Z^0. The relevant mass term in the Lagrangian is

$$\begin{aligned} \mathcal{L}_M^{Ne} &= \tfrac{1}{2} i g_1 \mathrm{W}^0 \left(v_1 \psi^1_{\mathrm{H}_1} - v_2 \psi^2_{\mathrm{H}_2} \right) - \tfrac{1}{2} i g_2 \mathrm{B} \left(v_1 \psi^1_{\mathrm{H}_1} - v_2 \psi^2_{\mathrm{H}_2} \right) \\ &+ \tfrac{1}{2} M_2 \mathrm{W}^0 \mathrm{W}^0 + \tfrac{1}{2} M_1 \mathrm{BB} + \mu \psi^1_{\mathrm{H}_1} \psi^2_{\mathrm{H}_2} + h.c \end{aligned} \tag{38}$$

Here B, W, $\psi^1_{H_1}$, $\psi^2_{H_2}$ are the superfields of the neutral gauginos and Higgsinos. g_2 is the second weak coupling constant and M_1 the mass parameter for the B-bosons. As I am working in the framework of a GUT M_1 is given by

$$M_1 = \frac{5}{3} \tan\theta_W M_2.$$

After introducing the Z^0-mass $m_{\mathrm{Z}} = \frac{1}{2}\sqrt{(v_1^2 + v_2^2)(g_1^2 + g_2^2)}$ and

$$\psi^0 = \left(-i\mathrm{B}, -i\mathrm{W}^0, \psi^1_{\mathrm{H}_1}, \psi^2_{\mathrm{H}_2} \right)$$

one can rewrite equation (38) using the neutralino mass matrix Y

$$Y = \begin{pmatrix} M_1 & 0 & -m_{\mathrm{Z}} \cos\beta \sin\theta_W & m_{\mathrm{Z}} \sin\beta \sin\theta_W \\ 0 & M_2 & m_{\mathrm{Z}} \cos\beta \cos\theta_W & -m_{\mathrm{Z}} \sin\beta \cos\theta_W \\ -m_{\mathrm{Z}} \cos\beta \sin\theta_W & m_{\mathrm{Z}} \cos\beta \cos\theta_W & 0 & -\mu \\ m_{\mathrm{Z}} \sin\beta \sin\theta_W & -m_{\mathrm{Z}} \sin\beta \cos\theta_W & -\mu & 0 \end{pmatrix} \tag{39}$$

in the form

$$\mathcal{L}_M^{Ne} = -\frac{1}{2} (\psi^0)^T Y \psi^0 + h.c \tag{40}$$

Y can be diagonalised using a unitary matrix N with the eigenvectors

$$\chi^0 = N \phi^1_{H_1} \qquad \text{and} \qquad M_N = N^* Y N^{-1}.$$

Using again Dirac-spinors

$$\tilde{\chi}^0_i = \begin{pmatrix} \chi^0_i \\ \overline{\chi}^0_i \end{pmatrix}$$

one finds the neutralino mass term

$$\mathcal{L}_M^{\mathrm{Ne}} = -\frac{1}{2} \left(M_1 \overline{\tilde{\chi}}^0_1 \tilde{\chi}^0_1 + M_2 \overline{\tilde{\chi}}^0_2 \tilde{\chi}^0_2 + M_3 \overline{\tilde{\chi}}^0_3 \tilde{\chi}^0_3 + M_4 \overline{\tilde{\chi}}^0_4 \tilde{\chi}^0_4 \right).$$

Thus the four neutralinos are majorana fermions. Unlike the case of the charginos, the composition of the neutralinos from their components can be calculated from the matrix N.

There exists a closed form solution for the eigenvalues of the neutralino mass matrix, but it is rather complicated. Thus in most cases it is more convenient to insert the values for the actual point in parameter space into the matrix and diagonalise it numerically. The masses are then taken from the diagonalised mass matrix. The composition of the neutralinos can be extracted from the matrix N.

3.5.3 The Sfermion Masses

In this subsection the mass spectrum of the scalar fermions (i.e. the squarks and sleptons) will be discussed. The sfermions aquire their masses directly through the Yukawa coupling to the Higgs fields. After applying the RGEs one finds

$$\begin{aligned}
\tilde{m}^2_{E_L} &= M_0^2 & & & & & K_2 &+ \tfrac{1}{4}K_1 &+ \Delta_e,\\
\tilde{m}^2_{\nu_L} &= M_0^2 & & & & & K_2 &+ \tfrac{1}{4}K_1 &+ \Delta_\nu,\\
\tilde{m}^2_{E_R} &= M_0^2 & & & & & & &+ \Delta_{\bar{e}},\\
\tilde{m}^2_{U_L} &= M_0^2 &+ K_3 &+ K_2 &+ \tfrac{1}{36}K_1 &+ \Delta_u,\\
\tilde{m}^2_{D_L} &= M_0^2 &+ K_3 &+ K_2 &+ \tfrac{1}{36}K_1 &+ \Delta_d,\\
\tilde{m}^2_{U_R} &= M_0^2 &+ K_3 & &+ \tfrac{4}{9}K_1 &+ \Delta_{\bar{u}},\\
\tilde{m}^2_{D_R} &= M_0^2 &+ K_3 &+ &+ \tfrac{1}{9}K_1 &+ \Delta_{\bar{d}},
\end{aligned}$$

The coefficients K_i with $i = 1, 2, 3$ are obtained from the RGEs. They result from the couplings of the sparticles and are proportional to the strength of the coupling constants g_i. Thus $K_3 \gg K_2 \gg K_1 > 0$ is generally valid, which leads to a mass ordering such that the squarks are heavier than the sleptons. The numerical constants before K_1 are due to the different electro-magnetical charges of the particles.

The Δ-terms are special for each sparticle type because they depend on the individual charges

$$\Delta_\phi = (T_3^\phi - Q^\phi_{\mathrm{EM}} \sin^2\theta_W) \cos 2\beta M_Z^2.$$

Although they are relatively small these terms are still important as they are e.g. responsible for the mass splitting of the selectron and the sneutrino. The Monte Carlo generater used in this analysis (ISAJET version 7.20) neglects the mass-splitting for the squarks completely while generating events. The squark masses are calculated correctly using the RGEs. For generating events a mean squark mass

$$\tilde{m}_q = \frac{1}{4}(\tilde{m}_{u_L} + \tilde{m}_{d_L} + \tilde{m}_{u_R} + \tilde{m}_{d_R})$$

is calculated. This average then is used for the production of first or second generation squarks.

Because left-handed and right-handed sfermions of one generation have the same quantum numbers they can mix. If mixing takes place the mass eigenstates are two sfermions with different masses but they are no longer the superpartners of the left– or right-handed leptons. The strength of sfermion mixing is proportional to the masses of the SM-fermions belonging to the same generation. Generally the mixing is very weak for the sleptons and first two generations of squarks. Still mixing can be strong for the third generation squarks.

Since this analysis does not cover the production of third generation squarks sfermion mixing is neglected.

3.5.4 The Mass of the Gluino

The gluino is the only colour octet fermion in mSUGRA and thus can not mix with any other particle. Its mass can be taken directly from the Lagrangian after applying the RGEs. Neglecting two-loop corrections in supergravity the gluino mass can be calculated from the bino and wino masses and the gauge coupling constants

$$M_3 = \frac{\alpha_s}{\alpha} \sin^2 \theta_W M_2 = \frac{3}{5} \frac{\alpha_s}{\alpha} \cos^2 \theta_W M_1.$$

It is probable that the gluino is heavier than the other gauginos because α_s is much larger than the other two couplings.

3.6 Introduction to R-parity Violation

The multipicative quantum number R_P was defined in section 3.2. As stated there one usually assumes that R_P is conserved. The reason for this is that R_P violating couplings violate lepton number (L) or baryon number (B). No processes with violation of these quantum numbers have been observed so far. Still, in contrary to quantum numbers like energy, momentum or charge, whose conservation is a consequence of a underlying symmetry, the non–existence of couplings violating L and B is based on observations only. Thus R_P violating couplings are allowed as long as they do not cause any effects which are excluded by measurements. Another argument against R_P violating couplings is the existence of dark matter, which could be explained by residual LSPs. There is no evidence, however that dark matter consists of LSPs, so this cannot rule out the $\not{R}_P$-MSSM. Both types of models can be constructed and are similar in many ways.

The model used in this thesis is based on mSUGRA. To distinguish between the cases with and without R_P-violation the model used will be called $\not{R}_P$-mSUGRA throughout this thesis, in comparison to the R_P-conserving case, which will be called mSUGRA For references to SUSY models without the requirement of SUGRA an analogous notation will be used.

If one allows R-parity violation [18], four additional terms in the superpotential are allowed [19] in addition to the terms given in eqn. (4)

$$W_R = \lambda_{ijk} L_i L_j \bar{e}_k + \lambda'_{ijk} L_i Q_j \bar{d}_k + \lambda''_{ijk} \bar{u}_i \bar{d}_j \bar{d}_k + \kappa_i H_2 L_i, \tag{41}$$

here λ, λ' and λ'' are coupling constants, i, j and k are generation indices. Summation over the generation indices is implied, color and weak isospin indices have been suppressed. The κ_i are mass factors.

All four terms in eqn. (41) describe couplings which violate R-parity. The last term couples the Higgs sector with the leptonic sector. Through a redefinition of H_1 and L_i this term can be rotated away [20]. In the following the κ_i-terms are not considered. The other three terms all couple two fermions with a sfermion.

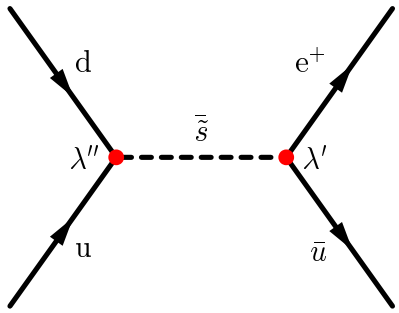

Abbildung 3.1: *Proton decay via λ' and λ'' coupling. The R_P-violating ($\not{R}_P$) vertices are marked with dots. The third quark in the proton is not shown.*

The λ'' term describes the coupling of three quark-superfields, thus violating baryon-number. This coupling could alter the decay of the top quark or lead to the production of single stops if the third generation is involved. If only the first and second generation are involved the effects will be very hard to detect at hadron-colliders because they are hidden in the large QCD-background.

The second term couples one lepton-superfield with two quark-superfields, violating lepton number. This coupling was proposed as a cause of the high-p_{T} HERA events [21] and was first investigated by CDF in [22]. At the moment there are ongoing CDF analyses regarding other aspects of a coupling λ'.

In this thesis the first term will be investigated. The term couples a slepton and two leptons, violating lepton number. Because of charge conservation two of the three particles have to be oppositely charged, while the third one has to be neutral. The λ-matrix is antisymmetric in the first two indices. This means that the diagonal elements are all zero and there are only 9 independent terms.

For simplicity one usually assumes that only one element of λ, λ' or λ'' is different from zero. This is an assumption based on the different coupling strengths of the SM interaction. It is probable that also in $\not{R}_P$ one coupling dominates the others. Once R-parity violating SUSY is discovered by observing effects of the dominating coupling one will measure the values of the smaller coupling as well.

3.7 Motivation for R-parity violating SUSY

The existance of R–parity violating couplings is intrinsic to SUSY, but their study been neglected for a long time. The main reason for this is that R-parity violating couplings can lead to fast proton decay. If λ' and λ'' both are non-zero, the proton can decay via the process shown in Fig. 3.1. This decay will be faster than the current experimental limit of 10^{32} years. Still, if only one of λ' and λ'' is non-zero, proton decay imposes no significant limit on its value. λ couples only lepton superfields and hence will not lead to proton decay at all.

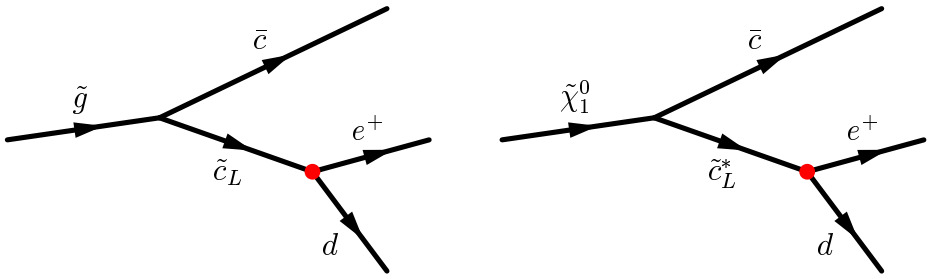

Abbildung 3.2: *The two scenarios investigated in the CDF like-sign dilepton channel. The dot indicates the $\not{R}_P$ vertex.*

In this chapter and in chapter 2 it has been explained that the SM Lagrangian and the superpotential of SUSY can be deducted from requiering the invariance under certain symmetries. To be consistent one can not just drop the terms in the superpotential responsible for R-parity violation because they would lead to proton decays. The reason for the non–existance of these couplings must be an additional symmetry, which was not considered so far. One such symmetry is R-parity. Still requiring R-parity conservation is an arbitrary choice, because there are other quantum numbers whose conservation will protect the proton in a similar way. These other symmetries generally allow one or two of the R-partiy violating couplings, while inhibiting the other couplings and thus forbiding rapid proton decay.

The interest for $\not{R}_P$ SUSY increased after the H1 and Zeus collaborations reported an excess of events with high Q^2 in e^+p collisions [21]. While seeing general agreement with the SM at low Q^2 both collaborations found an excess in the area of high momentum transfer. The excesses reported by the two collaborations can be explained by the exchange of a particle with a mass of roughly 200 GeV/c^2. This particle must couple to both the positron and one of the quarks of the proton. Candidates for such particles are leptoquarks, leptogluons or squarks in $\not{R}_P$–SUSY. Further studies of the HERA events with an increased luminosity could not confirm the excess of events.

If the exchanged particles are squarks, R-parity must be violated by a non-zero coupling λ'_{121}. The CDF-collaboration studied the effects of such a coupling investigating two scenarios. In the first one gluinos with a mass above 200 GeV are pair-produced. The gluinos decay through charm squarks with a mass of 200 GeV, which in turn decay into an electron and a down quark violating R-parity and lepton number. In the second scenario either two squarks or two top squarks are pair–produced and decay to the lightest neutralino (the LSP) through cascade decays. The LSP then decays into an electron and a down squark via a virtual charm squark. The decay of the virtual charm squark violates R-parity and lepton number. Feynman diagrams describing both channels are shown in figure 3.2. The final state of both scenarios will contain two like–sign electrons or two opposite–sign electrons with equal probaility. The analysis focusses on like–sign leptons because in this case the SM background is much smaller than in the

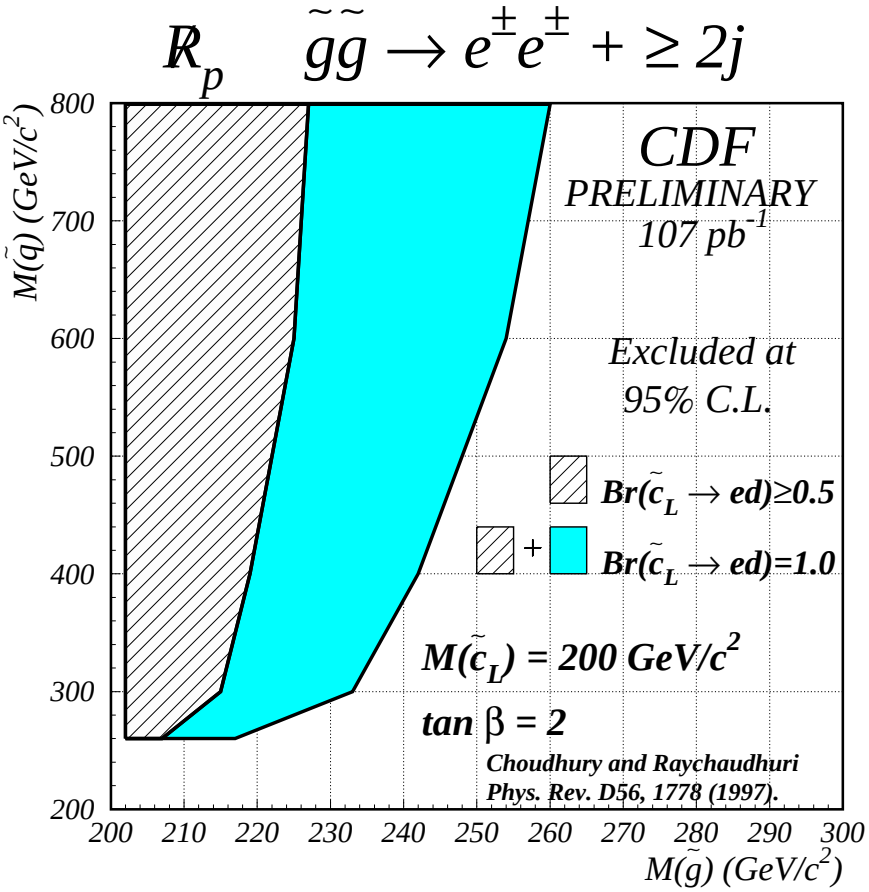

Abbildung 3.3: *The region excluded by CDF for gluinos decaying to like–sign dilepton channel through R-parity violating couplings.*

opposite–sign case. No evidence for non-SM contributions was found and thus limits on the masses of the primary produced particles were set. The limit set for the gluino decay channel is a function of the gluino and the squark mass and is given in figure 3.3. The neutralino decay analysis excludes top squarks lighter than 135 GeV/c^2 and degenerate squark up to 260 GeV/c^2. For further details on the anlysis and on the excluded region see [22].

The events observed at HERA and the following discussions have made it clear that an interesting area of physics had been neglected by both experimentalists and theorists. Investigating $R\!\!\!/_P$ scenarios is an important task in order to be sure not to miss SUSY looking into the wrong channels. Generally also searches for R_P SUSY can probe $R\!\!\!/_P$–SUSY models. Still, missing transverse momentum, the main SUSY signature used in previous searches is non-existing in the case of $R\!\!\!/_P$ SUSY. Thus it is not possible to simply apply the results from R_P–conserving SUSY searches to the case of $R\!\!\!/_P$. This

means that new searches optimised for $\not{R}_P$–SUSY will be able to probe a much larger parameter space than is accessible by the extrapolation of R_P–SUSY result to the R_P violating case. In order to examine as much of the SUSY parameter space as possible it is crucial to perform searches specially adapted to find $\not{R}_P$–SUSY.

3.8 The Decay of LSPs

In this analysis it is assumed that only one of the λ-couplings is non-zero. The diagonal elements have to be zero because of the anti-symmetry of λ. Therefore the element we choose has to be non-diagonal. We select λ_{121}, on which the most stringent limits are from charged current universality [23, 24]:

$$\lambda_{121} < 0.05 \, \frac{m_{\tilde{e}_{Rk}}}{100\mathrm{GeV}}.$$

The limit is given at the 1 σ level.

There are no quarks involved in this coupling. Thus the production processes at hadron colliders will not be changed compared to the MSSM. Still a non-zero value of λ_{121} would have several consequences in the SUSY–decays.

The Yukawa interactions for this case are given by the Lagrangian [24]:

$$\mathcal{L} = \lambda_{ijk} \left[\tilde{\nu}^i_L \bar{e}^k_R e^j_L + \tilde{e}^j_L \bar{e}^k_R \nu^i_L + (\tilde{e}^k_R)^* (\bar{\nu}^i_L)^C e^j_L - (i \leftrightarrow j) \right] + h.c.$$

For λ_{121} this becomes:

$$\mathcal{L} = \lambda_{121} \left[\tilde{\nu}^1_L \bar{e}^1_R e^2_L + \tilde{e}^2_L \bar{e}^1_R \nu^1_L + (\tilde{e}^1_R)^* (\bar{\nu}^1_L)^C e^2_L - \tilde{\nu}^2_L \bar{e}^1_R e^1_L + \tilde{e}^1_L \bar{e}^1_R \nu^2_L + (\tilde{e}^1_R)^* (\bar{\nu}^2_L)^C e^1_L \right] + h.c.$$

This Lagrangian can lead to two classes of processes:

1. Charged sleptons and sneutrinos can decay directly to leptons and neutrinos via the $\not{R}_P$ coupling. e.g., $\tilde{\mu}_L \to e_R \nu_e$.

2. Charginos and neutralinos can decay into a lepton or neutrino and a virtual charged slepton or sneutrino. The later slepton then will then decay into charged and neutral leptons.

If the value of λ_{121} if sufficiently small, both of these processes will be suppressed in comparison to the MSSM decays. Still the second process will be important for the LSP. For this particle there are no MSSM decays and it will decay only if there are R-parity violating processes.

In the following we assume that the LSP is the lightest neutralino and λ_{121} is so small that it's only visible effect is the LSP-decay via a virtual slepton. The channels for LSP-decay in the presence of a coupling λ_{121} are shown in Fig. 3.4.

The top two diagrams produce either $e\bar{e}\bar{\nu}_\mu$ or $\bar{\mu}e\bar{\nu}_e$, depending on the generation of the exchanged particle. Together with the charge conjugated processes they produce the following final states with equal probability.

$$\mu\bar{e}\nu_e, \quad \bar{\mu}e\bar{\nu}_e, \quad e\bar{e}\nu_\mu, \quad e\bar{e}\bar{\nu}_\mu. \tag{42}$$

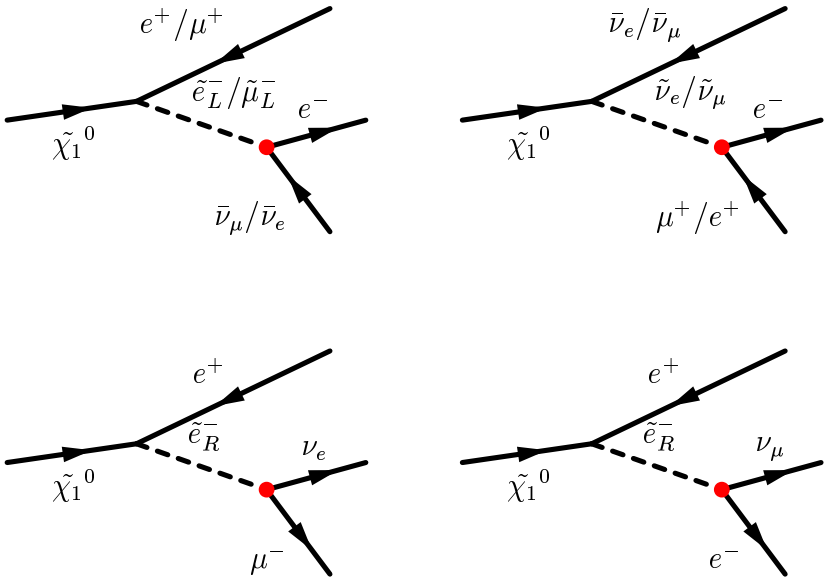

Abbildung 3.4: *The LSP decay channels for a non-zero coupling of λ_{121}. The R_P-violating vertex is marked with dots.*

The bottom left (right) process in Fig. 3.4 produces $\mu\bar{e}\nu_e$ ($e\bar{e}\nu_\mu$)in the final state. Together with the charge conjugate processes they produce the same four final states mentioned above, again with equal probability.

SUSY particles being pair produced, each decaying into an LSP will yield two LSPs per event. The signature will then be four leptons coming from the LSP-decay with possible additional leptons and jets being produced in the cascade decay. Two of the leptons have to be electrons, the others may be electrons or muons. Thus the signature is

$$p\bar{p} \to eeee + X \quad \text{or} \quad p\bar{p} \to eee\mu + X \quad \text{or} \quad p\bar{p} \to ee\mu\mu + X.$$

We will use a Monte Carlo (MC) to simulate the production and the decays to the LSP. The only new process we have to introduce to the MSSM is the decay of the LSP.

Assuming the LSP is a photino it's decay rate for the different channels is given as :

$$\Gamma_{\tilde{\gamma}} = \frac{\alpha\lambda_{ijk}^2}{127\pi^2}\frac{M_{\tilde{\chi}_0^1}^5}{\tilde{m}^4} \tag{43}$$

where α is the electro-magnetic coupling constant and $M_{\tilde{\chi}_0^1}$ and $\tilde{m}$ are the masses of the LSP and the slepton.

From the decay rate one can calculate a lower limit for λ. Below this value the LSP will not decay fast enough to see it with our current approach, because we assume a prompt LSP decay. There are about two orders of magnitude between the current

upper limit on λ and this lower limit. Thus we can see a signal if λ lies in this region or else can significantly constrain the mass of SUSY particles.

4 Supersymmetry at Colliders

At present (1999) research at the energy frontier is done exclusively with beam-beam experiments. In these experiments two particle beams are brought to collision at a fixed interaction point. Located around the interaction point are multi-purpose detectors, with which the products of the reaction are measured. The highest energetic colliders currently are:

- The LEP[8] at CERN[9], an e^+e^- collider currently running at a Center of Mass (CMS) energy of 200 GeV.
- The $e^{\pm}p$ collider HERA[10] at DESY[11]. This machine collides a 820 GeV proton beam and a 27.5 GeV beam of either electrons or positrons.
- The 1.8 TeV $p\bar{p}$ collider TEVATRON at FNAL[12]. The analysis presented in this thesis is based on data taken at the Tevatron, thus I will concentrate on hadron colliders for the remainder of this thesis.

In all three experimental setups beams of light particles are brought to collision. In the following reaction particles with a high invariant mass are produced. These heavy particles subsequently decay into lighter particles which are seen in the detectors. In the case of SUSY with R-parity conservation an even number of sparticles (usually two) are produced in the hard interaction. Each sparticle decays into an odd number (usually one) of LSPs and several SM particles. If R-parity is not conserved the production of single (in general of odd numbers of) sparticles is also allowed. The single sparticle production could lead to the first signals for supersymmetry. In this case only the energy to produce one sparticle must be provided. In contrast the energy equivalent to twice the sparticle mass is needed for pair production. R-parity violation allows also for additional decay channels for sparticles. In particular the LSP will not be stable as it can decay into SM particles.

In this chapter I will first discuss general properties of hadron colliders. Then I will focus on the production and decay of sparticles at these machines. Finally I will introduce the changes caused by allowing R-parity violation.

4.1 Particle Physics at Hadron Colliders

At hadron colliders the beams consist of protons or antiprotons. The antiproton is the anti-particle of the proton and ad high energy collisions has generally the same proper-

[8] Large Electron Positron collider

[9] European Organization for Nuclear Research, Geneva, Switzerland. (in French: Organisation Europeenne pour la Recherche Nucleaire). The acronym, still used, derives from the organisation's original name: Centre Europeen pour la Recherche Nucleair.

[10] Hadron Electron Ring Accelerator facility

[11] Deutsches Elektronen–Synchrotron

[12] Fermi National Accelerator Laboratory (Batavia, IL).

ties as the proton. I will not distinguish between the two particles in the remainder of this section, but will refrain to both as protons except where explicitly stated.

Protons are no fundamental particles, they are composed of three quarks, which are bound by the exchange of gluons. The kinetic energy and the momentum of the proton are divided up between these constituents. In hadron-hadron collisions a proton is probed with another proton. At high energies sometimes not the protons, but their constituents react with each other. The interaction of the proton constituents is called the hard interaction. In most of the cases only one constituent of one proton reacts with one constituent of the other proton. The other constituents (the proton remnant) rearrange and either continue on their path or end up in the detector as background. The interesting hard interaction will have on average only 1/5th of the beam energy if the participating particles are valence quarks, and still less for sea quarks and gluons. The rest of the energy remains with the proton remnant.

In order to understand the hard interaction it is necessary to know which of the constituents of the proton interact and which energy they have. The proton is a dynamical particle. This means that the energy and even the number of the constituents is not fixed, but distributed statistically. The fraction of the proton energy a specific quark constituent has is described by the Parton-Distribution Functions (PDFs).

From the previous paragraph it follows that at a hadron collider one does not know the exact energy of the hard interaction a priori. Only if all particles are recorded in the detector one can reconstruct the total energy from their measurement. However, if one or more of the particles do not react with the detector (like neutrinos or neutralinos), or if particles hit an uninstrumented area, one cannot determine the energy of the hard interaction.

The solution to this problem is using the transverse energy instead of the total energy. The transverse energy of the quarks and gluons in the proton is minimal, compared to the longitudinal energy the proton obtained during the acceleration phase. Thus one can assume $\vec{E}_{\mathrm{T}}(q_1) + \vec{E}_{\mathrm{T}}(q_2) = 0$ for the two interacting constituents. Then the total $\vec{E}_{\mathrm{T}}$ of the reaction products must also be 0. One defines the missing energy as $\not{E}_T = |\sum \vec{E}_{\mathrm{T}}|$,where the sum goes over all energy seen in the detector. Due to mismeasurements in the detector it is possible that one measures a small $\not{E}_T$, even if all particles interact with the detector. Still if there is a large amount of missing E_{T}, one knows that a particle has escaped undetected either because it hit an uninstrumented area of the detector or because one (or more) of the produced particles does not interact with the detector material.

In events recorded at hadron colliders the hard interactions have on average significantly less than the beam energy. The environment imposes still more difficulties because of beam remnants and an unknown interaction energy for each single interaction. However there are good reasons to build such machines, especially if one aims at finding new physics. To find new physics one has to construct a machine with as high an energy for the hard interaction as possible. The current generation of colliders are build as synchrotrons. In these machines a pre-accelerated beam is injected into the

circular synchrotron. In the synchrotron the beam is further accelerated and simultaneously the field of the bending magnets is increased in order to keep the beam on its circular path.

It is known from relativistic electrodynamics that a charged particle which is accelerated radiates off photons in the so-called bremsstrahlung. The energy lost because of bremsstrahlung in each cycle in the synchrotron is given by

$$E_{\text{Brems}} = \frac{4\pi}{3}\frac{e^2\beta^2\gamma^4}{r}.$$

e is the charge of the particle, $\beta = v/c$ is its velocity divided by the speed of light c, $\gamma = 1/\sqrt{1-\beta^2}$ and r is the radius of the synchrotron. As the particles are highly relativistic $\beta \approx 1$. Using $\gamma = E/m$, where E and m are the energy and mass of the particle one sees that the energy loss is proportional to E^4/m^4. A proton is about 2000 times as heavy as an electron. Thus, if it follows a path with the same radius a proton will only radiate off 1.610^{-13}th of the energy an electron radiates off. This can be seen directly in comparing the e^+e^- collider LEP with the pp collider LHC[13], which will be built in the LEP tunnel replacing LEP by 2005. The energy reach of LEP is limited by bremsstrahlung and the maximal energy it will be able to achieve lies near 100 GeV per beam. The LHC energy in contrary is limited by the magnetic field needed to bend the beams on their circular path. The expected beam energy of the LHC is 7 TeV, which is a factor of 70 higher than the LEP energy. Even if one looks only at the average energy of valence quarks in the hard interaction the LHC will have more than 14 times the energy of LEP.

Another point in favour of hadron colliders is the spread of the hard interaction energy. At an electron collider all hard interactions will have the nominal energy or lower. At a hadron collider the energy will be distributed around the mean. Many events will have less energy than the average, still also many events will have a lot more energy. The highest energetic events seen by the CDF-detector have energies in excess of 1000 GeV i.e. 1/3rd of the CMS-energy of 1.8 TeV. Translating this to the LHC one expects events with energies in excess of 10 TeV, while the maximal energy at LEP is a factor of 25 lower.

From this it is clear that a hadron synchrotron of the same dimensions has a much higher energy as an electron synchrotron. Put the other way a hadron collider with the same average energy as an electron collider will be much smaller (and thus easier to build) and it will also have a number of events well above the nominal energy, where unexplored new physics may be found. This makes hadron machines the ideal environment for new physics searches at the energy frontier.

[13] Large Hadron Collider

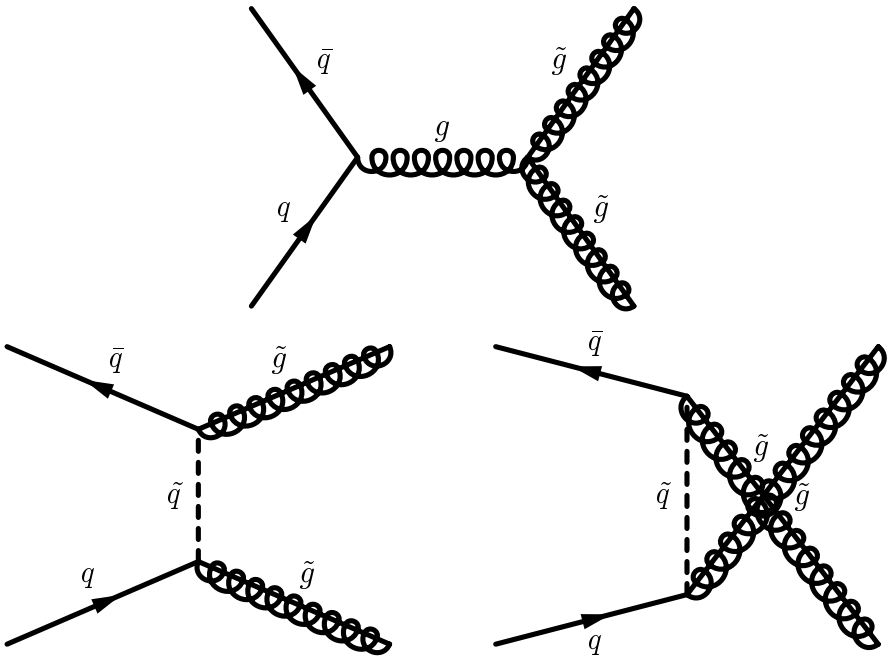

Abbildung 4.1: *The production of gluinos by $q\bar{q}$ scattering in lowest order.*

4.2 Sparticle Production

The hard interacting particles at a hadron collider are quarks, antiquarks and gluons. As the interacting particles have electro-magnetic, weak and colour charges, particles can be produced in many different ways [25]. I will describe the reactions possible at hadron colliders in lowest order of perturbation theory.

4.2.1 Gluino Pair Production

Gluinos have the same charges as gluons and thus couple to SM particles with the same coupling strengths. Thus also the production processes are identical to the ones for gluons in the SM. The only difference is that the particles exchanged in the u or the t channel are the superpartners of the quarks and gluons. There are two production processes depending on the particles taking part in the hard interaction.

- $q\bar{q} \to \tilde{g}\tilde{g}$. The quark and the antiquark either annihilate into a gluon which subsequently splits into two gluinos or the quark and the antiquark each radiate off a gluino while exchanging a t-channel or u-channel squark. The three processes are shown in figure 4.1.

- $gg \to \tilde{g}\tilde{g}$. Here either two gluons fusion and the resulting gluon splits up into two gluinos or both gluons radiate off a gluino exchanging a u– or t–channel gluino. The Feynman diagrams are identical to the ones for the gluinos production from

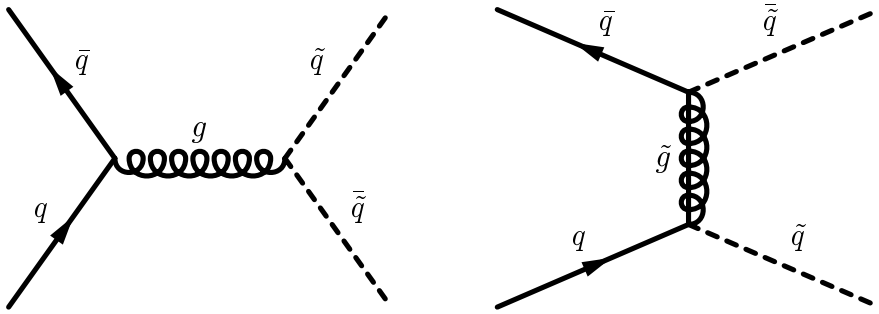

Abbildung 4.2: *Feynman diagrams for the production of squarks from a quark–antiquark initial state.*

$q\bar{q}$ with the quark and antiquark each substituted by a gluon and the squark substituted by a gluino.

4.2.2 Squark Production

The processes in which squarks can be produced are similar to the SM processes for quark production. Again the exchanged particles in the t and u-channel are the superpartners of the particles exchanged in the SM. Depending on the initial state of the hard interaction there are three types of processes.

- $q\bar{q} \to \tilde{q}\bar{\tilde{q}}$. A quark and an antiquark fusion to a gauge boson. The gauge boson may be any SM gauge boson, but because of the different coupling strengths the fusion to gluons will always dominate and the contributions due to the other gauge bosons can be neglected. A second possible process is the exchange of a gauge boson in the t-channel. The two contributing diagrams are shown in figure 4.2.

- $qq \to \tilde{q}\tilde{q}$. This process is similar to the second process in figure 4.2, with the addition of a crossed diagram. The crossed diagram occurs because the two produced squarks can not be distinguished from each other and thus both processes have to be considered. The two contributing diagrams are shown in figure 4.3.

- $gg \to \tilde{q}\bar{\tilde{q}}$. This process proceeds either via the fusion of two gluons and a following splitting into two gluinos or via the splitting of a gluon into two squarks, one of which is re-absorbed by the other gluon, while this second gluon emits another squark. The three corresponding diagrams are given in figure 4.4.

4.2.3 Slepton Production

Sleptons are produced if a quark and an antiquark annihilate into a photon or a Z^0, which subsequently decay into two oppositely charged sleptons or two sneutrinos. An alternative mechanism is the annihilation of two quarks into a $W^{\pm}$ boson, which then

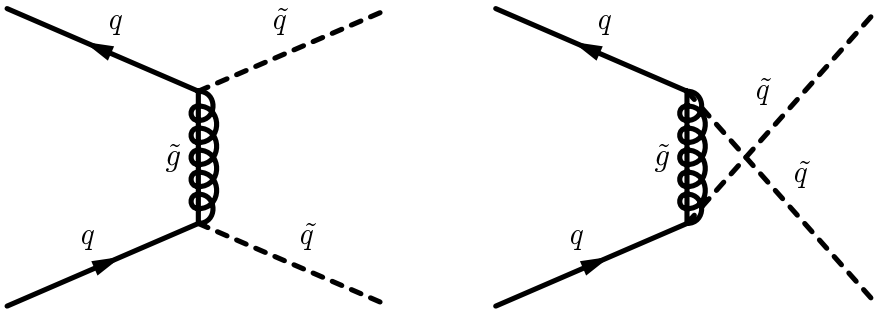

Abbildung 4.3: *Feynman diagrams for the production of squarks from a quark–quark initial state.*

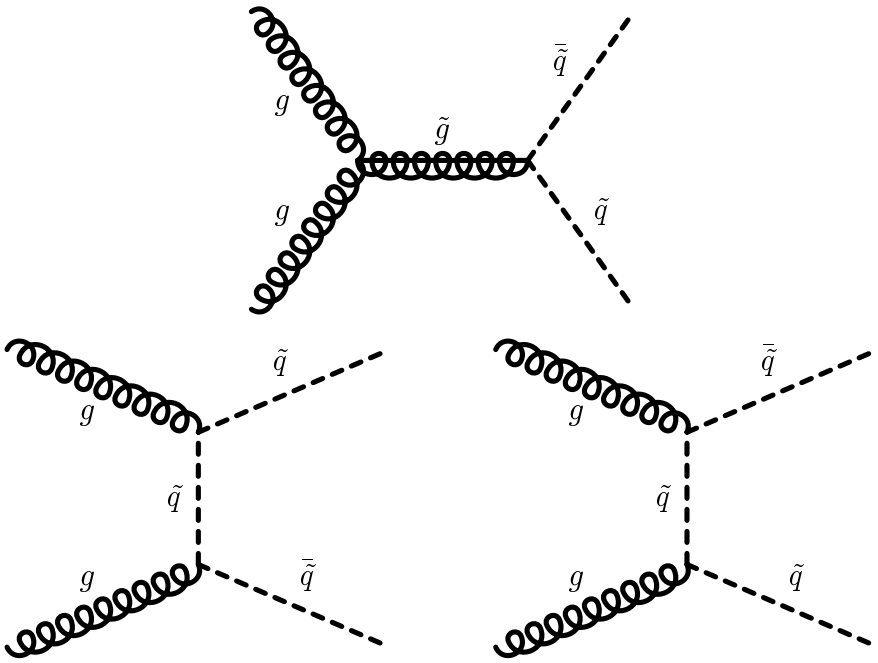

Abbildung 4.4: *The diagrams for the production of squarks pairs from a gluon–gluon initial state.*

decays into a slepton-sneutrino pair. The two corresponding diagrams are given in figure 4.5.

4.2.4 Chargino–Neutralino Production

Charginos and neutralinos can be produced in processes similar to diboson production in the SM. The diagrams for this can be obtained from the diagrams for gluino pair production given in figure 4.1. Two quarks can annihilate into a gauge boson, which then splits into two gauginos. The corresponding diagrams are shown in figure 4.6.

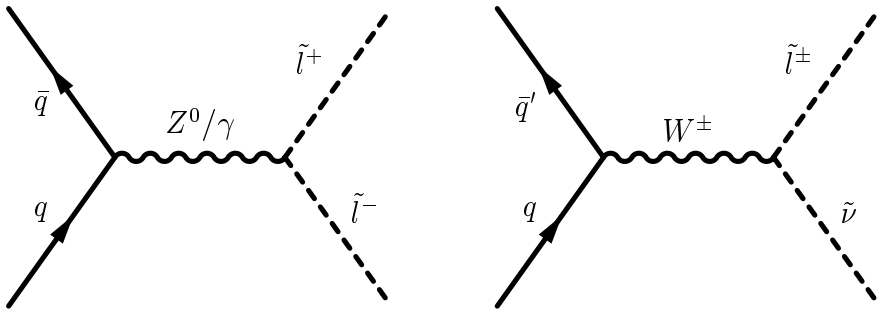

Abbildung 4.5: *The Feynman diagrams describing the production of sleptons at hadron colliders.*

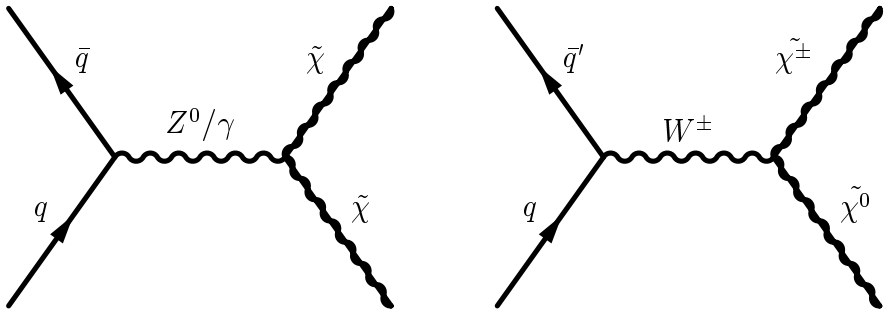

Abbildung 4.6: *s-channel production of charginos and neutralinos.*

The other possible process is the exchange of a squark in the t or the u channel. In this case both quarks radiate off a chargino or neutralino. If the particle radiated off is a neutralino then the incoming quark and the exchanged squark must have the same flavour. Thus if two neutralinos are radiated off the reaction can only take place with a quark-antiquark pair in the initial state. As the produced neutralinos are undistinguishable one must also consider the crossed diagram. If one of the particles radiated off is a chargino and the other one is a neutralino, the incoming particles must be a quark and an antiquark of different flavours. Two oppositely charged charginos are radiated off if a quark and its corresponding antiquark react. For the cases involving charginos one can distinguish between the two particles in the final state and thus needs not consider crossed diagrams. The Feynman diagrams describing chargino/neutralino production through t and u-channel exchange of squarks are shown in figure 4.7.

4.3 Sparticle Decays without R-Parity Violation

In this section the decays of the sparticles will be discussed under the assumption that R-Parity is conserved. The changes introduced by R-parity violation will be discussed in the next section.

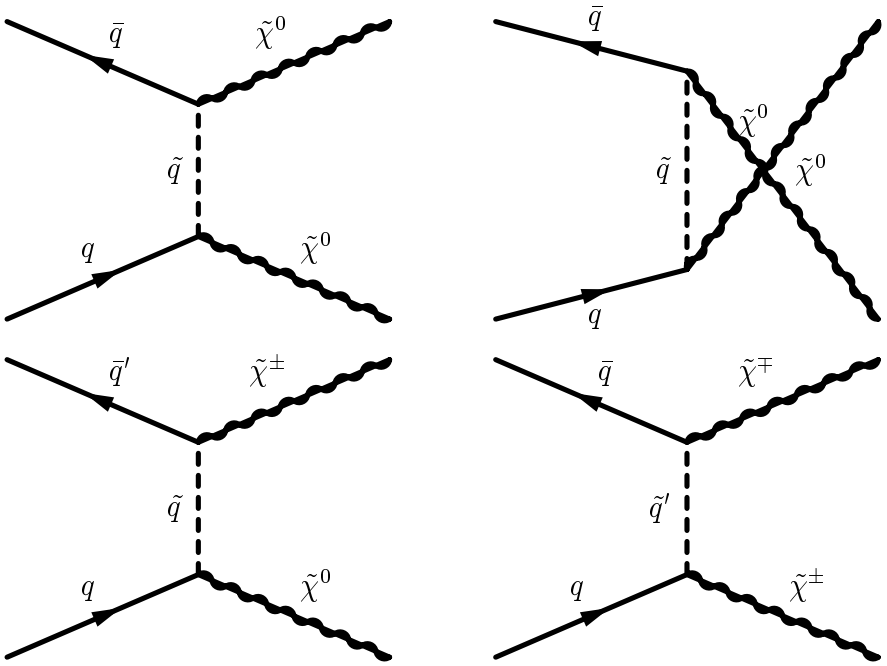

Abbildung 4.7: *t-channel and u-channel production of gauginos.*

All sparticles produced in high-energy collisions will decay into the LSP. It has been known for some time that these decays will not lead from the heavy particle to the LSP in one step. If there are sparticles with a mass between the original sparticle and the LSP, then in most of the cases the sparticles will first decay into the intermediate sparticle, which then decays into the LSP directly or via another intermediate sparticle. As these decays can go through various steps they are called cascade decays. In the remainder of this section I will discuss the decays of all superpartners. As it is impractical to list all possible cascade decays, which sometimes exist only in a small area of parameter space I will give the building-blocks for the decays, from which one may construct the complete cascade.

4.3.1 Squark and Gluino decays

A gluino can only decay into a quark and a squark. Thus the decay chain for a squark and a gluino are identical. I will give some possible decay channels for gluinos here. The corresponding channels for squarks can be obtained by omitting the initial gluino and the quark produced by its decay into the squark. The decays of squarks are similar to the decays of heavy quarks in the SM with one of the outgoing particles replaced by its superpartner. I assume that the squark is already on the mass shell and thus not discuss the radiation of SM gauge bosons. This radiation would only change the energy of the particle and produce a new SM gauge boson. The particle decaying in the next step of the cascade will still be a squark, which in the case of $W^\pm$ radiation

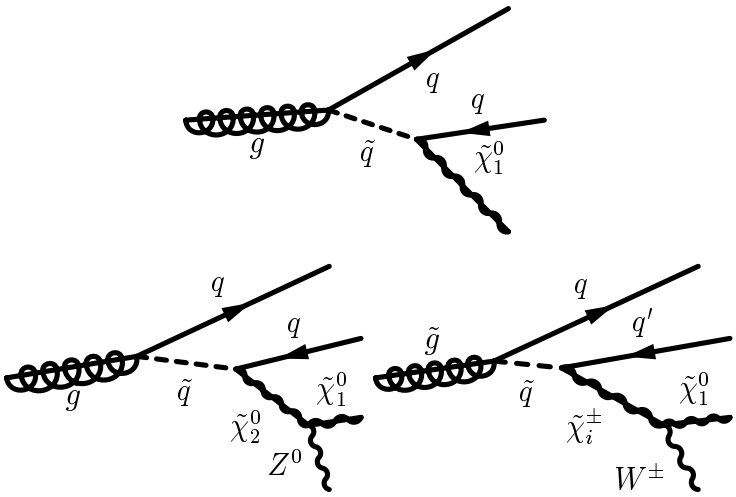

Abbildung 4.8: *Cascade decays of gluinos.*

would have a different flavour. For an on-shell squark the only decay paths are the decays into quarks and charginos or neutralinos if these particles are lighter than the squark. The two processes are shown in figure 4.8. As the chargino can not be the LSP it continues to decay. If the produced neutralino is not the LSP it will also decay in similar channels.

4.3.2 Decays of Charginos, Neutralinos and Sleptons

Charginos and neutralinos can decay through sleptons radiating off SM gauge bosons or through lighter charginos and SM leptons. The decays of sleptons can be obtained from this in the same way the squark decays can be obtained from the gluino decays, just by omitting the first vertex. A few examples of decay chains are given in figure 4.9.

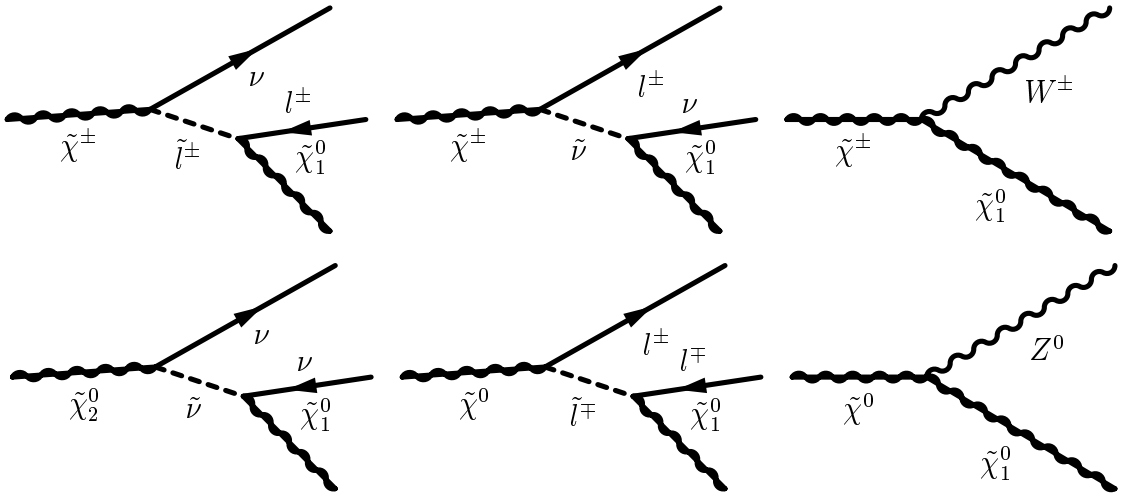

Abbildung 4.9: *Cascade decays of charginos and neutralinos.*

5 The Tevatron and CDF

The data used for this analysis were taken with the Collider Detector at Fermilab (CDF) in the years 1994-1996 (Run IB). In this chapter the used experimental apparatus is described.

5.1 The Tevatron

The Tevatron is the world's highest energy hadron collider, colliding protons and antiprotons with a center-of-mass energy of 1.8 TeV. To achieve these high energies several stages of acceleration are necessary. The acceleration process is described in this section. A schematic view of the accelerator is shown in Figure 5.1.

The acceleration process starts with hydrogen atoms, which are injected into the Cockcroft-Walton accelerator. Here an electron is added to each atom, resulting in negative ions, which then are accelerated to an energy of 750 keV. After leaving the Cockcroft-Walton the hydrogen ions enter a 150 m long linear accelerator (Linac), where they are accelerated to 400 MeV. At the end of the Linac the ions pass through a carbon foil, which strips off the electrons so that only protons enter the next stages. The Booster, a small synchrotron ring, subsequently accelerates bunches of protons to energies of up to 8 GeV. Having reached this energy the protons are injected into the Main Ring, where their energy is increased to 150 GeV. At this point, most of the protons are sent into the Tevatron, a 2 km diameter proton synchrotron containing 1,000 superconduction magnets. Here the protons reach their final energy of 0.9 TeV.

The high energetic antiprotons are created using a portion of protons from the Main Ring. These protons are shot on a tungsten target, producing $p\bar{p}$ pairs. The antiprotons are separated from the protons, then focused using a lithium magnetic lens and finally sent into the Debuncher. Here the energy spread of the beam is reduced by debunching and stochastical cooling. The monochromatic beam then is transfered into the accumulator, where it is stored until an amount of antiprotons sufficient for the desired luminosity is accumulated. From this point on the acceleration of the antiprotons is the same as the one of the protons. They are subsequently transfered to the Booster, the Main Ring and finally the Tevatron.

In the Tevatron six bunches each of protons and antiprotons are accelerated from 150 GeV to 900 GeV. The proton and antiproton beams travel in opposite directions and collide at two interaction points.

The Tevatron has had several collision runs so far. The first collisions were generated in 1985, followed by low luminosity runs in 1987 and 1988-1989. The two main run periods were Run IA (1992-1993) and Run IB (1994-1996).

During Run IA a proton bunch consisted typically of $12 \cdot 10^{10}$ protons, whereas an antiproton bunch typically consisted of $3.1 \cdot 10^{10}$ antiprotons. The luminosity recorded during this time was approximately 20 pb^{-1}. For Run IB the number of protons (antiprotons) per bunch was increased to $22.5 \cdot 10^{10}$ ($6.5 \cdot 10^{10}$). The luminosity recorded

during this run was approximately 90 pb^{-1}.

After a major accelerator and detector upgrade the Tevatron will start Run II in spring of 2001. The expected luminosity for this new run is 20 fb^{-1}.

5.2 The CDF Detector

Located at the interaction points of the Tevatron are two multi-purpose detectors: the D0 detector [26] and the CDF detector [27]. The data used for this analysis were taken with the CDF detector.

The interactions of protons and antiprotons are independent of the azimuthal angle and symmetric in forward-background direction. Thus the CDF detector was built symmetric in forward-backward direction and azimuthal angle.

To identify the produced particles the detector consists of a tracking system inside a 1.4 T magnetic field, fine-grained calorimeters and muon chambers.

A schematic view of the detector is shown in Figure 5.2. Because of the symmetries a cylindrical coordinate system, with the z-axis is pointing in the direction of the incoming protons, is used. For the observation of particle collisions it is not convenient to use the polar angle θ, because most interactions are boosted with respect to the laboratory

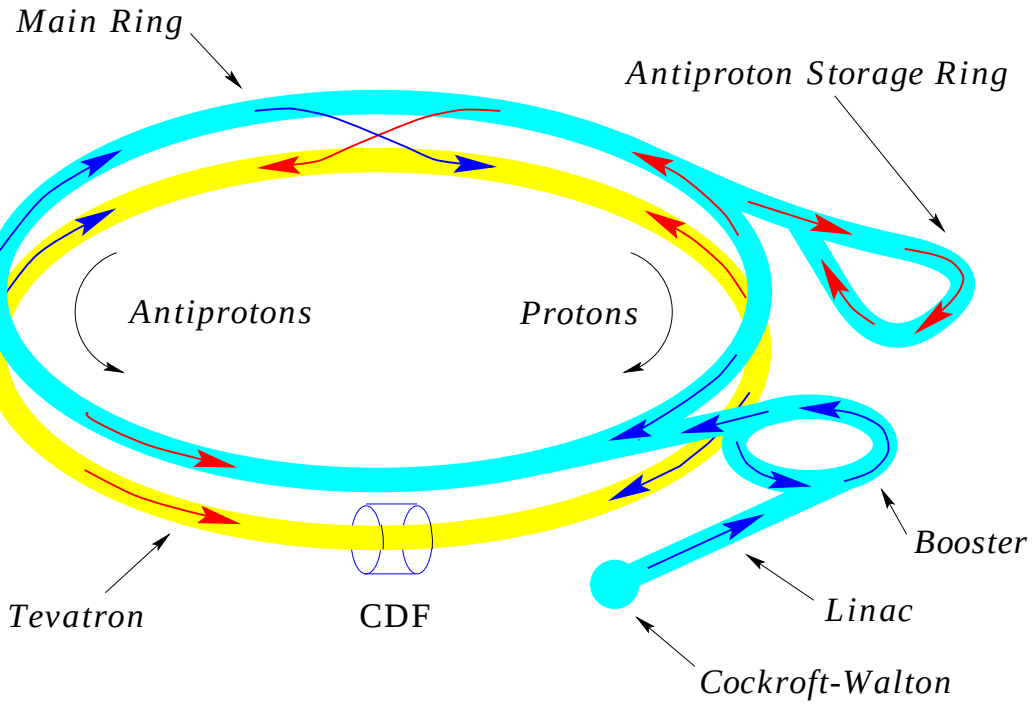

Abbildung 5.1: *Schematic view of the Tevatron collider during Run I.*

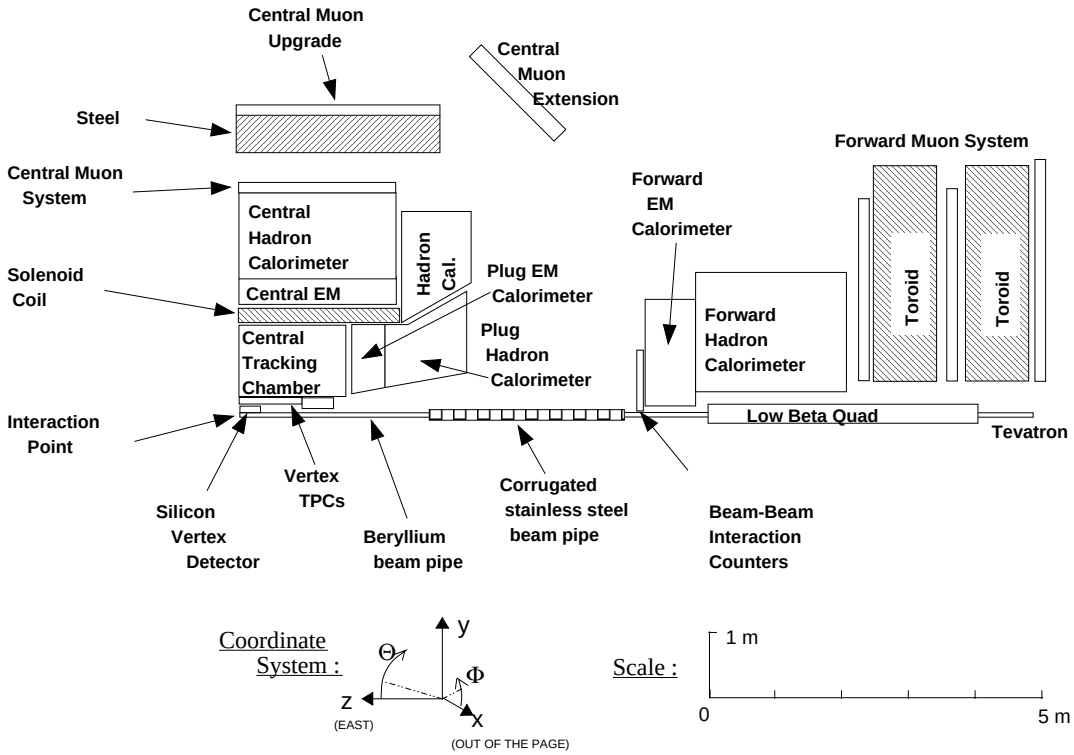

Abbildung 5.2: *Schematic view of one quadrant of the CDF detector during Run I.*

rest frame. Instead one uses the rapidity

$$y = 0.5 \ \ln \frac{E + P_z}{E - P_z},$$

which transforms under a Lorentz boosts along the z-axis in such a way that the shape of the rapidity distribution is invariant. In order to calculate the rapidity for a particle one needs to measure both its momentum and its energy. Thus instead of θ usually the pseudorapidity

$$\eta = -\log \tan(\theta/2)$$

is used. The pseudorapidity is a good approximation for the rapidity at high energies. It depends only on the angle of the particle with respect to the beam axis, which is easier to obtain than the energy and momentum of the particle.

In the following the various components of the CDF detector will be described. A detailed description of the detector components can be found in [27].

5.2.1 The Tracking System

The tracking system of the CDF detector is the part of the detector closest to the Tevatron beamline. It is contained within a solenoidal magnetic field of 1.4 T. The

system consists of three modules: the Secondary Vertex Detector (SVX), the Vertex Time Projection Chamber (VTX) and the Central Tracking Chamber (CTC). For this analysis the VTX and CTC were used.

The Silicon Vertex Detector

The CDF Silicon Vertex Detector (SVX) consists of two independent modules with a total length of 51 cm. It covers a rapidity region of $|\eta| < 2.9$ for the inner and $|\eta| < 1.9$ for the outer layer.

The modules are composed of four concentric cylindrical layers of silicon strip detectors arranged as twelve sided barrels. The radii of the barrels are between 3.005 cm and 7.866 cm. On each of the faces there are six detectors in groups of three. The individual detectors have a length of 8.5 cm, their width increases with the radius of the layer. The strips on the detectors have a pitch of 60 μm for the first three and of 55 μm for the last layer. The readout is done using the SVX chip Revision D.

The Vertex Time Projection Chamber

The Vertex Time Projection Chamber (VTX) consists of eight 2.8 m long time projection chambers, covering a pseudorapidity of $|\eta| < 3.25$. The chambers start directly outside the SVX and have an outer radius of 22 cm. The drift gas used is a 1:1 mixture of argon and ethane.

The VTX consists of 28 individual modules, which are divided into 2 drift regions in z and 8 octants in φ. All modules are 10 cm long and equipped with at least 16 sense wires. The 10 outer modules (five at each end) are larger because they are outside the rapidity region of the SVX. These chambers are equipped with 24 sense wires each. All sense wires are strung azimuthally. The z-position of a particle transversing the VTX can be determined with an accuracy of 2 mm. For particles passing through more than one module rudimentary φ information is available from the 15° tilt between neighbouring modules.

The Central Tracking Chamber

The CTC is a cylindrical drift chamber about 0.015 radiation lengths thick. Its inner (outer) radius is 30 cm (1.3 m). Being 3.2 m long it covers a pseudorapidity of $|\eta| < 1(2)$ at the outer (inner) layer. The drift gas used is an equal mixture of argon and ethane with an additional small amount of ethanol.

The chamber is equipped with 6,156 sense wires, arranged in 84 layers. The wire spacing is 10 mm. 60 layers of wires are parallel to the beamline. These axial layers are grouped into 5 superlayers containing 12 layers each. The remaining 24 layers are arranged into 4 groups of stereo superlayers containing 6 layers of wire each. The wires of the stereo layers are tilted by $\pm 3°$ with respect to the beamline.

The electrons created by a charged particle passing through the CTC move in a field with a gradient of 1340 V/cm. Their maximal drift time of 800 ns is significantly smaller than the beam-crossing time of 3.5μs. The resolution of the individual wires is

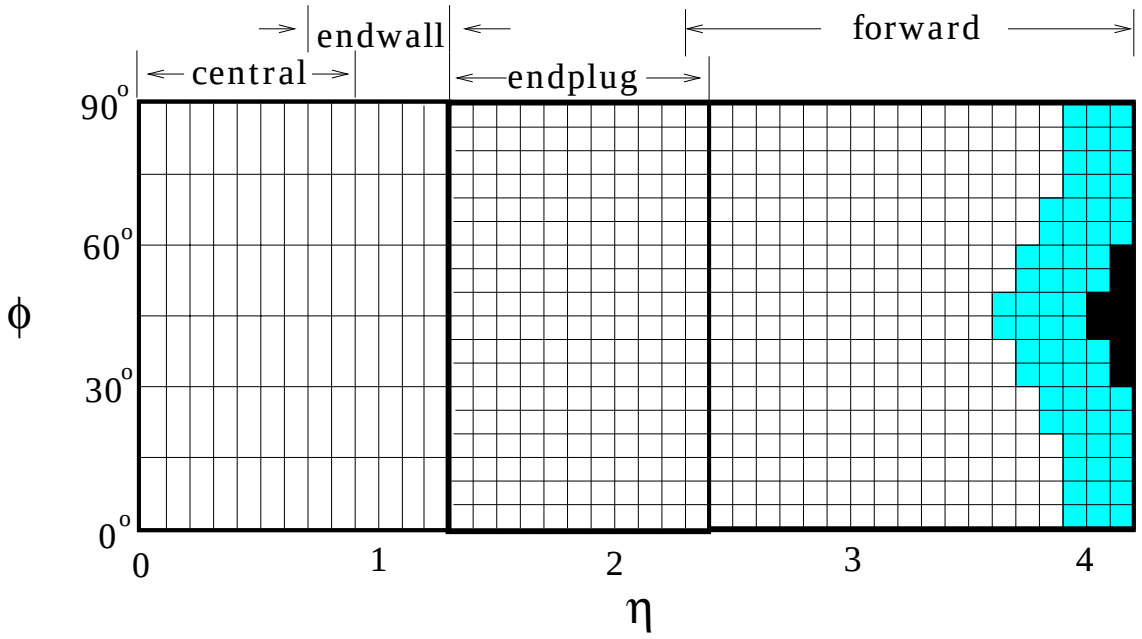

Abbildung 5.3: *The segmentation of the CDF calorimeters in the $\eta - \varphi$ plane.*

200 μm, which yields a two-track resolution of approximately 5 mm. The momentum resolution is further increased by requiring that tracks originate in the r-φ plane of the interaction region. The beam constrained momentum resolution of the CTC is $\delta p_{\mathrm{T}}/p_{\mathrm{T}} = 0.002 \times p_{\mathrm{T}}/\mathrm{GeV}$ for isolated tracks.

5.2.2 Calorimeters

The CDF calorimeters are built as projective towers covering a pseudorapidity of $|\eta| < 4.2$ (see Fig. 5.3). The calorimeters for the central ($|\eta| < 1.1$), plug ($1.1 < |\eta| < 2.4$) and forward ($2.4 < |\eta| < 4.2$) region each consist of an electromagnetic and a hadronic part. For this analysis only the central calorimeter was used.

The Central Calorimeter

The central calorimeter is composed of layers of scintillator and absorber material. It is divided into 480 towers with sizes of 0.1 in η and 15° in φ.

In the electromagnetic part (CEM) lead is used as absorber material. The CEM has a thickness of 18 radiation lengths and one absorption length. The scintillator is SCSN-38 polystyrene, which is connected via a Y7 UVA acrylic wavelength shifter to Hamamatsu R580 phototube readout. The energy resolution of the CEM is $13.5\%/\sqrt{E}$.

Located near the shower maximum at about 6 radiation lengths is a proportional multiwire chamber (CES). This chamber is used to measure the transverse shower profile of particles passing through the CEM. It has a spatial resolution of 2 mm. The

measurement is performed reading out the 64 anode wires in the x-direction and the 64 orthogonal cathode strips in z-direction. The strips (wires) are spaced by 18 mm (6.3 mm) and separated by a drift-volume filled with 95% argon and 5% CO_2.

The absorber used for the central hadronic calorimeter (CHA) is steel, the scintillator is acrylic PMMA. The CHA is read out with Thorn-EMI-9954 phototubes, which are connected to the scintillator with UVA PMMA doped wavelength shifters. The CHA is 4.7 absorption lengths thick and has an energy resolution of $80\%/\sqrt{E}$.

The Plug Calorimeter

The plug calorimeters use the same absorber material as the central calorimeters, but use drift chambers instead of scintillators. The segmentation is 0.09 in η and 5° in φ.

The drift gas used is a 1:1 mixture of argon and ethane in both cases. With a thickness of 18-21 radiation lengths and 0.9-1.0 absorption lengths the electromagnetic plug calorimeter (PEM) achieves an energy resolution of $28\%/\sqrt{E}$. The hadronic plug calorimeter (PHA) is 5.7 absorption lengths thick and has an energy resolution of $130\%/\sqrt{E}$. Similar to the construction of the CEM there is a proportional chamber located near the shower maximum in the PEM. This chamber (PES) has a spatial resolution of 2 mm.

The Forward Calorimeter

The forward calorimeter is similar to the plug calorimeter, but with a larger segmentation of 0.1 in η and 5° in φ. The electromagnetic part (FEM) is 25.5 radiation lengths and 0.8 absorption lengths thick and gives an energy resolution of $25\%/\sqrt{E}$. The hadronic part (FHA) is 7.7 absorption lengths thick and has an energy resolution of $141\%/\sqrt{E}$.

5.2.3 The Muon Chambers

The CDF muon chambers are placed on the outside of the detector. There are three different systems in the central area and one system in forward direction.

CMU and CMP

The central muon chambers (CMU) are located directly outside the CHA, covering the region $|\eta| < 0.6$. They consist of 4 layers of drift chambers located at a radial distance of 3470 mm from the beam axis. The chambers are segmented in wedges of 12.6°, fitting into the top of each central calorimeter wedge. Each wedge is in turn composed of three 4.2° modules. The modules contain four layers of aluminum drift cells filled with a 1:1 mixture of argon-ethane with a small addition of ethanol.

There are 4.9 interaction lengths of material between the interaction point and the CMU. Thus there is still a high probability for punch-throughs of high energetic jets to be identified as muons. This probability is reduced significantly by the four layers of drift chambers constituting the central muon upgrade (CMP). These are separated

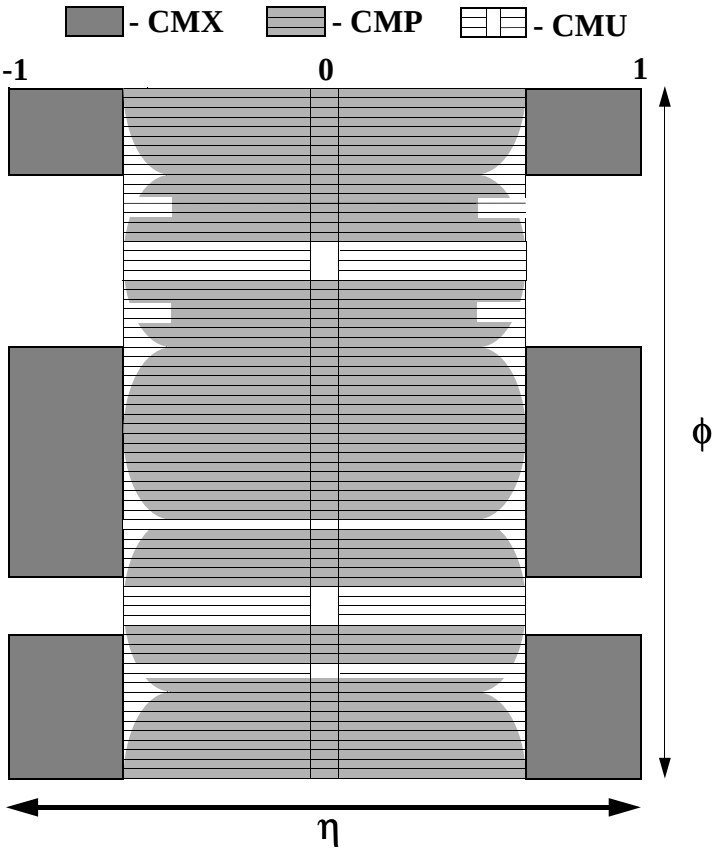

Abbildung 5.4: *The angular coverage of the central muon detectors.*

from the CMU chambers by 0.6 m of steel, corresponding to additional 8 interaction lengths.

The detector coverage of CMU and CMP is not complete. The CMU cover approximately 84% of the central area, whereas the CMP covers about 63%. An area of 53% is covered by both CMU and CMP. Details about the angular coverage of the central muon detectors are shown in figure 5.4.

CMX

In the rapidity region of $0.6 < |\eta| < 1.0$ muons are detected using the central muon extension (CMX). This detector consists of four free-standing conical arches of drift chambers. The drift chambers are sandwiched between scintillators, which are used for triggering. The CMX covers approximately 71% of the solid angle of the rapidity region. It has major gaps of 90° at the bottom, where it intercepts the collision hall floor and of 20° at the top, where the main ring and solenoid refrigerator are located.

CMIO

As described in the previous paragraphs the muon chambers do not cover the central region completely. In order to be able to detect all muons CDF uses Central Minimum Ionising Objects (CMIO). For this CTC tracks are extrapolated through the calorimeters and muon chambers. If the energy deposition is consistent with a minimum ionising particle and the track would not hit any muon chamber it is marked as a muon candidate. A CMIO muon is not detected in any muon chamber and thus the possibility of a track faking a CMIO muon is high.

FMU

The forward muon chambers (FMU) consists of a pair of magnetised iron toroids instrumented with three sets of drift chambers and two planes of scintillator counters. Each plane of drift chambers or scintillators is subdivided into 24 sectors covering an angle of 15° each. The layers of drift chambers are staggered relative to each other to eliminate detector dead spots. The drift gas is a 1:1 argon ethane mixture. The toroids create a magnetic field of 2.0 T at the inner and 1.6 T at the outer radius. The position resolution of the FMU is 130 μm.

5.2.4 The Beam Beam Counters

The beam beam counters (BBC) are two planes of scintillators covering the rapidity range of $3.24 < |\eta| < 5.88$ in both forward and backward direction. The detectors are used as triggers for minimum bias events and as primary luminosity monitors.

The rate of the coincidences in the two counters divided by the effective cross section of the counters gives the instantaneous luminosity. The effective cross section for the BBC in Run I and Run II was calculated using the measured total, elastic and inelastic cross sections:

$$\sigma_{\mathrm{BBC}} = \sigma_{\mathrm{total}} \frac{N_{\mathrm{BBC}}}{N_{\mathrm{inel}} + N_{\mathrm{el}}}.$$

The value obtained for the BBC cross section is 51.15 ± 60 mb. The total luminosity was calculated similarly using the total number of coincidences in the BBCs.

5.2.5 The Trigger System

The multi-purpose detectors used in todays high-energy physics experiments were developed to study the events containing reactions about which little or nothing is known yet. These events are hidden in a large background of other events, which are understood to a high degree and which are thus not considered to be of high interest. Even for some of the interesting events the rate is to high to save all events without loosing valuable information about rarer events. In order to separate the "importantëvents from the less important ones one uses several stages of events selection.

CDF uses a four level trigger system to select the events which are eventually written to 8 mm tapes.

Level 0: The lowest trigger level is used to decide if a collision has taken place during a beam crossing. The following trigger stages are only fired if there is a coincidence in the BBCs. The decision at level 0 must be made in less then 3.5 μs, which is the time that separates two beam crossings. This level thus operates at the full rate the collider delivers.

Level 1: The decision at level one is based on the states of several detector subsystems. If there is a certain amount of energy in the central calorimeters, a track in the CTC or hits in the muon chambers the event will be accepted and then be forwarded to the next trigger level. The decision is made by the detector hardware to obtain the necessary speed of less than 7 μs. Still the time needed for the level 1 decision means that the next event will be missed if the current event is accepted. The trigger rate at level one was slightly above 1 kHz during Run Ib.

Level 2: Like the two previous levels this level is a pure hardware trigger. The two main differences are the combination of different detector subsystems and the introduction of prescaling. The combination of detector elements can be e.g. the requirement that the part of the detector which a track points to (e.g. the calorimeter or a muon chamber) also shows a signal. The second level was the main data selection trigger. The prescaling is used because of the different importance of events. One is most interested in extremely rare events like top. Triggers in which such events are expected were not prescaled. On the other hand events containing a single lepton are useful in many cases, but one needs only a small percentage of the events produced. In order to keep all the important events a certain ratio of the less important events were rejected, although they would have passed the level two trigger. There were two different prescaling mechanisms depending on the process they were used on. One was the static prescale, which was set at the beginning of a data-taking run and was not changed for the several hours that run lasted. The dynamic prescaling, in contrary could be adapted to the luminosity changes during the individual runs. Thus it was possible to record a higher percentage of the events during low luminosity than one could have recorded during high luminosity. The typical trigger rate at level two was about 12 Hz.

Level 3: The last trigger level was implemented as a programmable software trigger. The trigger software ran on a farm of 60 Silicon Graphics Servers at a speed of about one billion instructions per second. Each server had several Motorola 68020 Processors. The computer farm ran a special version of the CDF offline code and had the complete detector information available. This level was mainly used to reject bad events and group the remaining events into several data sets according to the triggers they had passed. The output rate of this trigger level was 5-7 Hz.

Events passing all four trigger levels were written to disks, which subsequently were saved to 8 mm tapes for long-term storage. The process of saving the data to disk and tape was the main limiting factor to the trigger rate at level three.

6 Monte Carlo Simulations

6.1 Simulating the Signal Process

The masses and branching-ratios of the superpartners were calculated in the framework of R_P-mSUGRA [11].

The Monte Carlo generator used to simulate SUSY processes was ISAJET version 7.20 [14] with its extension ISASUSY. The LSP-decays were simulated assuming the same branching ratios for all possible LSP-decays.

For mSUGRA processes ISASUSY takes four input parameters:

1. M_0
2. $M_{1/2}$
3. A_0
4. $\tan(\beta)$
5. SGN(μ).

From these parameters ISASUSY calculates 13 MSSM parameters

1. $\tilde{m}_g$,
2. $\tilde{m}_q = \frac{1}{4}(\tilde{m}_{u_L} + \tilde{m}_{d_L} + \tilde{m}_{u_R} + \tilde{m}_{d_R})$,
3. $\tilde{m}_{l_L}$ with $l = e,\, \mu$,
4. $\tilde{m}_{l_R}$ with $l = e,\, \mu$,
5. $\tilde{m}_\nu$,
6. $\tilde{m}_{t_L}$,
7. $\tilde{m}_{t_R}$,
8. A_t,
9. $\tilde{m}_{b_L}$,
10. $\tilde{m}_{b_R}$,
11. $\tan(\beta)$,
12. μ,
13. $\tilde{m}_{h_a}$.

From these parameters the SUSY mass spectrum and the branching ratios are calculated.

For this analysis M_0 and $M_{1/2}$ were varied, while the other three parameters were kept constant at

$$A_0 = 0, \quad \tan(\beta) = 2, \quad \mathrm{SGN}(\mu) = -1.$$

The parameter A_0 describes the top-squark mixing. As stop production is not considered in this analysis the value of A_0 is not important and is arbitrarily set to 0.

In mSUGRA the value of μ is calculated using the RGEs. The sign of μ is not predicted by theory and has to be given to ISASUSY as input parameter. In this analysis $\mathrm{SGN}(\mu) < 0$ was used. This is consistent with $\mu = -400$ as used in previous searches at CDF. $\tan(\beta) = 2$ was the value used in most previous SUSY-searches at CDF and was kept for consistency.

ISAJET simulated $p\bar{p}$ collisions with a center of mass energy of 1.8 TeV. The structure function was CTEQ3L. The production of all superpartners except for stops was allowed. The momentum of the produced particles had to lie between 5 GeV and 600 GeV.

A sample configuration file containing the ISAJET setup :

```
PBAR + P --> b + bbar
1800.000000 15 1000 0
SUPERSYM
BEAMS
'P'       'AP'
TMASS
175.0000000 -1.000000000 -1.000000000
PDFLIB
'NPTYPE',1.D0,'NGROUP',4.D0,'NSET',29.D0,'TMAS',175.D0/
JETTYPE1
'GLSS','SQUARKS','GAUGINOSSLEPTONS'/
JETTYPE2
'GLSS','SQUARKS','GAUGINOSSLEPTONS'/
SUGRA
200.,100.,0.0,2.0, -1./
PT
5.000000000,600.0000000,5.000000000,600.0000000/
NTRIES
100000/
END
STOP
```

The decays of the LSP were introduced in the Mote Carlo by adding appropriate entries to the decay tables of ISAJET. There are two files containing the information for particle decays. The file "dktable.dbt" contains the particles decaying, together with

the branching ratios and the particles produced in the decay. For this analysis 4 decays of the LSP corresponding to the four final states shown in equation 42 were introduced. In addition in the file "cvtable.dbt" the decay of the LSP was enabled and flagged as a weak decay.

6.2 Simulating Background Processes

The same MC-generator (ISAJET version 7.20) was used for the background simulation as for the signal simulation. A number of background processes, which could produce real three or four-lepton events were taken into account. The three-lepton events serve as a cross-check for the event selection. If neutralinos decay via a non-zero coupling λ_{121} the decay products will be electrons, muons and neutrinos (see section 3.8). Taus can only originate from cascade decays and are difficult to identify in the detector. As they will not make a significant contribution to the signal there is no tau selection. If taus decay leptonically their decay products may pass the selection cuts. For the remainder of the thesis I will use lepton as a synonym for both electron or muon, but not for tau.

Processes which can give real four-lepton events are top-pair and heavy-quark ($b\bar{b}/c\bar{c}$) production. If both quarks decay with at least two leptonic decays in the decay chain, the final state will have at least four charged leptons. In addition there is a small contribution from Z-pair production with both Z^0s decaying leptonically.

All of the abovementioned processes can also produce three-lepton events. Either if only three leptons are produced or because of a lepton escaping undetected. In addition three-lepton events can come from WZ-production with both particles decaying leptonically and Drell-Yan with an additional lepton.

A detailed discussion of the background processes will be given in chapter 9.

6.3 Detector Simulation

We used QFL′ version 3.59 to simulate detector effects. Triggers were simulated with the MC_WGT function written by Stephan Lammel. This function contains all relevant information about the lepton triggers we used.

7 LSP Decays into Leptons

In the first part of this chapter the kinematics of the signal events are discussed. The results with and without R_P violation are compared in order to verify that the modified MC gives the expected results. In the second part of the chapter the efficiencies for identifying leptons in the signal events are studied. Here the relative importance of LSP decays and other sources of leptons is discussed.

7.1 Kinematics of the Signal Events

Comparing the kinematics of mSUGRA events with and without R_P-conservation the most important difference is the decay of the LSPs. In mSUGRA the LSPs escape undetected and thus cause a significant amount of $\not{E}_T$. In $\not{R}_P$-mSUGRA the LSP decays and the products of this decay are seen in the detector. In the case of a non-zero coupling λ_{121} there will still be $\not{E}_T$ in the event because each LSP decays into two leptons and a neutrino (see fig. 3.4). Still the $\not{E}_T$ will be smaller than in the mSUGRA. $\lambda_{121} \neq 0$ would thus result in events with 4 leptons from the LSP decay plus possible additional leptons and jets from the cascade decay. [28] predicts the highest range in the search for R_p violating SUSY in the 4-lepton channel.

In fig. 7.1 the lepton E_{T} (P_{T} for muons) spectrum for M_0=0 GeV $M_{1/2}$=170 GeV are shown. The solid line corresponds to the identified leptons form a scenario with R_P violation, while the broken line represents a line R_P conservation. For both cases 5000 events were processed. The $\not{R}_P$ scenario gives a higher number of leptons and a harder lepton spectrum. The scenario shown in figure 7.1 has a hard lepton spectrum in the R_P conserving case. Still the leptons from the LSP-decays are harder. With R_P conservation nearly no events containing three of four leptons are produced. The number of leptons passing the cuts for the first and second lepton are shown in figure 7.2 for three scenarios with and without R_P conservation. The events from scenarios with R_P violation contain more leptons and the multiplicity reaches up to five or six leptons while in the scenarios without R_P violation no more than two or three leptons are seen.

From this in the $\not{R}_P$-mSUGRA framework one expects events with a high number of leptons, a significant number of jets from the cascade decays and some $\not{E}_T$.

7.2 Identifying Leptons in the Signal

Leptons in signal events can originate from two sources: they can either come from the cascade decay of heavy SUSY particles or from the decay of the LSP.

Only scenarios with neutralino LSPs decaying into two charged leptons and a neutrino are investigated. Thus the leptonic branching ratio due to the decay of the LSP is constant. Here only kinematic effects influence the detection efficiency. These effects

generally lead only to small changes in the lepton identification efficiency.

The changes in the leptonic branching ratios in the cascade decays can be rather strong. About one third of the leptons are coming from cascade decays. Due to the opening and closing of several decay channels the leptonic branching can change significantly. The consequences of this behaviour are studied in chapter 7.2.2.

7.2.1 The Origin of Leptons in the Signal Scenarios

In this subsection the origin of the leptons identified in several signal scenarios will be investigated. The two sources of leptons are the cascade decays and the LSP decays.

In order to identify the source of the leptons selected by the analysis module one needs to find the corresponding generator level lepton. Similar to the data of identified leptons the information about the generator level leptons is stored in a YBOS bank.

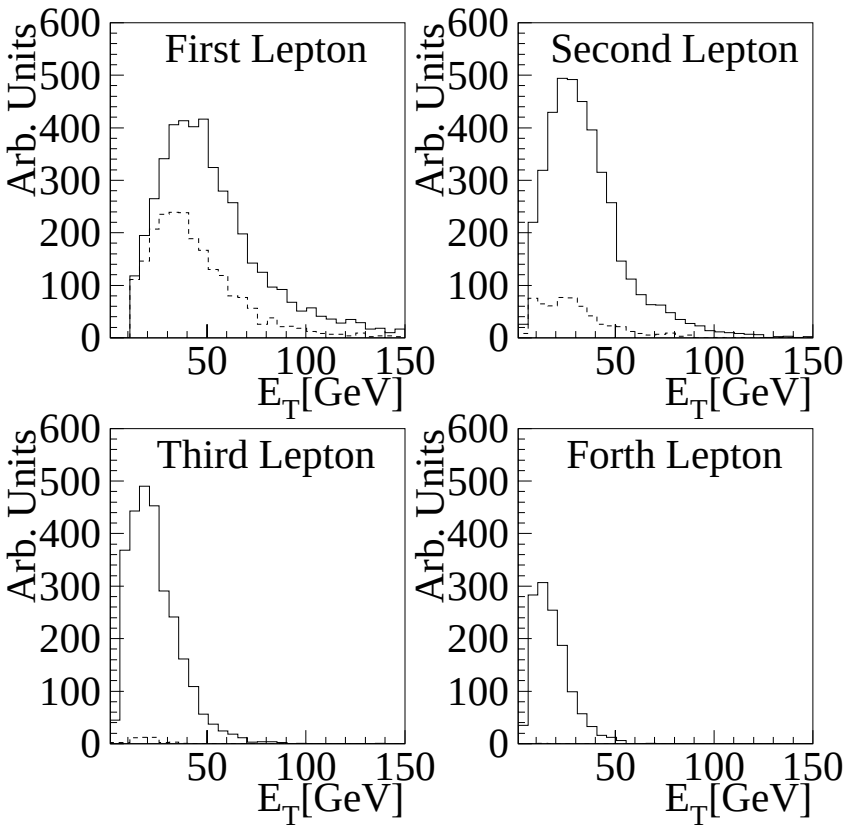

Abbildung 7.1: *The E_{T} (p_{T} for muons) spectra of the four leptons for one of scenarios studied. The solid lines give the spectrum for the scenario with R_P violation, the broken lines the spectrum with R_P conservation.*

This bank which is called the GENP bank is part of a simulated event and thus available at the analysis stage. The CDF Run I lepton banks do not contain links to the GENP bank generating the signal in the detector simulation. Thus the only way to determine the origin of a lepton signal is to compare the leptons at GENP level with the leptons identified in the analysis code.

One starts with the leptons identified by the analysis code. For each lepton the separation from all GENP leptons of the same flavour as the lepton is checked. The separation $\Delta R > 0.4$ is defined as

$$\Delta R = \sqrt{(\eta_1 - \eta_2)^2 + (\varphi_1 - \varphi_2)^2)}.$$

If the separation is less than 0.1 a flag is set, indicating that the lepton seen in the detector originates from a real lepton in the GENP bank. Most of the leptons seen

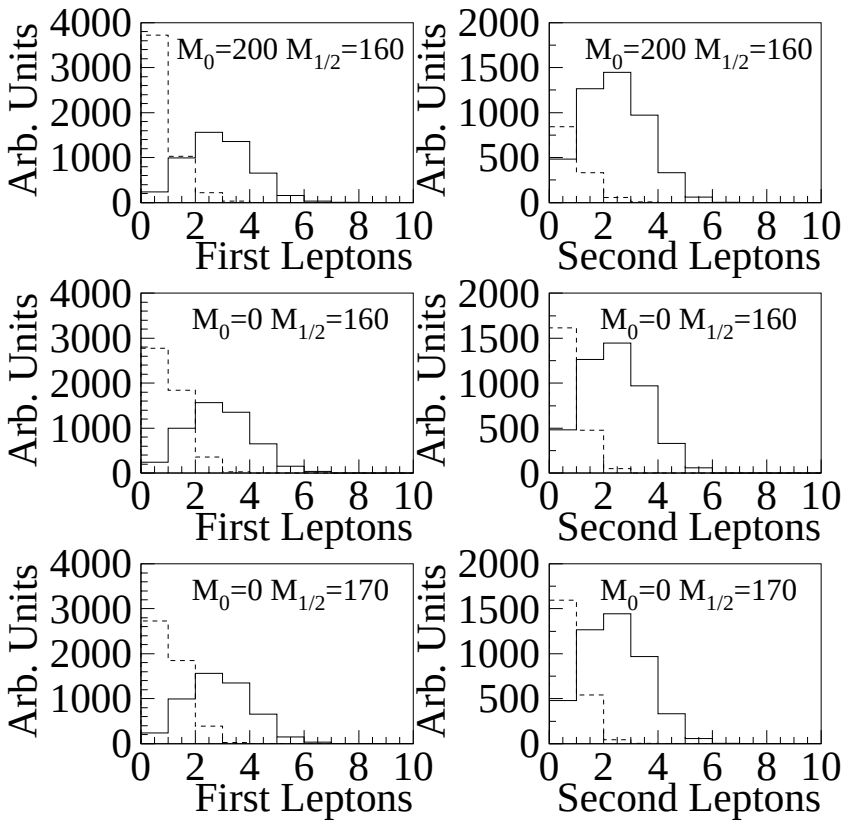

Abbildung 7.2: *The number of first (left) and second (right) leptons found for three scenarios. The solid lines give the spectrum for the scenario with R_P violation, the broken lines the spectrum with R_P conservation.*

in the detector should be flagged as originating from GENP leptons. Still due to the small size of the cone used some leptons will be flagged as not originating from GENP leptons. In a next step the parent of the GENP lepton is read from the GENP bank. If the parent is a LSP a flag is set to indicate this. If a lepton seen in the detector has more than one GENP lepton inside the cone of 0.1 only one flag is set. In this case the lepton is flagged as coming from the LSP if the parent particle of one of the candidates is an LSP. The signal MC runs were checked for leptons which can be associated to more than one GENP lepton. The maximum number found was 34 leptons in 5000 events. This means that about half a percent of the events contain leptons for which the parent can not be determined without ambiguities. As only events with 3 or more leptons are investigated this affects less than 0.2 percent of the leptons and thus does not change the results.

The scenarios used for the comparison of the lepton rates from LSPs and from cascade decays are given in table 7.1. One sees that most of the identified leptons originate from LSPs. The contribution from this source falls with rising $M_{1/2}$. This can be explained by the harder spectrum the cascade leptons have at higher $M_{1/2}$. Then the probability for a lepton from the cascade decay to be accepted rises. Another general feature is that with higher $M_{1/2}$ a higher percentage of the leptons are accepted, which can be explained with the harder spectrum at higher $M_{1/2}$. In most cases the dependence on M_0 is weaker than the one on $M_{1/2}$. Still due to the effects discussed in the next subsection changes in M_0 can also have large effects in some areas of the parameter space.

7.2.2 The Leptonic Branching Ratio in Cascade Decays

The changes in the leptonic branching ratio can be quite dramatic in a very small area of parameter space. As an example the number of leptons per decaying second lightest neutralino and lightest chargino are discussed in dependence of M_0 for $M_{1/2}$=140 GeV.

For high values of $M_{1/2}$ almost all produced SUSY particles will be charginos or neutralinos. Thus this discussion considers only their decays.

The number of leptons per produced particle is calculated by summing over the produced number of leptons in all decay channels. Here electrons and muons are taken into account, but contributions from the leptonic decay of taus are neglected:

$$R_L(\text{parent particle}) = \text{Number of leptons per parent particle.}$$

The Decay of Neutralinos

In the upper picture of figure 7.3 the average number of leptons per produced second lightest neutralino ($R_L(\tilde{\chi}_2^0)$) is given. For low values of M_0 a cascade decay of the second lightest neutralino to the lightest neutralino produces and average of about 0.3 leptons.

M_0	$M_{1/2}$	Total	Source Electron 1 (percent)			Total	Source Muon 1 (percent)		
		Electrons	LSP	Other	Unknown	Muons	LSP	Other	Unknown
0	170	1836	77	23	0	754	57	43	0
200	160	1595	84	16	0	587	65	35	0
0	160	1801	77	23	0	719	53	47	0
100	150	1826	78	22	0	738	55	45	0
50	150	1725	86	14	<0.1	684	66	34	0
100	100	1366	85	15	0.1	557	63	37	0
50	100	1395	88	11	0.3	489	70	31	0
50	50	901	82	18	0.4	330	55	45	0

M_0	$M_{1/2}$	Total	Source Electron 2 (percent)			Total	Source Muon 2 (percent)		
		Electrons	LSP	Other	Unknown	Muons	LSP	Other	Unknown
0	170	1580	80	20	0.2	1010	54	44	2
200	160	1448	87	13	0.3	587	67	30	3
0	160	1627	81	19	0.2	893	54	44	2
100	150	1653	83	17	0.4	911	55	43	2
50	150	1548	82	18	0.3	861	58	39	3
100	100	1220	84	16	0.4	703	62	34	4
50	100	1208	84	16	0.5	676	65	31	4
50	50	764	88	12	0.4	467	70	24	7

M_0	$M_{1/2}$	Total	Source Electron 3 (percent)			Total	Source Muon 3 (percent)		
		Electrons	LSP	Other	Unknown	Muons	LSP	Other	Unknown
0	170	1831	84	16	0.4	759	64	31	5
200	160	1482	88	12	0.4	700	63	27	10
0	160	1736	86	14	0.3	784	66	29	5
100	150	1720	81	19	0.3	844	54	42	4
50	150	1697	84	15	0.4	712	61	35	5
100	100	1300	85	14	0.7	623	61	31	8
50	100	1310	89	10	1.2	374	65	30	6
50	50	855	91	8	0.8	376	67	23	9

M_0	$M_{1/2}$	Total	Source Electron 4 (percent)			Total	Source Muon 4 (percent)		
		Electrons	LSP	Other	Unknown	Muons	LSP	Other	Unknown
0	170	846	83	17	0.6	359	60	32	8
200	160	610	78	21	1.0	260	56	31	13
0	160	766	86	13	0.5	381	65	29	6
100	150	779	78	22	0.5	430	49	45	6
50	150	735	85	14	0.1	324	56	35	8
100	100	461	84	16	0.4	244	59	33	8
50	100	488	86	14	0.4	210	70	21	9
50	50	248	92	8	0.4	112	71	19	10

Tabelle 7.1 : *The origin of the leptons seen in the detector for several signal scenarios. For each scenario 5000 events were processed.*

In this area of parameter space the dominant channels are

$M_0 = 10$ GeV

Decay Channels					Branching Ratio
$\tilde{\chi}_2^0$	$\rightarrow$	$\tilde{\nu}\nu$	$\rightarrow$	$\tilde{\chi}_1^0\nu\nu$	79.4
$\tilde{\chi}_2^0$	$\rightarrow$	$\tilde{l}_L^{\mp}l^{\pm}$	$\rightarrow$	$\tilde{\chi}_1^0 l^{\mp}l^{\pm}$	12.9
$\tilde{\chi}_2^0$	$\rightarrow$	$\tilde{\tau}_L^{\mp}\tau^{\pm}$	$\rightarrow$	$\tilde{\chi}_1^0\tau^{\mp}\tau^{\pm}$	6.5.

Smaller contributions come from the decay through the right handed charged sleptons including staus. About 80% of the neutralinos decay into neutrinos and the LSP, thus the leptonic branching ratio is small.

With rising M_0 the masses of the lightest chargino (127.5 GeV) and the two lightest

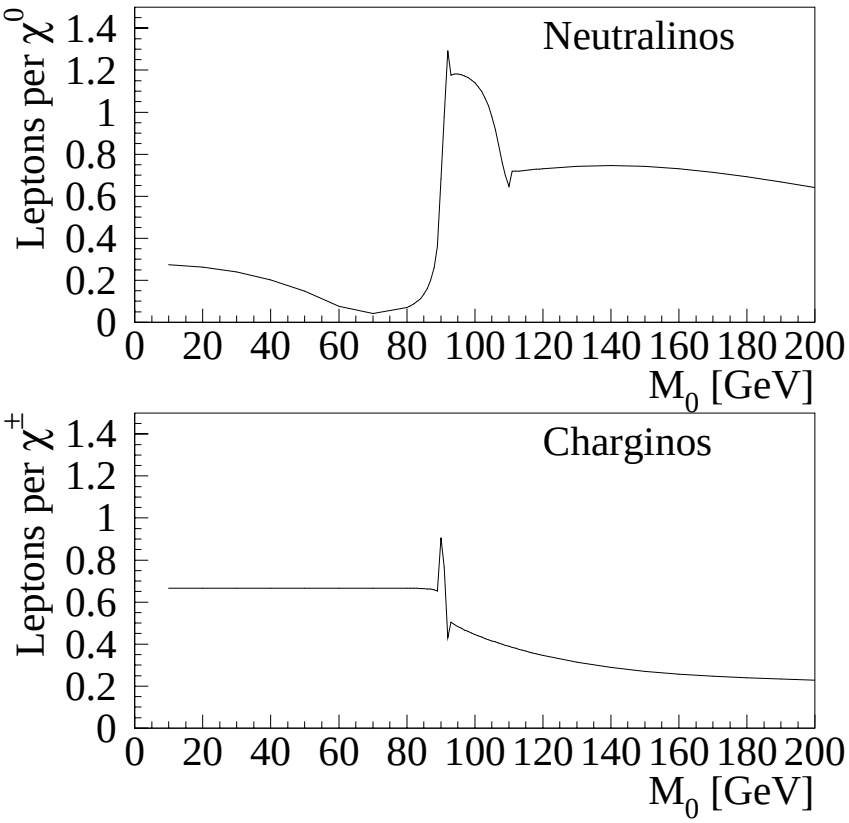

Abbildung 7.3: *The average number of leptons produced in the decay of neutralinos (top) and charginos (bottom). M_0 is fixed to 140 GeV, while M_0 is varied. The "jumps" that can be seen for M_0=93 GeV and M_0=110 GeV in the upper plot and at M_0=92 GeV in the lower plot are due to numerical effects in the MC generator.*

neutralinos (61.0 GeV and 127.5 GeV) change only slightly. On the contrary the masses of the squarks and sleptons change significantly. The dependence of the masses of the light gauginos and the sleptons on M_0 is shown in figure 7.4. The masses for all slepton generations are degenerate. For the scenario discussed here the mass difference between the second neutralino and the lightest chargino is negligible. The mass of the left handed charged sleptons is 108.4 GeV for $M_0 = 10$ GeV and has the same mass as the second lightest neutralino near $M_0 = 70$ GeV. The masses of the sneutrinos and the right handed charged sleptons rise in a similar way. Thus with rising M_0 the value of $R_L(\tilde{\chi}_2^0)$ falls slowly until it reaches a minimum of about 0.075 near $M_0 = 70$ GeV, where the decay into left-handed charged slepton becomes forbidden.

$M_0 = 70$ GeV

Decay Channels					Branching Ratio
$\tilde{\chi}_2^0$	$\rightarrow$	$\tilde{\nu}\nu$	$\rightarrow$	$\tilde{\chi}_1^0\nu\nu$	97.0
$\tilde{\chi}_2^0$	$\rightarrow$	$\tilde{l}_R^{\mp}l^{\pm}$	$\rightarrow$	$\tilde{\chi}_1^0 l^{\mp}l^{\pm}$	1.9
$\tilde{\chi}_2^0$	$\rightarrow$	$\tilde{\tau}_R^{\mp}\tau^{\pm}$	$\rightarrow$	$\tilde{\chi}_1^0\tau^{\mp}\tau^{\pm}$	1.0

In the region between M_0=70 GeV and $M_0 = 90$ GeV the decay into the sneutrino dominates. The branching ratios into right handed sleptons drop further because the parameter space for this channel is closing.

$M_0 = 89.8$ GeV

Decay Channels					Branching Ratio
$\tilde{\chi}_2^0$	$\rightarrow$	$\tilde{\nu}\nu$	$\rightarrow$	$\tilde{\chi}_1^0\nu\nu$	62.2
$\tilde{\chi}_2^0$	$\rightarrow$	$\tilde{l}_R^{\mp}l^{\pm}$	$\rightarrow$	$\tilde{\chi}_1^0 l^{\mp}l^{\pm}$	23.6
$\tilde{\chi}_2^0$	$\rightarrow$	$\tilde{\tau}_R^{\mp}\tau^{\pm}$	$\rightarrow$	$\tilde{\chi}_1^0\tau^{\mp}\tau^{\pm}$	11.8

At $M_0 = 90$ The mass of the sneutrino and the second neutralino are equal and the only allowed decays now are decays into right handed sleptons. At the same point $\tilde{\chi}_2^0 \rightarrow \tilde{\tau}_R^{\mp}\tau^{\pm}$ becomes kinematically impossible and fades out quickly. With all other processes forbidden the decay into the right handed selectron and smuon dominate. This has the net effect of increasing the number of leptons produced per neutralino dramatically. At $M_0 = 92.3$ GeV $R_L(\tilde{\chi}_2^0)$ reaches a maximum of 1.32. At this point the decays channel into real sneutrinos is closed. For still higher values of M_0 $R_L(\tilde{\chi}_2^0)$ falls again as the parameter space for the decay into the right handed sleptons closes. As a consequence the decays through virtual sneutrinos in the channel $\tilde{\chi}_2^0 \rightarrow \tilde{\chi}_1^0\nu\bar{\nu}$ become more important. At $M_0 = 110$ GeV all sleptons are heavier than the second neutralino and thus all decays into real sleptons are forbidden. For still higher values of M_0 the leptonic branching ratio falls slowly. The exchanged sleptons become heavier and thus have to be more virtual. As there are no more channels opening or closing, the branching ratio is a continuous function of M_0.

The "jumps", in $R_L(\tilde{\chi}_2^0)$, which can be seen at the point of the maximum in the upper plot of figure 7.3 and again at M_0= 110 GeV are due to numerical effects in the

MC. As long as a decay into two real particles is kinematically allowed the MC will disregard the decays where one of these two particles is slightly virtual. The effect of this is small as long as the parameter space for the decay is large. If a channel closes the decay into a real particle will first be followed to the point where the channel is completely closed. Then the channel containing virtual particles is considered. This leads to a "jump" in the number of leptons per particle.

The Decay of Charginos

The M_0–dependence of the leptonic branching ratio of the charginos is smoother than the one of the neutralinos. Still there are drastic changes at several points. The

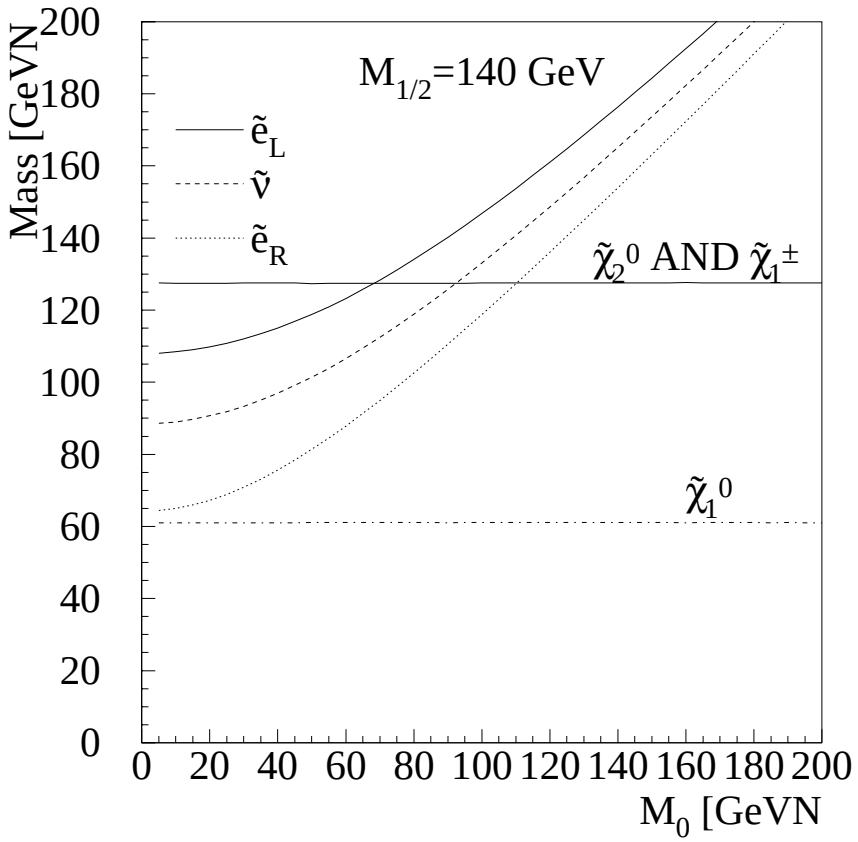

Abbildung 7.4: *The M_0 dependence of the masses of the charged left-handed slepton (solid line), right-handed slepton (dotted line) and sneutrinos (broken line). The three slepton generations are mass degenerate. The lower straight line gives the mass of the lightest neutralino, which is the LSP. The upper straight line gives the masses of the second neutralino and the lightest chargino, which have degenerate masses.*

behaviour of the branching ratio can be read from the lower picture in figure 7.3.

For low values of M_0 the decay of a chargino produces an average of 0.66 charged leptons. The most important channels are

$M_0 = 10$ GeV

Decay Channels			Branching Ratio
$\tilde{\chi}_1^{\pm}$	$\rightarrow$	$\tilde{\nu} l$	50.2
$\tilde{\chi}_1^{\pm}$	$\rightarrow$	$\tilde{\nu}_\tau \tau$	25.1
$\tilde{\chi}_1^{\pm}$	$\rightarrow$	$\tilde{l}_L \nu$	16.5

With rising M_0 the decay into $\tilde{\chi}_1^0 \tilde{l} \nu$ fades out because the mass of the left handed charged sleptons approaches the mass of the lightest chargino. At the same time the decay into $\tilde{\chi}_1^0 \tilde{\nu} l$ increases, leaving $R_L(\tilde{\chi}_1^{\pm})$ almost constant up to a M_0 value of 89.5 GeV.

$M_0 = 89.5$ GeV

Decay Channels			Branching Ratio
$\tilde{\chi}_1^{\pm}$	$\rightarrow$	$\tilde{\tilde{\nu}} l$	61.3
$\tilde{\chi}_1^{\pm}$	$\rightarrow$	$\tilde{\tilde{\nu}}_\tau \tau$	30.6

At this point the decay into sneutrino and tau becomes forbidden because of the tau mass and $R_L(\tilde{\chi}_1^{\pm})$ jumps to 0.929. The leptonic branching ratio will increase significantly at this point. Within a small area of M_0 the channel leading to $\tilde{\chi}_1^0 \tilde{\nu} l$ also fades out as the sneutrino mass approaches the chargino mass. $R_L(\tilde{\chi}_1^{\pm})$ reaches a minimum of 0.426 at $M_0 = 92.1$ GeV. At this point all decay channel to real sleptons have closed and the only decays still possible are through virtual sleptons.

$M_0 = 92.2$ GeV

Decay Channels			Branching Ratio
$\tilde{\chi}_1^{\pm}$	$\rightarrow$	$\tilde{\chi}_1^0 l \nu$	0.515
$\tilde{\chi}_1^{\pm}$	$\rightarrow$	$\tilde{\chi}_1^0 \tau \nu_\tau$	0.258
$\tilde{\chi}_1^{\pm}$	$\rightarrow$	$\tilde{\chi}_1^0 q \bar{q}$	0.227

For still higher values of M_0 the decay channels stay the same as there are no more channels opening and closing. As the masses of the squarks rise more slowly than the slepton masses, the leptonic branching ratio slowly falls. At $M_0 = 200$ GeV the value of $R_L(\tilde{\chi}_1^{\pm})$ is 0.229.

7.3 The Influence of the Cascade Decays on the Signal Strength

The contribution of the cascade decays to the total number of leptons in the signal events is below 50 % for all scenarios investigated and in the order of 20 % for electrons and 30 % for muons for most scenarios. This is large enough to make a significant influence. If one of the leptonic channels closes this will have a non–negligible effect on number of leptons seen. For the scenarios discussed in this subsection the rate of

leptons per neutralino reaches a minimum around $M_0 = 70$ GeV. The rate rises slowly after this point while at the same time the mass of the right handed slepton approaches the mass of the second neutralino. At M_0=80 GeV the mass difference is more than 30 GeV, while it has dropped to about 15 GeV at M_0=90 GeV. The leptons produced in this region will have low momenta because of the small mass difference. Concluding one expects a minimum of the signal strength in the area between M_0=70 GeV, where the decay into the left handed charged sleptons closes and M_0=92 GeV, where the decay into the sneutrinos closes.

7.4 Signal Cross Sections and Efficiencies

The efficiency for finding four leptons depends on the values of M_0 and $M_{1/2}$. It is lowest for scenarios with small values of $M_{1/2}$. The signal in this regions is still visible, because the cross-sections rise faster than the efficiencies drop. The efficiencies for scenarios with cross-section below 5 pb^{-1}, which corresponds to event numbers of less than 440 were checked. Here the efficiencies vary between 10 and 20 %.

Tables 7.2 and 7.3 show the ISAJET cross section, efficiency, and number of events for various scenarios. The cross section depends mainly on $M_{1/2}$, as shown in Fig. 12.1 but changes only slightly with M_0 (see Fig. 12.2).

The detection efficiency on the other hand depends only weakly on $M_{1/2}$, but strongly on M_0. In general the detection efficiency rises with M_0, however there is a dip at $M_0 = 90$ GeV. For $M_{1/2} = 140$ GeV the efficiency drops from 20% at $M_0 = 80$ GeV to about 11% for $M_0 = 88$ GeV and then again rises sharply to 24% at $M_0 = 100$ GeV. The behaviour is often seen in mSUGRA searches in leptonic channels [42]. The cause of this behaviour is rather complex and can be understood by looking at the SUSY particle spectrum, decay channels and cross sections.

The mass of the lightest neutralino changes only slightly with M_0. This means that the kinematics of the LSP decay remains unchanged and the effect is caused by changes in the cascade decays only.

For low values of M_0 the cross sections for chargino pair production and chargino-neutralino production are of similar size. The number of charged leptons from cascade decays is relatively high because of the large number of charginos which on average produce more leptons. With increasing M_0 chargino-neutralino production starts dominating. The ratio of the two cross sections reaches a maximum of

$$\frac{\sigma(p\bar{P} \to \chi^0\chi^0)}{\sigma(p\bar{P} \to \chi^0\chi^\pm)} = 1.8$$

at $M_0 = 90$ GeV and then gets closer to 1 again for still higher values of M_0. At $M_0 = 90$ GeV the number of charginos produced is only one fifth of the number of neutralinos. The number of leptons per chargino is still about 0.7, while the number of leptons per neutralino has dropped to about 0.1.

This explains why the number of leptons originating from cascade decays has a minimum in this region.

M_0(GeV)	$M_{1/2}(GeV)$	Cross Section (pb)	Efficiency	Four-lepton Events in 87.5 pb^{-1}
0	130	0.89	0.16	12.7
0	140	0.59	0.17	9.0
0	150	0.42	0.19	7.0
0	160	0.29	0.20	5.0
50	130	0.89	0.15	11.8
50	140	0.60	0.16	8.3
50	150	0.41	0.18	6.3
50	160	0.29	0.19	4.9
90	140	0.56	0.11	5.6
90	150	0.40	0.10	3.6
100	130	0.80	0.14	10.0
100	140	0.56	0.19	9.1
100	150	0.40	0.21	7.4
100	160	0.28	0.22	5.4
100	170	0.21	0.17	3.1
150	130	0.73	0.14	9.0
150	140	0.53	0.14	6.6
150	150	0.39	0.15	5.0
150	160	0.28	0.16	3.8
200	130	0.70	0.13	7.8
200	140	0.51	0.14	6.3
200	150	0.37	0.14	4.5
200	160	0.27	0.15	3.5

Tabelle 7.2 : *Cross section, efficiency and number of four-lepton events for various scenarios with $M_0 \leq 200$ GeV.*

M_0(GeV)	$M_{1/2}(GeV)$	Cross Section (pb)	Efficiency	Four-lepton Events in 87.5 pb^{-1}
250	140	0.50	0.13	5.5
250	150	0.37	0.13	4.3
250	160	0.27	0.13	3.1
300	130	0.71	0.10	6.5
300	140	0.50	0.11	4.8
300	150	0.37	0.12	4.0
350	130	0.71	0.10	6.5
350	140	0.52	0.11	5.0
350	150	0.38	0.11	3.9
400	130	0.73	0.10	6.6
400	140	0.54	0.11	5.0
400	150	0.39	0.11	3.7
450	130	0.76	0.09	6.3
450	140	0.55	0.10	4.8
450	150	0.41	0.10	3.7
500	130	0.77	0.09	5.9
500	140	0.57	0.10	4.9
500	150	0.42	0.11	3.9

Tabelle 7.3 *: Cross section, efficiency and number of four-lepton events for various scenarios with $M_0 \geq 250$ GeV.*

8 Data Sample and Event Selection

The analysis starts from the Run IB SUSY-Dilepton sample, which is described in [29]. This sample contains 457,478 events passing the Run IB level 3 dilepton trigger (COMBINED_EXOB_DIL). The events passing this trigger were written to the XDLB_5P PAD tapes. The trigger accepts any two leptons at level three without a level two prerequisite.

The data taken during Run I with CDF were divided up into three streams labelled stream A, B and C. The data were processed according to the stream they belonged to and written to EXABYTE 8mm tapes. The XDLB_5P tapes were part of stream B. The 5P in the name indicates that the tapes contain one of the 28 PAD streams of Run IB. Events passing the COMBINED_EXOB_DIL trigger have to contain at least one central lepton ($|\eta| < 1$) with a transverse momentum (transverse energy for electrons) of more than eight GeV/c. They also must have a second lepton, which may be either central or a plug electron. Its energy (momentum for muons) must be higher than three GeV.

The leptons of the events selected for the SUSY dilepton sample must pass tighter requirements than the ones demanded in the trigger. The first lepton must be a CEM electron or a CMU/P muon meeting the requirements in table 8.1. The other lepton may be either a CEM or PEM electron or a CMU/P, CMX or CMIO muon fulfilling the requirements given in table 8.2.

First Electron	
CEM	
P_{T}	$\geq$ 6.0 GeV/c
E_{T}	$\geq$ 8.0 GeV
E/P	$\leq$ 2.0
H/E	$\leq$ 0.05
$\mathrm{L_{SHR}}$	$\leq$ 0.2
$\lvert\Delta x\rvert$	$\leq$ 3.0 cm
$\lvert\Delta z\rvert$	$\leq$ 5.0 cm
χ^2	$\leq$ 10.0

First Muon	
CMU/CMP	
P_{T}	$\geq$ 7.5 GeV/c
E_{EM}	$\leq$ 2.0 GeV
E_{Had}	$\leq$ 6.0 GeV
d_0 (raw)	$\leq$ 0.5 cm
CMU matching	$\lvert\Delta x\rvert \leq 2$ cm or $\chi^2_{\mathrm{CTC}} \leq 9$
CMP matching	$\lvert\Delta x\rvert \leq 5$ cm or $\chi^2_{\mathrm{CTC}} \leq 9$

Tabelle 8.1 : *The selection requirements for the SUSY dilepton sample tight leptons.*

The lepton identification cuts follow closely the cuts and definition of [30]. The electron identification cuts are based on the properties measured in the calorimeters and on the associated track measured in the CTC

Second Electron	
CEM	PEM
$P_{\mathrm{T}} > 2.8$ GeV/c	–
$E_{\mathrm{T}} > 4.0$ GeV	$E_{\mathrm{T}} > 4.0$ GeV
$E/P < 2.0$	–
$H/E < 0.055 + 0.045 * E/100$	$H/E \leq 0.1$
$\mathrm{L_{SHR}} < 0.2$	–
$\Delta x < 3.0$ cm	–
$\Delta z < 5.0$ cm	–
$\chi^2_{\mathrm{strip}} < 15$	$\chi^2_{3\times3} \leq 3.0$
–	$\mathrm{VTX_{occupancy}} \geq 0.5$

Second Muon		
CMU/CMP	CMUO	CMIO
$P_{\mathrm{T}} > 2.8$		$P_{\mathrm{T}} > 10$
$E_{\mathrm{EM}} < 2.0$ GeV		
$E_{\mathrm{Had}} < 6.0$ GeV		
$D_0 < 0.8$ cm		
CMU matching $\lvert\Delta x\rvert \leq 2$ cm or $\chi^2_{\mathrm{CTC}} \leq 9$		–
CMP matching $\lvert\Delta x\rvert \leq 5$ cm or $\chi^2_{\mathrm{CTC}} \leq 9$		–
CMX matching $\lvert\Delta x\rvert \leq 5$ cm or $\chi^2_{\mathrm{CTC}} \leq 9$		–

Tabelle 8.2 : *The SUSY dilepton sample loose lepton selection cuts.*

- p_{T} is the transverse momentum of the track associated with the electron candidate as measured in the CTC.

- E_{T} is the transverse energy of the electro–magnetic cluster associated with the candidate.

- The ratio of the momentum and the energy of the candidate E/p. The requirement of $E/p < 2$ assures that the electron energy and its momentum agree roughly. cutting on this variable allows rejection of photons from π^0 decays.

- H/E is the ratio of hadronic to electro magnetic energy associated with the cluster. This variable will have small values for electrons, while having larger values for hadrons. The sliding cut for loose CEM electrons was originally introduced for Z' searches and is still used for historical reasons. The cut is always looser than the fixed cut used for the primary electron.

- L_{SHR}, the transverse shower profile of the electromagnetic tower. This variable is defined as

$$L_{SHR} = 0.14 \sum_i \frac{E_i^{adj} - E_i^{prob}}{\sqrt{0.14^2 E + (\Delta E_i^{prob})^2}},$$

  where the sum goes over all towers in the electro-magnetic cluster. E_i^{adj} and E_i^{prob} are the measured and the expected energy in the tower. The expected energy is calculated from parametrised test beam data for electrons. The denominator normalises the addends to their total error. $0.14E$ is the uncertainty in the energy measurement and ΔE_i^{prob} is the uncertainty of the energy estimate. Hadrons will have a shower profile different from electrons and thus will be rejected by a cut on L_{SHR}.

- To calculate the track-shower matching parameters Δx and Δz the track position is extrapolated to the CES. The extrapolated position is compared to the position measured in the CES. The Δx and Δz are the differences between the two values in x and z-direction respectively. Cutting on the two variables allows rejecting background from overlap between charged and neutral hadrons.

- χ^2_{strip} is a fit of the energy deposited in the CES strips to the profile determined during the test beam. The fit uses the 11 strips in z-direction per CES chamber.

- For plug electron candidates the $\chi^2_{3\times3}$ is the result of a fit of the lateral energy sharing in three towers each in ϕ and η. The shape used in the fit was determined in a test beam.

- The $VTX_{occupancy}$ cut gives the ratio of VTX layers in which the electron deposited energy compared to the layers in which it could deposit energy according to its trajectory. The cut serves to reject photons in the plug.

For the muon selection the main cuts are based on information obtained from the CTC and the muon chambers. Cuts on calorimeter data serve to verify that a minimal ionising particle passed through the detector.

- p_T is as for electrons the transverse momentum of the associated track measured in the CTC. The difference to the electron selection is that there is no independent measurement of the energy for muons.

- The cuts on the electromagnetic E_{EM} and the hadronic energy E_{Had} reject hadron punch-throughs. Hadrons would deposit a significant amount of energy in the calorimeters.

- The impact parameter d_0(raw) measures the distance of the origin of the muon to the interaction point. The cut mainly rejects cosmic muons.

- The CMU/CMP/CMX matching cuts require that the CTC track extrapolated to the muon chambers matches with the muon chamber stubs. Either the distance in $r-\phi$ direction ($|\Delta x|$) or the fit of the track to the muon stub must meet the requirement.

For this analysis the cuts on the two trigger leptons are further tightened. The first and second lepton must pass the tightened cuts. In addition two more leptons passing the same cuts as the second lepton are required. There is no discrimination between electrons and muons at any stage. Thus any of the four leptons may be either an electron or a muon. The tightened selection criteria are the ones used in most electron-based analyses of the CDF SUSY working group. The E_{T} and p_{T} cuts are tightened to assure that they are outside the region of the trigger turn on. The first lepton has to be central with a corrected E_{T} (P_{T} for muons) of at least 12 GeV. If the lepton candidate is an electron the p_{T} cut is tightened from 6 GeV/c to 8 GeV/c. The other three leptons are accepted if their E_{T} (p_{T} for muons) is above 5 GeV (10 GeV for CMIO muons). For electrons the p_{T} must be higher than 3 GeV/c. Also the electron matching cuts are tightened to $|\Delta x| \leq 1.5$ cm and $|\Delta z| \leq 3.0$ cm. In addition to the trigger requirements there are several new constraints.

- The Good Tracks cut requires the CTC-track associated with the lepton to be a 3-dimensional helix with hits in 6 layers. There have to be three hits in an axial layer or 2 hits in a stereo layer. This ensures that the track is well defined.

- The event must have a vertex of class 10 or higher within 60 cm of the interaction point. The class describes the quality of a vertex. A vertex with class ten or higher is consistent with a beam-beam interaction.

- The distance between the first lepton and one vertex of class 10 or higher must be less than 5 cm. The distance between this vertex and all other leptons must be less than 10 cm. This cut ensures that the leptons all come from the same, good vertex.

- The sum of electro-magnetic and hadronic energy deposited in the calorimeter must be higher than 0.1 GeV for muons in order to make sure that there was really a particle that passed through the calorimeter.

- For muons in addition to the raw impact parameter cut there is a tighter cut on the beam constrained impact parameter.

- The leptons have to be separated by $\Delta R > 0.4$. Here ΔR is defined as

$$\Delta R = \sqrt{(\eta_1 - \eta_2)^2 + (\varphi_1 - \varphi_2)^2)}.$$

  If the distance of a lepton to an already identified lepton is less than 0.4 the new lepton is rejected.

Electron 1	other Electrons
CEM	CEM
$P_{\mathrm{T}} > 8$ GeV/c	$P_{\mathrm{T}} > 3$ GeV/c
$E_{\mathrm{T}} > 12$ GeV	$E_{\mathrm{T}} > 5$ GeV
$E/P < 2$	$E/P < 2$
$H/E < 0.05$	$H/E < 0.055 + 0.045 * E/100$
$\mathrm{L_{SHR}} < 0.2$	$\mathrm{L_{SHR}} < 0.2$
$\Delta X < 1.5$ cm	$\Delta X < 3.0$ cm
$\Delta Z < 3.0$ cm	$\Delta Z < 5.0$ cm
$\chi^2 < 10$	$\chi^2 < 15$
$\Delta Z_0 < 5$ cm	$\Delta Z_0 < 10$ cm
Good Tracks	–

Tabelle 8.3 : *The electron requirements used in this analysis. The first column giving the cuts for the high E_{T} electron, the second column the cuts for the other three electrons.*

- Plug electrons are rejected.

The lepton cuts are summarised in table 8.3 for electrons and table 8.4 for muons.

The SUSY dilepton sample includes events from runs in which part of the detector was not in working order. All events from these runs were rejected using the offline routine BADRUN. This routine compares the run number to a database containing information about the state of the detector during the data taking [31]. Only runs for which BADRUN reports a fully operational detector were accepted for analysis.

Muon 1
CMU/CMP
$P_{\mathrm{T}} > 12$ GeV/c
$E_{\mathrm{EM}} < 2$ GeV
$E_{\mathrm{Had}} < 6$ GeV
$E_{\mathrm{EM}} + E_{\mathrm{Had}} > 0.1$ GeV
D_0(raw) < 0.5 cm
CMU/CMP matching
Good Tracks
D_0(Beam) < 0.2 cm
$\Delta Z_0 < 5$ cm

other Muons		
CMU/CMP	CMUO	CMIO
$P_{\mathrm{T}} > 5$ GeV/c		$P_{\mathrm{T}} > 10$ GeV/c
$E_{\mathrm{EM}} < 2$ GeV		
$E_{\mathrm{Had}} < 6$ GeV		
$E_{\mathrm{EM}} + E_{\mathrm{Had}} > 0.1$ GeV		
D_0(raw) < 0.8 cm		
CMU/CMP matching	CMUO matching	–
Good Tracks		
D_0(Beam) < 0.5 cm		
$\Delta Z_0 < 10$ cm		

Tabelle 8.4 : *The muon selection cuts used in this analysis. The first table gives the cuts for the central high P_{T} muon. The second table shows the cuts for the other three muons.*

9 Standard Model Background

The production of four real leptons in one event is a very rare occurrence in the SM. Processes that can produce four real leptons have either a small cross-section (Z^0-pair production) or a small branching fraction into leptons (top-pair and heavy-quark ($b\bar{b}$) production). In the rare cases in which an event contains four real leptons they will not necessarily all be seen. The central detector of CDF covers a pseudorapidity range of $|\eta| < 1.1$. All leptons with higher pseudorapidity will not be accepted. If the rapidity of the leptons is less than 1.1 they can hit an uninstrumented area of the detector or their energy can be too low for them to be detected. This further reduces the number of SM-events with four real leptons seen in the detector.

The main source of four lepton events will be processes with three real leptons, where a jet passes all lepton requirements and is misidentified as a lepton. This is the more probable as the lepton cuts used in this analysis are very loose. In this chapter the SM backgrounds to the signal will be investigated. First the number of three and four lepton events expected from MC will be investigated. Then the main background, the fake leptons will be considered.

9.1 Real Lepton Background

The definition of real and fake leptons is somewhat arbitrary. There is no way of knowing if a particle which fulfilled all lepton requirements was really a lepton. It is always possible that such a particle really is a hadron which passed the requirements by pure chance.

The SM MCs used do not simulate the low energy resonances correctly. In addition the detector MC does not model the mis-identification of jets as leptons correctly. In the remainder of this thesis real leptons are defined as leptons which are simulated by our MC programs.

To determine how many events with three and four real leptons are expected in the data a large number of background MC was studied. All simulated processes can produce events with three real leptons. All except Drell-Yan and $W^{\pm}Z^0$ can produce events with four real leptons.

1. $t\bar{t}$ ($m_t = 175$ GeV)
2. Dibosons (ZZ, WZ)
3. Drell-Yan
4. Heavy quark ($b\bar{b}$, $c\bar{c}$)

In order to determine the contribution of real leptons from SM processes to the signal channel we used the full statistics from the CDF SUSY working group MC samples [35] relevant to this analysis.

The generation of MC events consumes a lot of computing time. In order to make optimal use of the available computers one avoids to generate events which will not pass the event selection cuts. In the case of the MC used for this analysis the parameters used was the exchanged momentum p_{T}. Not limiting this variable would yield the best results because all events in a certain channel would be simulated. Still most of the events with small p_{T} will result in particles with small momenta, whose decay products would not pass the selection cuts. Not generating these events changes the results only slightly, but saves a significant amount of computing time. The lower limits were set as high as possible without missing events. Decay products of heavy particles can be seen even if the particles are produced at rest. Thus the momentum limit decreases with increasing mass of the produced particles. The limit was set to be efficient for dileptons with transverse momenta of 8 GeV/c for the first and 3 GeV/c for the second lepton Similarly the upper limit of the exchanged momentum was set to 500 GeV/c. This is legitimate because the number of events with momentum transfer in excess of this value will be negligible, although the computing time necessary to calculate these events is no.

$b\bar{b}/c\bar{c}$ Production

Tho estimate the number of leptons expected from heavy quarks a MC for $b\bar{b}/c\bar{c}$–production was used. The main contribution will come from $b\bar{b}$, because b quarks may decay leptonically into c–quarks, which then may continue to decay leptonically. The production of $b\bar{b}/c\bar{c}$ MC was split up into 3 generation processes: direct production, production including initial state gluon radiation (ISR) and production including final state gluon radiation (FSR). Each of these processes was again split up in three areas according to the exchanged momentum q. The nine data sets were generated as separate runs. For each of the runs the event generation was performed for at least the three structure functions CTEQ2L, MRSD0' and GRV_LO. For runs with high q also the function CTEQ3L was used. In addition the function GRV_94 was used for the direct production with 25 GeV $< q <$ 50 GeV and for the two runs including FSR and having $q >$ 25 GeV. Cuts on the generator level particles were applied in order to minimise the computing time for the detector simulation. These cuts were designed to reject events which would not pass the selection cuts. $b\bar{b}/c\bar{c}$ events must contain the following particles at generator level to be accepted:

- At least one b or c quark with a transverse momentum above 10 GeV/c in the rapidity region of $|y| < 4$.
- At least one lepton with a transverse momentum larger than 9.0 GeV/c in the pseudo–rapidity range $|\eta| < 1.5$ or alternatively two leptons with a $p_{\mathrm{T}} > 2.8$ GeV/c and a pseudorapidity less than 3.

The number of events generated for each run exceeds the number of events expected with the luminosity accumulated during Run IB by at least a factor of two. There are

Run Number	Type of Production	q range [GeV]	Additional Structure functions	Integrated Luminosity [pbarn^{-1}]
81	direct	10–25	–	175.1
82	direct	25–50	CTEQ3L, GRV_94	442.7
83	direct	50–500	CTEQ3L	1401.4
84	ISR	10–25	–	286.1
85	ISR	25–50	CTEQ3L	581.2
86	ISR	50–500	CTEQ3L	1852.6
87	FSR	10–25	–	286.5
88	FSR	25–50	CTEQ3L, GRV_94	545.9
89	FSR	50–500	CTEQ3L, GRV_94	1425.9

Tabelle 9.1 : *The $b\bar{b}/c\bar{c}$ MC samples. The structure functions CTEQ2L, MRSD0' and GRV_LO were used for all samples. Additional functions are listed.*

no significant changes in the results using different structure functions. Table 9.1 gives details on the event generation.

Running the analysis code over the $b\bar{b}/c\bar{c}$ MC samples yielded a total of 47.0 ± 2.6 events with exactly three leptons. The number was calculated by adding up all events with exactly three leptons with the weight according to MC_WGT. The number was multiplied by a factor of 0.85 to correct for the efficiency of QFL'. An additional correction had to be applied because MC_WGT assumes an integrated luminosity of 88.76 pb^{-1}, while the SUSY dilepton sample has an integrated luminosity of 87.5 pb^{-1}. The error given is the statistical error due to the number of MC-events which passed the three-lepton requirement. Using the same methods the number of events with four was calculated to be 0.28 ± 0.14.

Drell-Yan production

Three runs of Drell-Yan MC were used to determine the number of events expected from this background. All runs restricted the transfered momentum to the region 5 GeV$< q <$ 500 GeV. The first run was photon-exchange only, while the two other runs were Z^0-exchange in two regions of exchanged transverse momentum q_{T}. Only events containing either on high–p_{T} lepton or two low–p_{T} leptons were passed on to the detector simulation. The cuts on the leptons were the same that were used for $b\bar{b}/c\bar{c}$ production. For each of the three runs the integrated luminosity was more than a factor 6 higher than the luminosity recorded by CDF during Run IB. Details of the generation can be seen in table 9.2. Using the calculations described for the $b\bar{b}/c\bar{c}$ sample the number of events with exactly three events was found to be 18.7 ± 1.4, while there were no events found with four or more leptons.

Run Number	Exchanged Particle	q_T range [GeV]	Additional Structure functions	Integrated Luminosity [pbarn^{-1}]
92	γ	5–500	CTEQ3L,GRV_94	819
93	Z^0	5–500		1268.5
94	Z^0	0.1–5		585.5

Tabelle 9.2 : *The Drell-Yan MC sample used. For all runs the structure functions CTEQ2L, MRSD0' and GRV_LO were used. Additional structure functions are listed.*

$t\bar{t}$ Production

The generation of $t\bar{t}$ events was done in one single run. Direct top production with a top mass set to $m_t = 175$ GeV was considered. The transfered momentum was limited by the requirement 0.1 GeV$< q <$ 500 GeV. The four used structure functions CTEQ2L, MRSD0', GRV_LO, CTEQ3L showed no significant differences in the number of events passing the selection cuts. All events containing at least one lepton with a transverse momentum larger than 7.5 GeV/c and a pseudorapidity of less than 1.5 were processed by the detector simulation. In total a number of events corresponding to 21,842 pb^{-1} were investigated. After applying the correct weight to the events 1.21 ± 0.10 three-lepton events and 0.08 ± 0.02 events with four or more lepton are expected from Run IB.

Diboson Production

Events containing $W^{\pm}W^{\pm}$, $W^{\pm}Z^0$ and Z^0Z^0 were generated in three separate runs. For each run the transverse momentum was limited to be 0.1 GeV/c $< p_T <$ 500 GeV/c. For all three runs the structure functions CTEQ2L, MRSD0' and GRV_LO were used. There were no additional cuts on generator level. The integrated luminosity for each run was more then 75 times the Run IB luminosity. Details of the generation are given in table 9.3. Due to the tiny cross section for diboson production only few events pass the requirements. The number of three lepton events from this source is 0.53 ± 0.08, while the number of four lepton events is 0.02 ± 0.01. The dibosons give a cross-check for our selection procedure. While all three channels give three lepton events only the Z^0Z^0 channels produces events containing four or more leptons.

Combining the Results

Three-lepton events are identified in all considered backgrounds. The dominant contributions are 47.0 events from $b\bar{b}$ and 18.7 events from Drell-Yan. A minor contribution of 1.2 events comes from top production. The contribution from dibosons is below one event. Summing up one expects a total of 67.5 ± 3.0 3-lepton events.

The main source of events with four real leptons is $b\bar{b}$ production with a total of 0.28 ± 0.14 events. $t\bar{t}$ and dibosons give minor contributions of 0.08 ± 0.02 and 0.02 ± 0.01,

Run Number	Dibosons Particle	Integrated Luminosity [pbarn^{-1}]	Events with Exactly three leptons	Events with Four or more Leptons
95	$W^{\pm}W^{\pm}$	6870	0.09	0.0
96	$W^{\pm}Z^{0}$	16684	0.35	0.0
97	$Z^{0}Z^{0}$	20582	0.64	0.02

Tabelle 9.3 : *The MC samples used to estimate the background due to diboson production. For all three runs the structure functions CTEQ2L, MRSD0' and GRV_LO were used.*

	3 leptons	≥ 4 leptons
bb	47.02 ± 2.61	0.28 ± 0.14
Drell-Yan	18.71 ± 1.4	$0 \pm^{0.10}_{0.0}$
$t\bar{t}$	1.21 ± 0.10	0.08 ± 0.02
ZZ, ZW, WW	0.53 ± 0.08	0.02 ± 0.01
Sum MC	67.5 ± 3.0	$0.37 \pm^{0.17}_{0.14}$
Fakes expected	$154 \pm 2 \pm^{268}_{39}$	$1.19 \pm 0.08 \pm^{2.08}_{0.3}$
MC and Fakes	$221.5 \pm 4 \pm^{268}_{39}$	$1.56 \pm^{0.19}_{0.16} \pm^{2.08}_{0.3}$
DATA	185	1

Tabelle 9.4 : *The expected number of three- and four-lepton events for this analysis. Errors on background MC are statistical errors only.*

while none of the Drell-Yan events pass the selection cuts. Summing up all background contributions one expects a total of $0.37 \pm^{0.17}_{0.14}$ real four-lepton events from background. Table 9.4 combines the results of the SM background study using MC samples.

9.2 Fake Lepton Background

In this section the background expected from events with at least one fake lepton is discussed. There are several possible ways to calculate the rate of expected fakes. The estimate can be based on the number of events or alternatively on the structure and the objects contained in these events. Both methods will be discussed in this section.

9.2.1 Event Based Fake Rate

For an event based fake rate study a sample with similar properties as the data sample is needed. If the q of the hard processes and the structure of the events in the data sample and the sample used for the fake study are similar one can expect a good prediction for the fake rate. The main problem with this method is finding a sample with high

enough statistics and a well understood or negligible background of extra leptons.

The Z^0–Sample

The most convenient sample for such a study is the Z^0-sample, because Z^0–events are well defined by the existence of two high energetic leptons. In the region of the Z^0 mass peak the production of Z^0s clearly dominates all backgrounds. Still using the Z^0 sample for a fake study is impossible due to small statistics.

The $W^\pm$ Sample

For the CDF-trilepton analysis [36] a fake lepton rate study based on the $W^\pm$ sample was performed. In 262.537 events 48 leptons in addition to the ones coming from the $W^\pm$ were found. The event-based fake-rate obtained from this is $0.289 \pm 0.042\%$. The results of this study and the modules used for it are described in [37].

For this thesis the study was re-done using the identical analysis module (CleanW) to select a clean $W^\pm$ sample. An event is accepted as a $W^\pm$ candidate if it has a lepton with $p_{\mathrm{T}} > 20$ GeV/c, significant missing transverse energy $\not\!\!E_T > 20$ GeV and a transverse mass of lepton-$\not\!\!E_T$ between 40 and 100 GeV. Details of the lepton cuts can be found in [37]. The number of events seen in the approximately 21 pb^{-1} of scanned data was 271,939, slightly higher than the number reported in the trilepton analysis. Of the pre-selected events 17,437 passed the $W^\pm$ cuts imposed by CleanW. On these events a slightly modified version of the analysis code was run. The modifications were introduced to allow the analysis code to accept most of the leptons pre-selected by CleanW. The vertex requirement and the good track requirement for the lepton from the $W^\pm$ were removed completely. Leaving in these requirements the analysis code would have removed approximately 10% of the events from the sample. Due to small differences in the lepton selections only 17,336 of the events selected by CleanW are identified as events with at least one good lepton by the analysis module. In order to avoid contamination with Z^0s all events containing a pair of either electrons or muons of opposite charge and with an invariant mass between 75 and 105 GeV are rejected. After this cut a total of 68 events containing CEM electrons and 73 events containing CMUO muons remained. The higher number of leptons found in this analysis can be explained by the fact that the leptons are not required to be isolated. If the same isolation cut as was used in the trilepton analysis is required only 33 CEM electrons and 46 CMUO muons totalling to 79 leptons remain. The number is further reduced by mimicking also the other cuts of the previous study.

The fake rate determined from the $W^\pm$ sample by this method is $0.81 \pm 0.07\%$, where the error is the statistical error due to the number of leptons used to calculate the fake rate. In addition to the statistical error there is a significant systematic error in this study. The definition of a good $W^\pm$ event is non-trivial. The selection is based on identifying a high energetic central lepton and a significant amount of $\not\!\!E_T$ carried away by the neutrino. Although one is looking for events with two leptons one has to reject events where the invariant mass of the leptons is compatible with the Z^0 mass.

Additional problems arise from the use of the MC programs. In the previous subsection MC programs were being used to calculate the number of events with three and four real leptons expected in the SM. Any jets that QFL' misidentifies as leptons would be double-counted, once from the MC and once from the $W^{\pm}$ sample. A cross-check was made using a $W^{\pm}$+2 jets MC sample generated using the VECBOS generator [38]. In 18,217 events passing CleanW, the first lepton cut and the Z-removal cut I found 38 leptons. In order to properly account for these events it would be necessary to understand the jets spectrum of W events, which is not modelled correctly by the MC generators. Then the events counted twice could be subtracted. Still this method then would rely heavily on MC programs. From this I conclude that a fake rate estimate should preferably be based on a different sample.

The SUSY Dilepton Sample

Another possible lepton-based sample is our data sample. The number of three lepton events with at least one fake lepton can be determined from comparing the two– and three lepton samples. Assuming that the fake rate is the same for the step from three- to four leptons one will get an estimate of the fake rate. The method gives an over-estimate because of the topological properties of the events. Our event selection includes a ΔR cut, which prohibits two leptons closer than $\Delta R = 0.4$ to each other. The fake rate calculated from the dilepton sample excludes all lepton candidates closer than this distance to the two already identified leptons. Using this rate to calculate the number of expected four lepton events will not take into account that there are less possibilities left to place the lepton without getting to near to one of the leptons already identified.

A way to calculate the number of fake events is using like-sign dilepton and trilepton events. All trilepton events that are not described by the MC are defined as fake events. This implies no statement about the number of fakes in the dilepton sample which is not of interest. The number of dileptons is accepted as is. The question asked is: "having this number of dilepton events, how many events containing an additional fake lepton can one expect".

The main problem here is to find a sample in which one knows the number of dileptons from which it originated. E.g. if one uses the trilepton sample where the first two leptons are same charge and the third is not, one does not know if the two real leptons are the first two, the first and the third or the last two. The problem can be overcome by using the like–sign trilepton sample. Here one knows that the events must already have been like–sign at the dilepton stage. All like-sign trilepton events not explained by the MC are per definition fake events. The probability for a fake lepton to have the same charge as the like–sign dileptons is assumed to be 50%. Thus the number of fake leptons is twice the difference between data and MC. Having obtained the number of events with a fake third lepton originating from the like–sign dilepton sample one calculates the fake rate by dividing this number by the number of like–sign

dilepton events

$$\frac{\text{FAKE LEPTONS}}{\text{EVENT}} = \frac{2 * (N_{\text{Data}}(l^{\pm}l^{\pm}l^{\pm}) - N_{\text{MC}}(l^{\pm}l^{\pm}l^{\pm}))}{N_{\text{Data}}(l^{\pm}l^{\pm})}.$$

Inserting the number of like–sign events found in the dilepton, the trilepton and the MC sample $N_{\text{Data}}(l^{\pm}l^{\pm}) = 10776$, $N_{\text{Data}}(l^{\pm}l^{\pm}l^{\pm}) = 32 \pm 5.7$ and $N_{\text{MC}}(l^{\pm}l^{\pm}l^{\pm})) = 2.2 \pm 1.1$ we arrive at a fake rate of $0.51 \pm 0.10\%$ and thus expect 178 ± 35 fake trilepton events. The fake rate agrees roughly with the rate obtained from the $W^{\pm}$ sample.

The method used here makes use of part of the data sample and thus is not safe against contamination from signal events. The possible contamination is negligible for several scenarios we investigated. Still it is preferable to have a fake estimate which is derived from a completely different sample and thus can not be contaminated by the signal. In the next subsection such a fake rate calculation will be introduced.

9.2.2 Track Based Fake Rate

The estimate of the lepton fake rate will be more reliable if one uses more of the information contained in the events. So far only the number of events has been used. If the exact structure of the events is used the estimate should describe reality better. In order to use most of the information contained in the event a fake rate per track in the event will be calculated in this subsection.

In principal the samples discussed for the event-based fake rate could also be used to estimate the track-based fake rate. Still for the event based fake rate one needs events with a similar q as the sample one is investigating. This is not necessary for a track based approach. Here it is sufficient to have a sample which has a structure similar to the data-sample minus the already identified leptons. Keeping this in mind one can turn to the minimum bias and the jet samples. These samples have a higher statistics than the samples considered so far. The three samples cover different regions of p_{T}. In order to be able to cover the whole p_{T} range with our samples and have high enough statistics in all p_{T} ranges we decided to use the minimum bias, the Jet 20 and the Jet 50 sample.

The level 2 trigger used to select the jet samples is based on the energy deposited in calorimeter clusters. The cluster containing the object passing our lepton cuts may have fired the trigger. If this is the case the spectrum of the leptons as well as their number would be biassed by the trigger requirement [39]. A way to avoid this bias is to require in the event a second cluster capable of firing the level two trigger. In the remainder of this subsection only tracks and leptons will be discussed for which the trigger bias has been removed. No trigger bias removal is necessary for the minimum bias sample because the trigger used here is the beam-beam counter.

The analysis of the samples proceeds in two steps. In the first step all tapes containing the samples are scanned for events containing lepton banks (ELES, CMUP or CMIO). These events are saved to disk. In the same step all events are scanned for

tracks with a p_T larger than 3 GeV/c and the properties of the tracks are saved to an n-tuple. From this step one obtains detailed information about the good tracks in each sample and a sub-sample containing all events with lepton banks. This sub-sample can be re-used if one later wants to repeat the study for another analysis using different lepton ID cuts. On the reduced sample another modified version of the analysis code is run. No central high-p_T lepton is required, all leptons passing the loose cuts are counted and their properties saved to an n-tuple. At this point all information needed to calculate the fake rate is available.

The track p_T spectra for the data samples, the minimum bias sample and the jet samples are shown in figure 9.1. The trilepton sample is a subsample of the dilepton sample and the spectra agree well. The spectrum for the minimum bias sample is systematically lower than the data sample. The jet 50 sample is systematically higher than the lepton samples, while the spectrum of jet 20 sample agrees well with the lepton samples. In order to take into account the different p_T spectra of the samples they were divided up into bins according to the p_T of the tracks and leptons.

The muon-momentum is taken directly from the associated track. Thus the fake rate for muons can be calculated by counting the number of muons identified and dividing by the number of tracks in the same p_T-bin. The p_T cut on muons is 5 GeV/c. Thus only tracks with a $p_T > 5$ GeV/c are considered. For the minimum bias sample there are two 1 GeV/c-wide bins between 5 GeV/c and 7 GeV/c and a third bin containing all transverse momenta above 7 GeV/c. For the jet samples the statistics is much higher and thus it is possible to use a finer binning and still maintain high statistics. The bins defined for both jet samples are five 1 GeV/c bins between 5 GeV/c and 10 GeV/c. Between 10 GeV/c and 50 GeV/c there are another 4 bins. Everything above 50 GeV/c is summarised in one high p_T bin.

For electrons the case is more complicated than for muons. Here the E_T is measured in the calorimeter independent of the track p_T. There are only two constraints on the track p_T for electrons:

1. $p_T > 3$ GeV/c^2,
2. $E_T/p_T < 2.0$.

An electron candidate must pass both these cuts to be accepted in the four-lepton analysis. Investigating the spread of E/P in the data sample we concluded that the difference between the two values is negligible in general. Thus we assume that if a track is misidentified as a lepton its E_T will agree with the track p_T. Using this assumption we can use the same calculation for electrons as we did for muons.

The main dependence of the fake rate on the momentum is given on the left side of figure 9.2 for electrons and on the right side for muons. Shown in this figure are only the rates calculated from the jet samples, because the minimum bias sample has not enough statistics above 7 GeV. The fake rate from the jet 20 sample is higher than the one from the jet 50 sample for all but the last two points. The rate for electrons rises for both jet samples.

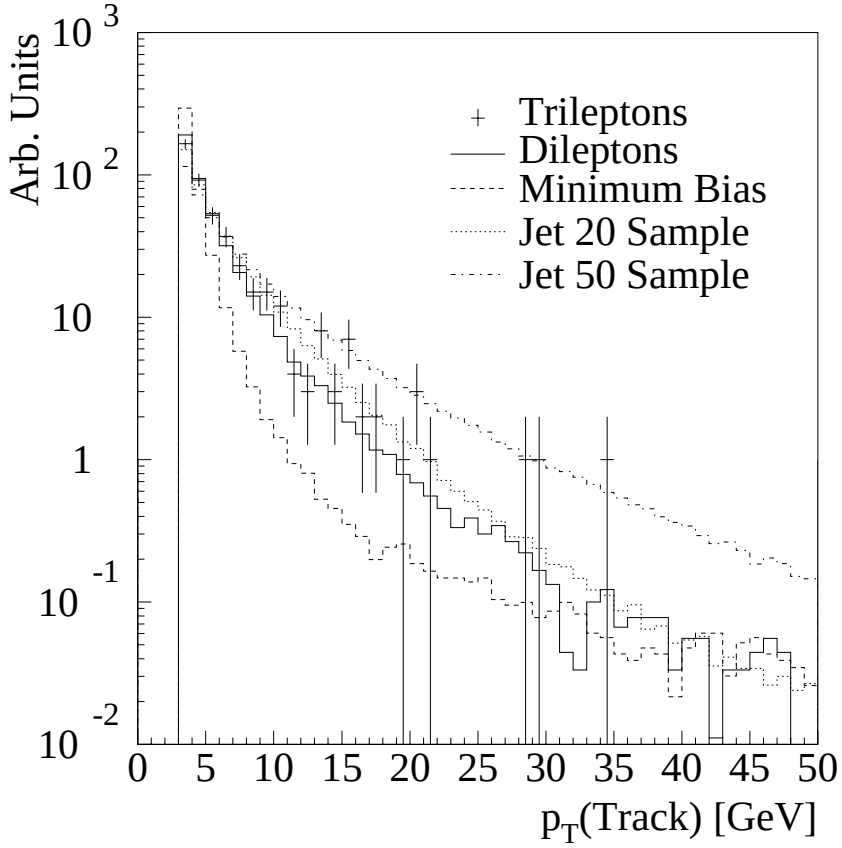

Abbildung 9.1: *The p_T spectra of the trilepton (crosses) and the dilepton sample (solid line). The spectra are compared with the spectra from the minimum bias (broken line), the Jet 20 (dotted line) and the Jet 50 sample (dashed line).*

This behaviour can be understood if one considers the data sample and the way electrons are selected. The jet p_T spectrum is steeply falling. Looking at a track with a small p_T, the possibility that this track is part of a jet containing more energy is high. Thus this track is unlikely to pass the electron selection cuts. On the contrary a jet containing a track with large transverse momentum will only have a few other tracks, which in most cases will be very low energetic. Thus such a track can more easily pass the electron selection cuts.

The muon fake rate falls with the transverse momentum up to about 30 GeV/c and the slowly rises again. It is not obvious if the rise is a physical effect or a consequence of small statistics. The drop of the fake rate can be understood with the same arguments that explained the rise for the electrons. If a track contains many low energetic tracks, the tracks can pass the muon selection in the calorimeter because the energy deposited

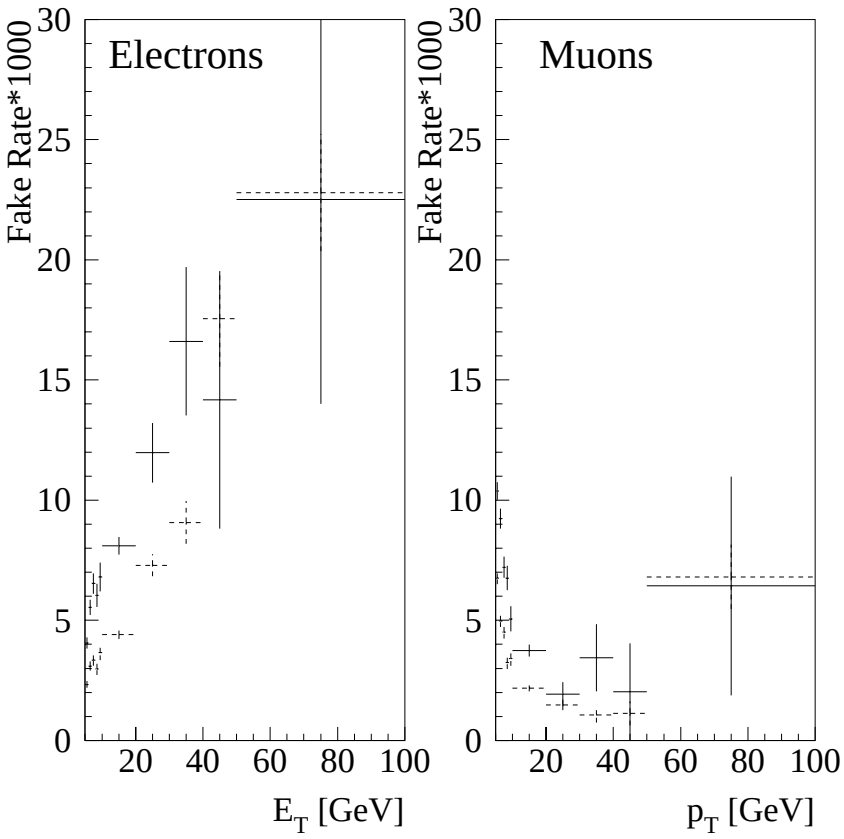

Abbildung 9.2: *The dependence of the fake rate from the transverse momentum p_T. The left plot shows the behaviour for electrons, the right one the behaviour for muons. The solid lines are for Jet 20 and the broken lines are Jet 50. Minimum Bias is not shown. The last bin on the right side is an overflow bin containing the fake rate for all lepton momenta above 50 GeV/c.*

is rather low. Still the larger number can result in a punch-through. If the jet contains only one high energetic track, then it will most likely be rejected by cuts requiring the deposited energy to be below the threshold for electrons and hadrons.

In figure 9.3 the fake rate for the low p_T range is shown. In this area the minimum bias sample and the jet samples have been considered. The general behaviour is the same as seen before. The fake-electron rate rises with the track momentum, while the fake muon rate drops. One sees that the fake rate obtained from the minimum bias sample is always higher than the one from the Jet 20 sample, which in turn is still higher than the rate for the Jet 50 sample. The study presented here uses loose lepton cuts and thus the statistics are higher than in other analysis using tighter cuts. With

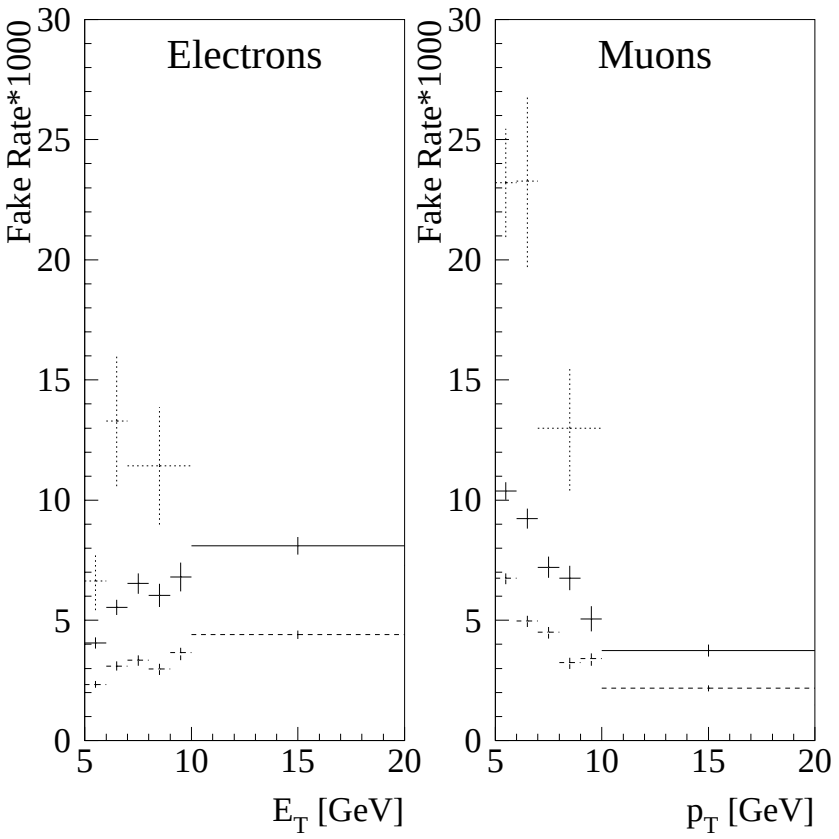

Abbildung 9.3: *The dependence of the fake rate from the transverse momentum p_T for momenta below 20 GeV. The left plot shows the behaviour for electrons, the right one the behaviour for muons. The solid lines are for Jet 20, the broken lines are Jet 50 and the dotted lines are Minimum Bias. For Minimum Bias the highest bin is an overflow bin containing all momenta above 7 GeV.*

the high statistics the difference between the three samples is statistically significant.

The important difference between the three samples is in the event structure. Minimum bias events most of the time contain only very few tracks, which are not clustered in any way. In the jet samples all events contain clusters which have fired a jet trigger. The number of central jets per events for the dilepton sample, compared to non-normalised sub-samples of the minimum bias, the Jet 20 and the Jet 50 sample is shown in figure 9.4. Only central jets are important for this study because no leptons from the plug or forward detectors are accepted. In the dilepton sample about 20% of the events have no additional jet. In contrary in the jet samples most of the events contain jets passing our selection criteria, while in the minimum bias sample only one out

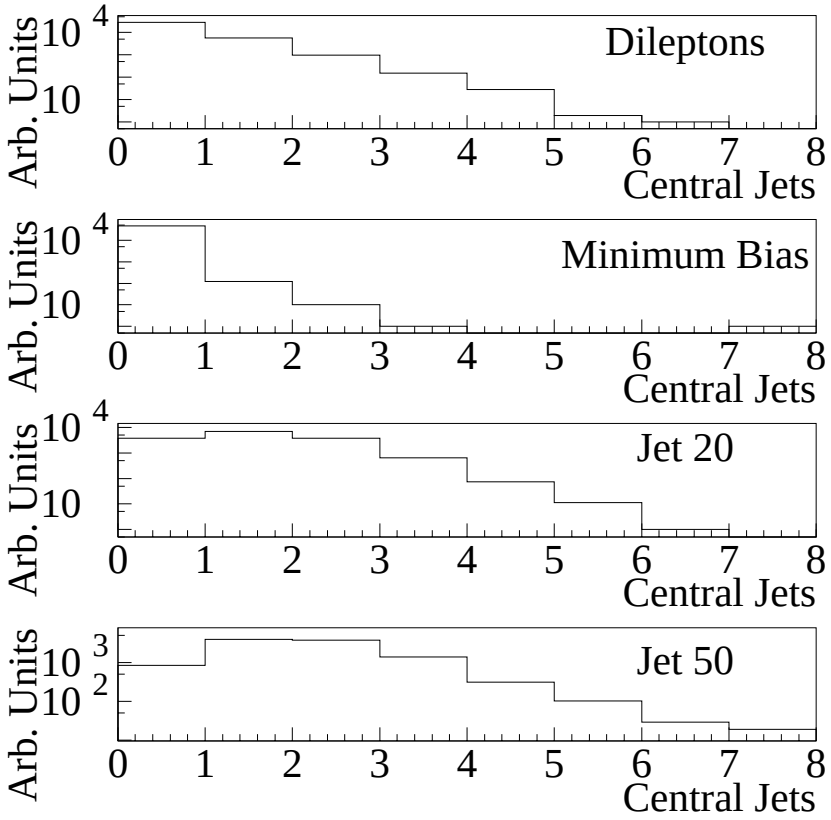

Abbildung 9.4: *The number of central jets for the dilepton sample (top), the minimum bias sample (second from top), the Jet 20 sample (third from top) and the Jet 50 sample (bottom).*

of thousand events contains a jet. The p_{T} spectra of the central jets of the four samples are shown in figure 9.5. For the dilepton sample the spectrum is monotonously falling. The minimum bias sample contains mostly jets with very low momentum, but has a similar p_{T} dependence as the dilepton sample. The p_{T} spectra of the two jet samples peak at about 40 GeV and 80 GeV respectively. The spectrum at high momentum is comparable to the spectrum from the dilepton sample.

No jet spectrum of any of the three samples models the spectrum of the dilepton sample well. The jet samples have on average more jets, the minimum bias sample has significantly less jets. The p_{T} spectrum of the minimum bias sample is closest to the dilepton sample, but runs out of statistics much to early to describe the dilepton sample accurately. In order to find the most general estimate of the fake rate a rate averaged over all three samples will be calculated. Using the weighted average will suppress the

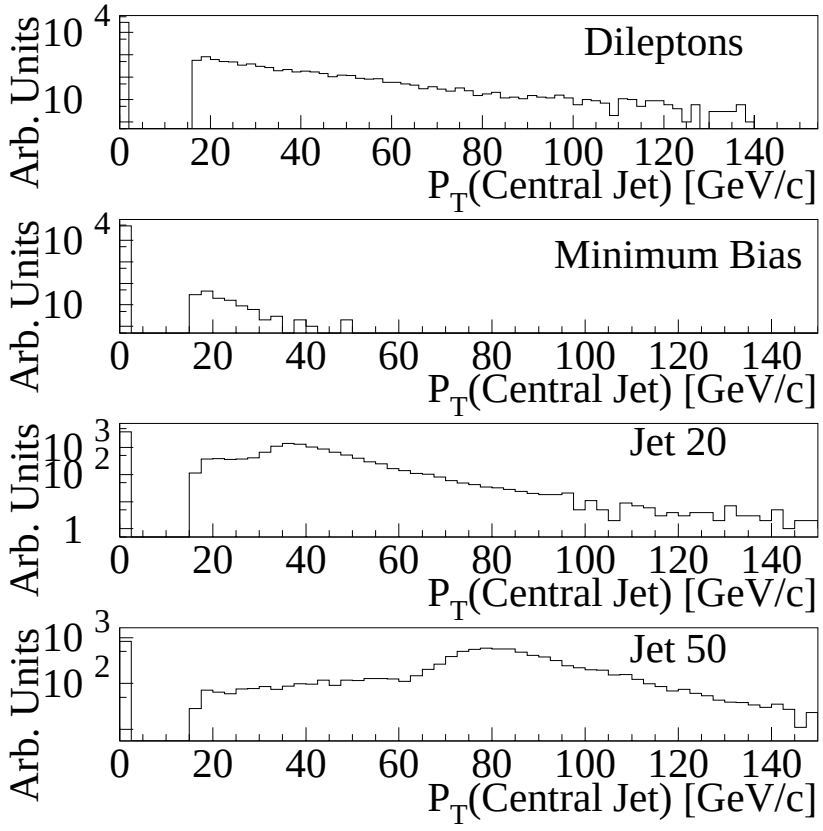

Abbildung 9.5: *The transverse momentum spectrum of the first central jet for the dilepton sample (top), the minimum bias sample (second from top), the Jet 20 sample (third from top) and the Jet 50 sample (bottom).*

contribution of the low-statistics minimum bias sample. Still, because it is not known which of the three sample is closest to the dilepton sample, the minimum bias sample dominates the systematical uncertainty of the fake estimate.

Due to its low statistics the E_{T} binning used for the minimum bias sample was different than the one used for the two jet samples. Thus the fake rates of the three samples cannot be simply added. To bypass this problem the error of the MB fake rate for the bins greater then 7 GeV was increased consistent with statistics. The statistical error obtained for 1 bin is σ_1. Applying the fake rate to eight bins instead of one means decreasing the statistics by a factor of eight. Assuming that all eight bins contain the same number of events the error for 8 bins σ_8 is given by $\sigma_8 = \sigma_1 * \sqrt{8}$. This corrected error for the Minimum bias sample was used in the calculations. The numbers used in the calculations as well as the results are summarised in tables 9.5 for

p_T Bin	Rate $*$ 1000 MB	Rate $*$ 1000 Jet 20	Rate $*$ 1000 Jet 50	Weighted Mean	Uncorrected MB mean
$5-6$	23.2 ± 2.26	10.38 ± 0.36	6.52 ± 0.36	$8.63 \pm 0.25 \pm^{14.57}_{2.11}$	$8.63 \pm 0.25 \pm^{14.57}_{2.11}$
$6-7$	23.28 ± 3.59	9.23 ± 0.42	4.69 ± 0.36	$6.72 \pm 0.27 \pm^{16.56}_{2.03}$	$6.72 \pm 0.27 \pm^{16.56}_{2.03}$
$7-8$	12.99 ± 7.35	7.21 ± 0.44	4.23 ± 0.40	$5.56 \pm 0.30 \pm^{7.43}_{1.33}$	$5.64 \pm 0.29 \pm^{7.35}_{1.42}$
$8-9$	12.99 ± 7.35	6.76 ± 0.51	3.38 ± 0.40	$4.71 \pm 0.32 \pm^{8.28}_{1.33}$	$4.82 \pm 0.31 \pm^{8.18}_{1.44}$
$9-10$	12.99 ± 7.35	5.06 ± 0.52	3.21 ± 0.45	$4.02 \pm 0.34 \pm^{8.98}_{0.81}$	$4.15 \pm 0.33 \pm^{8.85}_{0.94}$
$10-20$	12.99 ± 7.35	3.74 ± 0.25	2.13 ± 0.18	$2.69 \pm 0.15 \pm^{10.3}_{0.56}$	$2.72 \pm 0.15 \pm^{10.27}_{0.59}$
$20-30$	12.99 ± 7.35	1.93 ± 0.50	1.72 ± 0.34	$1.80 \pm 0.28 \pm^{11.19}_{0.09}$	$1.92 \pm 0.28 \pm^{11.08}_{0.2}$
$30-40$	12.99 ± 7.35	3.44 ± 1.40	1.25 ± 0.51	$1.55 \pm 0.48 \pm^{11.45}_{0.3}$	$1.88 \pm 0.47 \pm^{11.12}_{0.63}$
$40-50$	12.99 ± 7.35	2.02 ± 2.02	0.54 ± 0.54	$0.71 \pm 0.52 \pm^{12.29}_{0.16}$	$1.13 \pm 0.52 \pm^{11.86}_{0.59}$
> 50	12.99 ± 7.35	6.43 ± 4.55	6.83 ± 2.06	$7.14 \pm 1.82 \pm^{5.85}_{0.31}$	$8.9 \pm 1.52 \pm^{4.1}_{2.07}$
> 7	12.99 ± 2.6				

Tabelle 9.5 : *The binned fake rate for muons. The error of the rates from the Minimum Bias sample in the bins above 7 GeV was increased in order to account for the statistics as described in the text. For comparison the mean obtained without this corrections is given in the last column. Also the original value of the last bin of the minimum bias sample is given in the last row.*

muons and 9.6 for electrons. The fake rates for the three samples are given in columns 2-4 of both tables. The resulting average fake rate is given in the fifth column. Here the statistical error is calculated by summing the statistical errors in quadrature. The systematical uncertainty is estimated by the difference of the measured value to the highest and lowest of the input values. The last row gives the results of the analogous calculation with the original weight for the minimum bias rates. The effect of including this correction is small.

The corrected average fake rate was applied to the dilepton and trilepton sample to calculate the number of three– and four–lepton events with a fake lepton. The number of tracks in the p_T bins together with the fake rates and the expected number of events for electrons and muons for the dilepton and the trilepton sample are given in tables 9.7 and 9.8 respectively.

The last row in each table gives the total number of expected events. Here the

p_T Bin	Rate $*$ 1000 MB	Rate $*$ 1000 Jet 20	Rate $*$ 1000 Jet 50	Weighted Mean	Uncorrected MB mean
$5-6$	6.63 ± 1.21	4.06 ± 0.23	2.57 ± 0.23	$3.37 \pm 0.16 \pm^{3.26}_{0.8}$	$3.37 \pm 0.16 \pm^{3.26}_{0.8}$
$6-7$	13.3 ± 2.72	5.54 ± 0.32	3.06 ± 0.29	$4.23 \pm 0.22 \pm^{9.08}_{1.17}$	$4.23 \pm 0.22 \pm^{9.08}_{1.17}$
$7-8$	11.43 ± 6.9	6.53 ± 0.42	3.41 ± 0.36	$4.72 \pm 0.27 \pm^{6.72}_{1.3}$	$4.79 \pm 0.27 \pm^{6.65}_{1.38}$
$8-9$	11.43 ± 6.9	6.04 ± 0.48	2.9 ± 0.37	$4.1 \pm 0.29 \pm^{7.33}_{1.2}$	$4.2 \pm 0.29 \pm^{7.24}_{1.3}$
$9-10$	11.43 ± 6.9	6.80 ± 0.60	3.09 ± 0.44	$4.39 \pm 0.35 \pm^{7.04}_{1.31}$	$4.52 \pm 0.35 \pm^{6.91}_{1.43}$
$10-20$	11.43 ± 6.9	8.10 ± 0.37	4.31 ± 0.26	$5.56 \pm 0.21 \pm^{5.87}_{1.25}$	$5.6 \pm 0.21 \pm^{5.83}_{1.29}$
$20-30$	11.43 ± 6.9	11.97 ± 1.24	7.77 ± 0.73	$8.87 \pm 0.63 \pm^{3.1}_{1.1}$	$9.01 \pm 0.61 \pm^{2.96}_{1.24}$
$30-40$	11.43 ± 6.9	16.61 ± 3.08	7.06 ± 1.21	$8.42 \pm 1.11 \pm^{8.19}_{1.36}$	$8.88 \pm 1.02 \pm^{7.73}_{1.82}$
$40-50$	11.43 ± 6.9	14.17 ± 5.36	13.07 ± 2.67	$13.09 \pm 2.26 \pm^{1.08}_{1.66}$	$12.38 \pm 1.71 \pm^{1.79}_{0.95}$
> 50	11.43 ± 6.9	22.51 ± 8.51	24.21 ± 3.88	$21.33 \pm 3.14 \pm^{2.88}_{9.89}$	$15.47 \pm 2.01 \pm^{8.74}_{4.03}$
> 7	11.43 ± 2.44				

Tabelle 9.6 : *The binned fake rate for electrons. The error on the rates for the minimum bias sample in the bins with $E_T > 7$ GeV was multiplied with a factor of $\sqrt{8}$ in order to account for the splitting of the bin. The effect of this correction can be seen by comparing the last two columns. For completeness the fake for the bin larger 7 GeV/c of the minimum bias sample is given in the last row.*

statistical errors have been added in quadrature. The systematical errors stem from the different fake rates obtained from the three samples investigated. Thus they cannot be added in quadrature, as would be the case for independent errors. Instead the systematical errors have been added linearly. From this calculation one expects $89 \pm 2 \pm^{181}_{22}$ fake muons and $66 \pm 1 \pm^{86}_{17}$ fake electrons in the trilepton sample. Adding these two the expected total number of fakes is

$$154 \pm 2 \pm^{268}_{39},$$

where the statistical errors have been added in quadrature and the systematical errors have been added linearly. The analogous calculation for the trilepton sample gives $0.54 \pm 0.05 \pm^{0.71}_{0.14}$ fake muons and $0.65 \pm 0.07 \pm^{1.38}_{0.16}$ fake electrons. The total number of expected fake four lepton events is

$$1.19 \pm 0.08 \pm^{2.08}_{0.3}.$$

p_T Bin	Tracks	Fake muon Rate $*$ 1000	Fake Muons Expected	Fake Electron Rate $*$ 1000	Fake Electrons Expected
$5-6$	4797	$8.63 \pm 0.25 \pm^{14.57}_{2.11}$	$41.4 \pm 1.35 \pm^{69.9}_{10.1}$	$3.37 \pm 0.16 \pm^{3.26}_{0.8}$	$16.2 \pm 0.8 \pm^{15.6}_{3.8}$
$6-7$	2866	$6.72 \pm 0.27 \pm^{16.56}_{2.03}$	$19.3 \pm 0.86 \pm^{47.5}_{5.8}$	$4.23 \pm 0.22 \pm^{9.08}_{1.17}$	$12.1 \pm 0.7 \pm^{26.0}_{3.4}$
$7-8$	1861	$5.56 \pm 0.30 \pm^{7.43}_{1.33}$	$10.4 \pm 0.60 \pm^{13.8}_{2.5}$	$4.79 \pm 0.27 \pm^{6.65}_{1.38}$	$8.9 \pm 0.5 \pm^{12.4}_{2.6}$
$8-9$	1266	$4.71 \pm 0.32 \pm^{8.28}_{1.33}$	$6.0 \pm 0.43 \pm^{10.5}_{1.7}$	$4.2 \pm 0.29 \pm^{7.24}_{1.3}$	$5.3 \pm 0.4 \pm^{9.2}_{1.6}$
$9-10$	934	$4.02 \pm 0.34 \pm^{8.98}_{0.81}$	$3.8 \pm 0.34 \pm^{8.4}_{0.8}$	$4.52 \pm 0.35 \pm^{6.91}_{1.43}$	$4.2 \pm 0.4 \pm^{6.5}_{1.3}$
$10-20$	2542	$2.69 \pm 0.15 \pm^{10.3}_{0.56}$	$6.8 \pm 0.40 \pm^{26.2}_{1.4}$	$5.6 \pm 0.21 \pm^{5.83}_{1.29}$	$14.2 \pm 0.6 \pm^{14.8}_{3.3}$
$20-30$	335	$1.80 \pm 0.28 \pm^{11.19}_{0.09}$	$0.6 \pm 0.10 \pm^{3.8}_{0.03}$	$9.01 \pm 0.61 \pm^{2.96}_{1.24}$	$3.0 \pm 0.3 \pm^{1.0}_{0.4}$
$30-40$	69	$1.55 \pm 0.48 \pm^{11.45}_{0.3}$	$0.11 \pm 0.04 \pm^{0.89}_{0.02}$	$8.88 \pm 1.02 \pm^{7.73}_{1.82}$	$0.6 \pm 0.1 \pm^{0.5}_{0.1}$
$40-50$	30	$0.71 \pm 0.52 \pm^{12.29}_{0.16}$	$0.02 \pm 0.02 \pm^{0.37}_{0.00}$	$12.38 \pm 1.71 \pm^{1.79}_{0.95}$	$0.37 \pm 0.08 \pm^{0.05}_{0.03}$
> 50	34	$7.14 \pm 1.82 \pm^{5.85}_{0.31}$	$0.24 \pm 0.07 \pm^{0.20}_{0.01}$	$15.47 \pm 2.01 \pm^{8.74}_{4.03}$	$0.53 \pm 0.11 \pm^{0.3}_{0.14}$
Total			$88.5 \pm 1.9 \pm^{181.4}_{22.4}$		$65.5 \pm 1.4 \pm^{86.3}_{16.7}$

Tabelle 9.7 : *The number of tracks seen in the dilepton sample together with the fake rate and the number of expected events. The statistical errors for the tracks and the fake rate are added in quadrature.*

p_T Bin	Tracks	Fake muon Rate $*$ 1000	Fake Muons Expected	Fake Electron Rate $*$ 1000	Fake Electrons Expected
$5-6$	29	$8.63 \pm 0.25 \pm^{14.57}_{2.11}$	$0.25 \pm 0.05 \pm^{0.42}_{0.06}$	$3.37 \pm 0.16 \pm^{3.26}_{0.8}$	$0.1 \pm 0.02 \pm^{0.09}_{0.02}$
$6-7$	20	$6.72 \pm 0.27 \pm^{16.56}_{2.03}$	$0.13 \pm 0.03 \pm^{0.33}_{0.04}$	$4.23 \pm 0.22 \pm^{9.08}_{1.17}$	$0.08 \pm 0.02 \pm^{0.18}_{0.02}$
$7-8$	15	$5.56 \pm 0.30 \pm^{7.43}_{1.33}$	$0.08 \pm 0.02 \pm^{0.11}_{0.02}$	$4.79 \pm 0.27 \pm^{6.65}_{1.38}$	$0.07 \pm 0.02 \pm^{0.1}_{0.02}$
$8-9$	13	$4.71 \pm 0.32 \pm^{8.28}_{1.33}$	$0.06 \pm 0.02 \pm^{0.11}_{0.02}$	$4.2 \pm 0.29 \pm^{7.24}_{1.3}$	$0.05 \pm 0.02 \pm^{0.09}_{0.02}$
$9-10$	11	$4.02 \pm 0.34 \pm^{8.98}_{0.81}$	$0.04 \pm 0.01 \pm^{0.1}_{0.01}$	$4.52 \pm 0.35 \pm^{6.91}_{1.43}$	$0.05 \pm 0.02 \pm^{0.08}_{0.02}$
$10-20$	23	$2.69 \pm 0.15 \pm^{10.3}_{0.56}$	$0.06 \pm 0.01 \pm^{0.24}_{0.01}$	$5.6 \pm 0.21 \pm^{5.83}_{1.29}$	$0.13 \pm 0.03 \pm^{0.13}_{0.03}$
$20-30$	4	$1.80 \pm 0.28 \pm^{11.19}_{0.09}$	$0.01 \pm 0 \pm^{0.04}_{0}$	$9.01 \pm 0.61 \pm^{2.96}_{1.24}$	$0.04 \pm 0.02 \pm^{0.01}_{0}$
$30-40$	2	$1.55 \pm 0.48 \pm^{11.45}_{0.3}$	$0.003 \pm 0 \pm^{0.02}_{0}$	$8.88 \pm 1.02 \pm^{7.73}_{1.82}$	$0.02 \pm 0.01 \pm^{0.02}_{0}$
$40-50$	0	$0.71 \pm 0.52 \pm^{12.29}_{0.16}$	0	$12.38 \pm 1.71 \pm^{1.79}_{0.95}$	0
>50	0	$7.14 \pm 1.82 \pm^{5.85}_{0.31}$	0	$15.47 \pm 2.01 \pm^{8.74}_{4.03}$	0
Total			$0.54 \pm 0.05 \pm^{0.71}_{0.14}$		$0.65 \pm 0.07 \pm^{1.38}_{0.16}$

Tabelle 9.8 *: The number of tracks seen in the trilepton sample together with the fake rate and the number of expected events. The statistical errors for the tracks and the fake rate are added in quadrature.*

Leptons	Number of events
eee	27
$ee\mu$	29
$e\mu e$	14
μee	3
$e\mu\mu$	33
$\mu e\mu$	18
$\mu\mu e$	17
$\mu\mu\mu$	44
total	185

Tabelle 10.1 : *The leptons identified in the three-lepton events.*

10 Experimental Results

In 87.5 pb^{-1} of CDF data the analysis code identifies 185 three-lepton and one four-lepton candidate event, this last event is discussed in section 10.2.

10.1 The Three Lepton Events

The number of background events in the three lepton sample is much to high to identify any signal contribution in this sample. The sample is used to cross-check the analysis and show that the background is well understood. The sample can also be compared to the three lepton analysis, which serves as a further cross-check.

A split-up of the events by the type of leptons is given in Table 10.1. There are 73 events containing two or more electrons and 112 containing two or more muons. The invariant masses of the highest p_{T} pair are shown in the top and center plot of Fig. 10.1. In this figure the entries plus the overflow bin correspond to the number of events in the channel, while the underflow bin contains all events that do not have two leptons of the specified types. There are two ee and four $\mu\mu$ events in the area of the Z-peak. One of the dielectron pairs (from an $e\mu e$-event) has an invariant mass of 152.5 GeV. One of the dimuon events (Run: 67757, Event: 333537) has an invariant mass of 365.7 GeV.

The invariant mass distribution of the 115 events containing electrons and muons is shown in the bottom plot of Fig. 10.1. Here we see four events in the Z-region, one event each at 126 and 213 GeV.

10.1.1 Verification of the Background Calculation

The background calculation presented in the previous chapter can be verified by comparing the mass spectrum of the two leading leptons in the trilepton sample with the

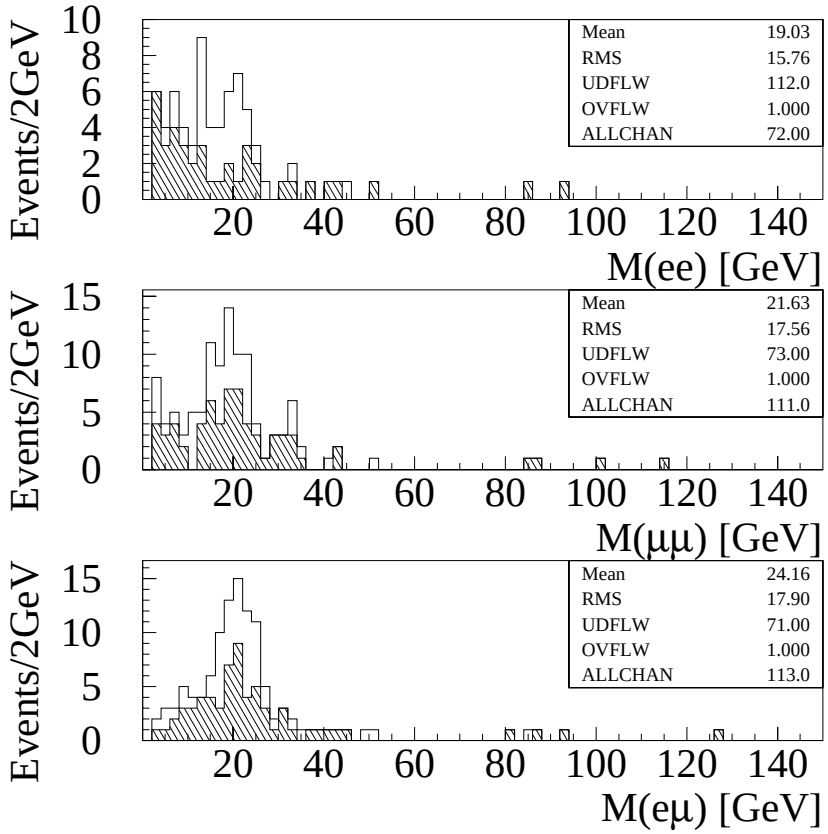

Abbildung 10.1: *The invariant mass of the highest energetic ee– (top), μμ– (middle) and eμ–pair (bottom) in the trilepton sample. The open histograms show all candidate events of the specified type, the hatched histograms only the candidates with opposite charge.*

spectrum expected from the background calculation. The leading background contribution are dilepton events with a jet mis-identified as third lepton. With the assumption that the fake lepton has always the smallest momentum the leading two leptons are the ones already seen in the dilepton sample. Then one can use the dilepton mass spectrum from the dilepton sample and scale it down with the factor corresponding to the fake rate. After adding the contributions from the $b\bar{b}/c\bar{c}$ and Drell-Yan MCs the spectrum should agree with the one from the trilepton sample. The other two backgrounds are small enough to be neglected here. The comparison is shown in figure 10.2. The points show the invariant mass of the two leading leptons from the dilepton sample. The histograms show the spectrum from the dilepton sample scaled down by a factor of 0.004 and of the two dominant backgrounds. The upper plot compares the spectra for

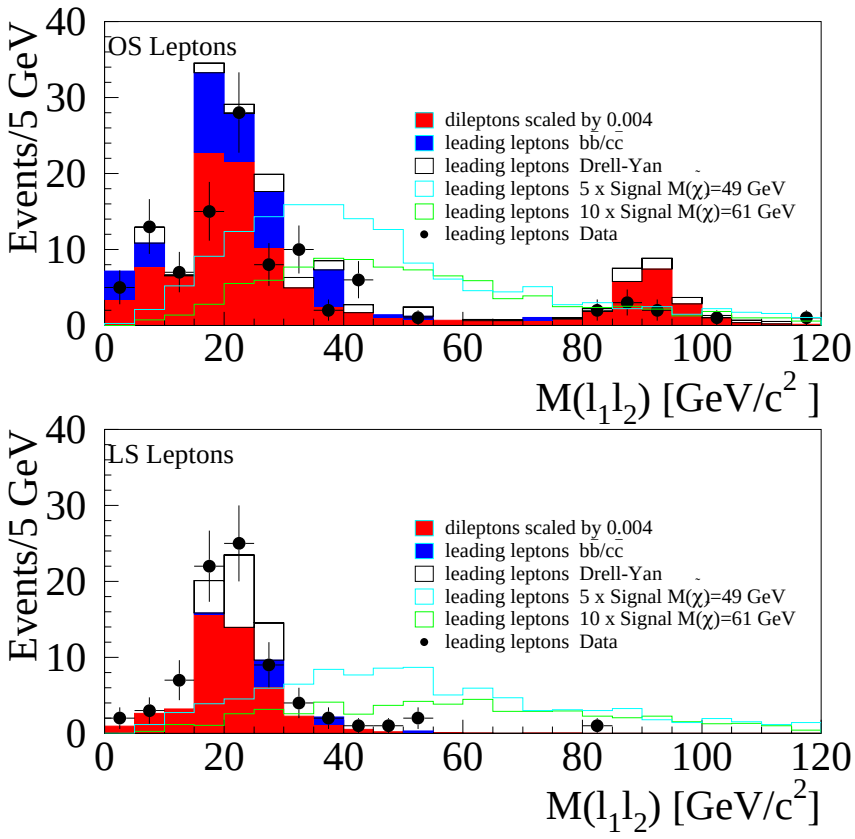

Abbildung 10.2: *The mass spectrum of the two leading leptons found in trilepton data compared to predictions from MC and dilepton events. The top (bottom) plot shows the distribution for opposite (like) sign leptons. For comparison the mass distributions expected for two signal scenarios are shown. The signal scenarios have been scaled up by factors of 5 and 10 to make them visible.*

opposite sign leptons, the lower one the spectrum for like sign leptons. The agreement is good for the like sign leptons. For the opposite sign leptons one would expect more events near the Z^0 mass, most of which would contain fake leptons. This can be explained either by assuming a different fake rate for Z^0 events than for the events at lower masses. An alternative explanation is that the fake lepton is not always the one with the smallest momentum. If the fake lepton is the first or second lepton the spectrum of the two leading leptons of the trilepton sample will not necessarily follow the spectrum of the dileptons.

Run	Event	Leptons	passes our cuts	passes trilepton analysis cuts	Reason for rejection
61024	463506	$ee\mu$	YES	YES	—
61232	89857	$\mu\mu e$	YES	YES	—
61416	336906	$\mu\mu e$	YES	YES	—
65918	197201	$\mu\mu\mu$	YES	YES	—
66185	194780	$\mu\mu\mu$	YES	YES	—
61167	268854	$\mu\mu\mu$	NO	YES	different Muon p_{T} cut
61528	124487	$\mu\mu\mu$	NO	YES	different Muon p_{T} cut
65085	13516	$\mu\mu\mu$	NO	YES	different Muon p_{T} cut
66103	125718	$\mu\mu e$	NO	YES	vertex ?
70945	215609	$\mu e\mu$	YES	NO	conversion e
67538	31023	$\mu\mu\mu$	YES	NO	μ fails soft-μ cuts ?
66539	267899	$\mu e\mu$	YES	NO	conversion e

Tabelle 10.2 : *List of the three-lepton candidates found by the CDF trilepton analysis and our analysis.*

10.1.2 Comparison with the CDF Trilepton Analysis

As this analysis is similar in many points to the CDF trilepton analysis [40] the 3-lepton events seen here are compared with the ones found in the trilepton analysis. In this analysis there were 0 events after all cuts. Several selection cuts which were used in the trilepton analysis are not used in the present analysis, some other cuts were used with different values. Especially in the present analysis the low mass resonances are not removed and there is no $\not\!\!E_T$ or isolation requirement. In the trilepton analysis 23 events are found after the isolation cut of 2 GeV. After the ΔR-cut 9 events remain. As the selection includes plug electrons one expects to see less leptons in the trilepton sample of the present analysis, after the corresponding plots have been applied. Requiring all leptons to have an isolation less than 2 GeV there are 8 events left of the 185 events that make up the trilepton sample. 5 of these events are also found by the trilepton analysis. Three events found in the trilepton analysis contain a muon which has a momentum between 4 and 5 GeV. The loose lepton p_{T} cut use in the present analysis is 5 GeV, not 4 GeV as in the trilepton analysis. Thus the three events are not selected. The rejection of the fourth event is probably due to differences in the vertex cuts.

The rejection of three leptons found in the present analysis by the selection in the trilepton analysis has not yet been investigated but is probably due to looser cuts used in the present analysis. All events are listed in Table 10.2

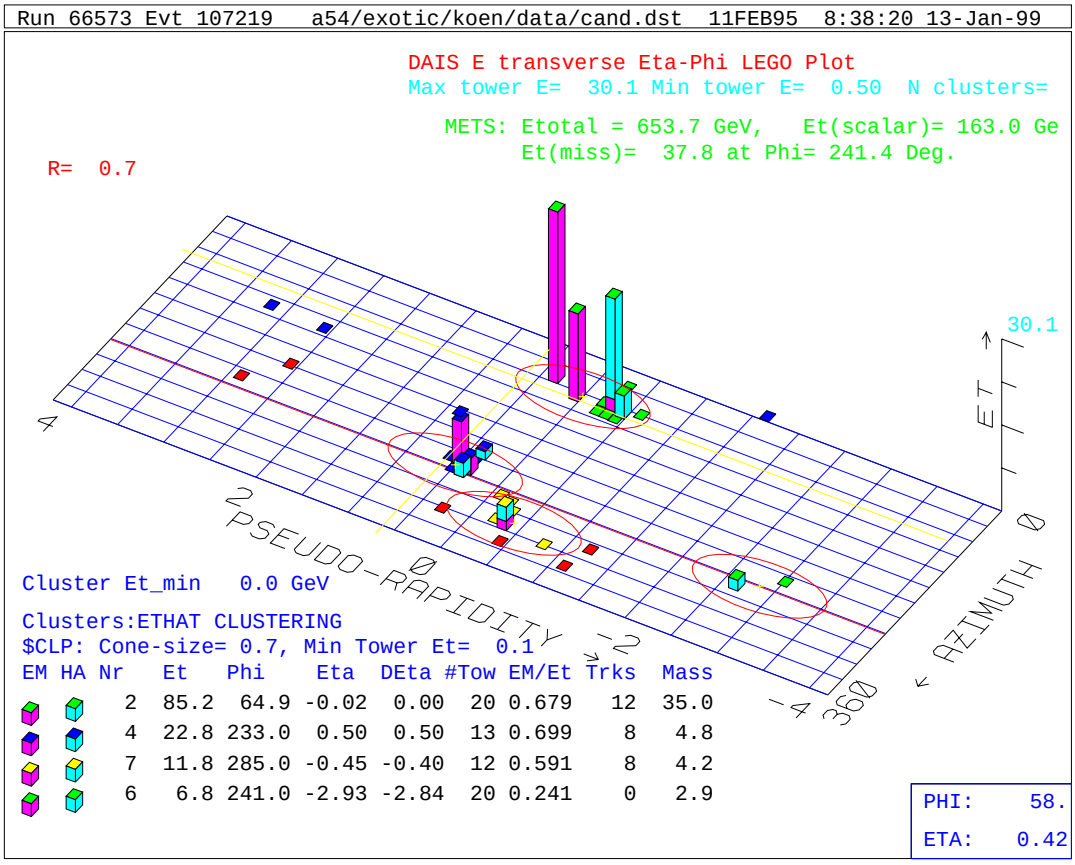

Abbildung 10.3: *Lego-plot of the four-lepton candidate event.*

10.2 The Four Lepton Candidate Event

From the background calculation $0.37\pm^{0.17}_{0.14}$ real and $1.19 \pm 0.08\pm^{2.08}_{0.3}$ fake four lepton events are expected. The total number of four lepton events expected is $1.56 \pm^{0.19}_{0.16} \pm^{2.08}_{0.3}$, in agreement with the one event found. The candidate event is

Event: 107219 Run: 66573

The dominant background for the trilepton and for the four-lepton sample is $b\bar{b}/c\bar{c}$ production. Thus, if the event is not signal, it will most probably contain heavy quarks.

The event contains 2 electron candidates and 3 hadronic clusters. Two of the clusters contain one muon candidate each. The parameters of the four leptons are given in Table 10.4. The event-displays are shown in Figs. 10.3 and 10.4. The second electron is near to the 90°-crack in the detector and thus does not pass the FIDELE cuts. The E/p ratio is 1.028 for this electron, which indicates that no energy vanishes in the crack. Table 10.3 gives the triggers which were fired by the event. In level one and two it fires the dielectron, dilepton, and $\not\!\!E_T$-triggers. The first muon has fired the level 2 CMNP

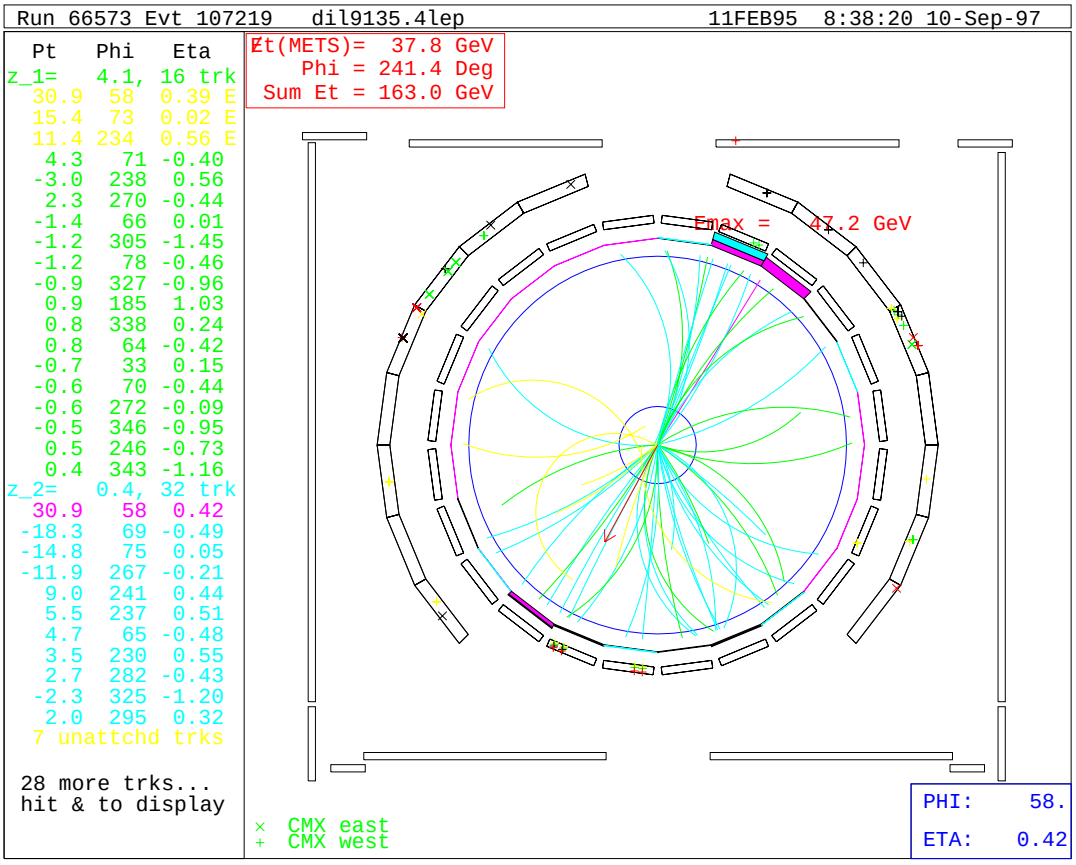

Abbildung 10.4: *CTC-plot of the four-lepton candidate event.*

trigger. The first electron fired the CEM_8_CFT_7_5_XCES electron trigger. In level three a variety of lepton and $\not\!\!E_T$ triggers were fired.

Apart from the electron not passing the FIDELE cuts there are other features that make it an unlikely $\not\!\!R_P$-MSSM candidate. The second muon is not isolated, it has more than 16 GeV in a cone of 0.4. In addition to this the jet containing this muon has a SECVTX b-tag. Both facts together clearly indicate that the jet is a likely b-jet.

Assuming the validity of all four leptons, the corrected invariant mass of the two electrons is 10.34 GeV, which is on the Υ(3s) resonance. On the other hand the transverse momentum of the two-electron system is 45.3 GeV, compared with 9 GeV for the highest Υ-momentum found in Run IA [41].

The probability that the event is an Υ is very low. If the event is not signal, it is most probably a b-event were both bs decay leptonically.

The event has two primary vertices (4.1 cm and 0.4 cm), about 4 cm apart. All leptons are coming from the same vertex ($z_{\rm vtx} = 0.4$cm).

Level 1:
L1_CALORIMETER_V3
L1_DIELECTRON_4
CMU_CMP_6PT0_HTDC_V1
TWO_CMU_3PT3_HTDC_V1
TWO_CMU_CMX_3PT3_V1
CEM_CMU_OR_CMX_V1

Level 2 Electron triggers:
CEM_16_CFT_12
CEM_8_CFT_7_5_XCES_V1
CEM_12_CFT_12_XCES_V2
TWO_CEM_6_CFT_4_7

Level 2 Muon triggers:
CMNP_JET_15_CFT_12_5DEG_V4
TWO_CMU_TWO_CFT_2_2_V4

Level 2 Met triggers:
MET_35_TWO_JETS
MET_35_TEX_2_NOT_GAS
MET_20_CEM_16_XCES

Level 3:	
QCDB_JET1_100_V1	EXOA_DIL_V2
COMBINED_ELEB_CEM	COMBINED_STRC
ELEB_CEM_8_6_V2	PSIC_E_CMU_V2
ELEB_CEM_18_LOOSE	PSIC_DIMUON_V2
ELEB_NO_CFT	COMBINED_EXOB_DIL
COMBINED_EXOB_MET	EXOB_DIL_TOP
EXOB_MET_30_TRK_3	EXOB_DIL_EWK
EXOB_MET_30_COSFL	EXOB_DIL_EXO
COMBINED_EXOA	
COMBINED_ELEA_CEM	
ELEA_CEM_18	
ELEA_CEM_22_W	
ELEA_CEM_25GEV_W_NOTRK	

Tabelle 10.3 : *The triggers fired by event 107219 of Run 66573.*

Object	Type	E_{T} or p_{T} (GeV)	ϕ	η	Calorimeter Isolation (GeV)	E/p
1	e^+	30.123	58.9°	0.4247	0.5226	0.974
2	e^-	14.395	74.0°	0.0455	2.8231	1.028
3	μ^-	10.664	266.9°	−0.2074	2.6892	–
4	μ^+	9.401	241.0°	0.4410	16.2690	–
	$\not\!\!E_T$	31.16713	239.8°	–	–	–

Tabelle 10.4 : *The measured properties of the lepton candidates in the four-lepton event candidate (Event 107219 of Run 66573). The second electron does not pass the FIDELE cuts because it is too near the 90°-crack. The isolation is measured in a cone of $\Delta R = 0.4$ around the lepton. The isolation is corrected for the first muon and two jets.*

11 Systematic and Theoretical Uncertainties

In this chapter we investigate several sources of systematic and theoretical uncertainties relevant to the analysis.

11.1 Theoretical Uncertainties

Effects which influence the cross section of the signal processes are considered as theoretical uncertainties. There are two such uncertainties

- The error resulting from the uncertainty of the structure function was estimated by running ISAJET at the point $M_0 = 200$ GeV, $M_{1/2} = 160$ GeV for the structure functions CTEQ2L, CTEQ4L, GRV and MRS_D0′ in addition to CTEQ3L, which was our nominal choice. The minimal (maximal) cross section was 0.259 (0.275) pb^{-1}, found using CTEQ4L (MRS_D0′), compared to 0.2730 for CTEQ3L. This is a relative difference of 5% (1%).

  The difference in the efficiency is of similar size. Of 5000 generated events a minimum (maximum) of 854 (917) events generated using MRS_D0′ (CTEQ3L) pass our cuts. The minimum number of events is 6.8 % less than the maximum of 917 events found using the nominal CTEQ3L structure function.

- We used cross section calculations from a R_P-conserving framework. The introduction of $\not{R}_P$ will change the values of about 10% [32]. Calculations including $\not{R}_P$ are not yet available.

Source	Relative Uncertainty (%)
Cross section (LO R_P vs. LO $\not{R}_P$)	10
Structure Functions	6.8
Total	12.1

Tabelle 11.1 : *Theoretical uncertainties for this analysis.*

Summing up the theoretical uncertainties in quadrature the total relative uncertainty is 12.1% (see Tab. 11.1).

11.2 Systematic Uncertainties

Effects which change the acceptance or which are due to detector effects or statistics are considered as systematical uncertainties. The sources of these uncertainties are

- Statistics of the MC generation: For each signal MC point 5000 events were generated. The worst acceptance for all scenarios was found for the point $M_0 =$ 150 GeV, $M_{1/2} = 110$ GeV, where 578 events were accepted. The statistical error resulting from this is 4.2%.

- The uncertainty in the acceptance due to gluon radiation was estimated by running several scenarios with gluon radiation turned off. To achieve this a modified version of the function DECJET was used. The modified function does not allow any gluon radiation.

  The region of $M_{1/2} \sim 160$ GeV was chosen in order to have points in the sensitive region, and M_0 was varied between 0 GeV and 500 GeV. The differences in acceptance were between 1 and 6 %. The worst point was $M_0 = 0$ GeV, $M_{1/2}$=160 GeV. To be conservative the worst values found (6 %) was used as uncertainty due to gluon radiation.

- The luminosity of the SUSY dilepton sample is: 87.5 pb^{-1} [29]. The systematics given in the reference are overestimated by a factor of about 2. The correct uncertainty of the luminosity is 4.1% according to [33]. This is used as the value for the uncertainty of the luminosity measurement.

- Lepton identification: The lepton identification efficiencies used were reported in [34]. In this analysis the same lepton identification cuts were used.

  The uncertainty on the lepton identification efficiency is 0.98 % (0.74 %) for tight electrons (muons). To be conservative 0.98 % was used. All except the first lepton are selected using loose cuts. Here the uncertainty is 0.94 % (0.64 %) for central electrons (central muons). For CMX (CMIO)–muons the error is 1.07 % (1.54 %). Looking at our signal-MC points we see that a mean of 27.3% (Max: 32.5%) of the events have one CMIO or CMX muon. Less than 7% have two and at most 1 % of the events have three CMX or CMIO muons.

  To estimate the uncertainty it is assumed that there is exactly one CMIO muon in each event. The possibility of having a second or third CMX/CMIO muon is neglected. To be conservative the other three leptons are assumed to be electrons. Doing this gives an uncertainty of 2.25 %. Assuming three CMIO muons and one tight central electron per event would raise this value to 2.84 %.

- Trigger Efficiency. The most important triggers for our data sample are shown in Table 11.2. We take the uncertainty in the trigger efficiency to be 5.6% [40].

Summing up all systematic uncertainties we find a total relative uncertainty of 10.1% (see Tab. 11.3).

Trigger
CEM_8_CFT_7_5_XCES
CMNP_CFT_12_5DEG
TWO_CMU_TWO_CFT_2_2
CMUP_CFT_12_5DEG
CMX_CFT_12_5DEG
CEM_8_CFT_7_5
TWO_CMU_ONE_CFT_2_2_6TOW
CMUP_CFT_7_5_5DEG
CEM_5_CFT_4_7_CMU_2_7
CMX_CMU_TWO_CFT_2_2
CEM_16_CFT_12

Tabelle 11.2 : *The most important triggers for the dilepton sample.*

Source	Relative Uncertainty (%)
MC Statistics	4.2
Gluon Radiation	6.0
Lepton ID	2.3
Trigger Efficiencies	5.6
Luminosity	4.1
Total	10.3

Tabelle 11.3 : *Systematic uncertainties in this analysis.*

12 Limit on R-Parity violating SUSY

Finding one event in 87.5 pb^{-1} with $1.33 \pm^{0.16}_{0.19} \pm^{2.08}_{0.3}$ expected events from SM background I proceed to set a limit on the $\not{R}_P$-MSSM with a coupling λ_{121}. The systematic uncertainty is calculated to be 10.3% and the theoretical uncertainty to be 12.1%

The statistical and systematic errors on the background estimate are large. To avoid any bias from this source no background subtraction is performed. Instead the number of expected background events is set to zero giving a conservative estimate of the limit.

The 95% confidence level upper limits can be calculated using either a frequentist or a Baysian algorithm. Both methods require a large amount of numerical calculations. A frequentist method is implemented in the FORTRAN program POILIM described in [43], which performs a number of pseudo-experiments until it can determine the limit. A baysian approach is implemented in the FORTRAN program BAYES described in [43]. Here the limit is obtained by solving an integral numerically. Both programs can be run with a reasonable amount of computing time and were used to determine the limits. Generally the baysian method gives larger limits.

12.1 Cross Section Limit

The cross-section limit is calculated using the systematic uncertainty of 10.3%. POILIM gives 4.841 with an accuracy of 0.001, the limit given by BAYES is higher at 4.883 with an integration step size of 0.01. This excludes scenarios where

$$\sigma \geq \frac{N_{95\%}}{A^{MC} \cdot \epsilon_{ID} \cdot \int \mathcal{L} dt}.$$

To be conservative the 95% confidence level upper limit given by BAYES $N_{95\%} = 4.883$ is used. The MC acceptance, which includes the trigger efficiency given by MC_WGT, varies from point to point. Its value is typically between 10 and 25 %. The MC electron efficiency factor is $\epsilon_{ID} = 0.8$. The cross section and the lines corresponding to the 95 % confidence level exclusion are shown in figures 12.1 and 12.2. The variations in the limit result from changes in the acceptance mainly. The band in figure 12.1 gives the ISAJET cross section in dependence of $M_{1/2}$ for $M_0 = 200$ GeV, $\tan\beta = 2$ and $\mu < 0$. The cross section is monotonously falling. The black line gives the CDF 95% confidence level limit. The limit is almost a straight line.

The band in figure 12.2 shows the cross section in dependence of M_0 for $M_{1/2}$ fixed to 140 GeV. The dependence of the cross section on M_0 is weaker than the dependence on $M_{1/2}$. The black line gives the CDF 95% confidence level limit exclusion. The exclusion shows a strong dependence on M_0 in the region of $M_0 \approx 90$ GeV. This dependence is due to the minimum in the leptonic branching ratios of the cascade decays in this area. This effect leads to a drop of the acceptance and thus de-creases the limit in this region.

12.2 Limit in the $M_{1/2}$–M_0 Plane

In order to examine points in the $M_{1/2}$–M_0 plane the systematic and theoretical uncertainties are added in quadrature. The uncertainty of 16% resulting from this is used as input for both programs. (BAYES) POILIM gives (5.115) 4.993 with the same accuracy/integration step size as before.

To decide if a particular point is excluded we correct the number of events found for the differences between QFL′ and the detector. In Fig. 12.3 we show the exclusion plot in the $M_{1/2}$–M_0 plane. The crosses correspond to points which we can exclude. Note that the points we used are separated by 10 GeV in $M_{1/2}$ and thus the exclusion line "jumps". An extrapolation between the points is not feasible because of the fast changes in the leptonic branching ration in the cascade decays. The region marked as "unphysicalcorresponds mainly to scenarios without electroweak symmetry breaking. In the region marked with "LSP= $\tilde{\nu}$" the sneutrino is the LSP. As we do not include the $\not{R}_P$ decays of sneutrinos in our simulation we can not determine if we can exclude this region.

For low values of M_0 we exclude $M_{1/2} < 150$ GeV. For $M_0 = 90$ GeV the limit drops to 140 GeV, then rises again to 160 GeV for $M_0 = 100$ GeV For 150 GeV $< M_0 <$ 300 GeV the limit is lowered to 140 GeV and then drops still further to 130 GeV.

12.3 Comparison with other SUSY searches at CDF

Comparing the limits obtained in this analysis with previous results one has to careful. The introduction of R-parity violation means that the limits can not just be applied to the R-parity conserving case. Another important thing to keep in ming is that the present analysis was performed using a mSUGRA framework. This framework closely links the masses of the superpartners. Previous studies at CDF often used a SUGRA inspired framework and excluded a mass range of the produced sparticles. In this analysis an area of the mSUGRA parameter space is excluded, which than can be translated into sparticle masses. Still a comparison with previous analysis can reveal how strong the limit is compared to these analysis.

A summary of the SUSY searches for squarks and gluinos performed during Run Ia is given in figure 12.4. In these searches squarks and gluinos were excluded up to approximately 225 GeV/c^2 for equal mass of squark and gluino. The limit on the squark mass from the search for R-parity violating SUSY in the like–sign dilepton channel are also in the order of 200 GeV/c^2, but expand to squark masses up to 260 GeV/c^2. In the present analysis the indirect limit on squarks and gluinos is approximately 400 GeV/c^2 for equal mass of squarks and gluinos.

The limit on chargino masses from the trilepton analysis is $M(\tilde{\chi}_1^{\pm}) > 81.5$ GeV/c^2. While the excluded chargino masses in the present search are 118 GeV/c^2.

The limits obtained in this analysis are much more stringent than the ones obtained from other analyses. This is mainly due to the fact that the relatively background–free four–lepton channel is used. In this channel only very loose cuts on the leptons have to

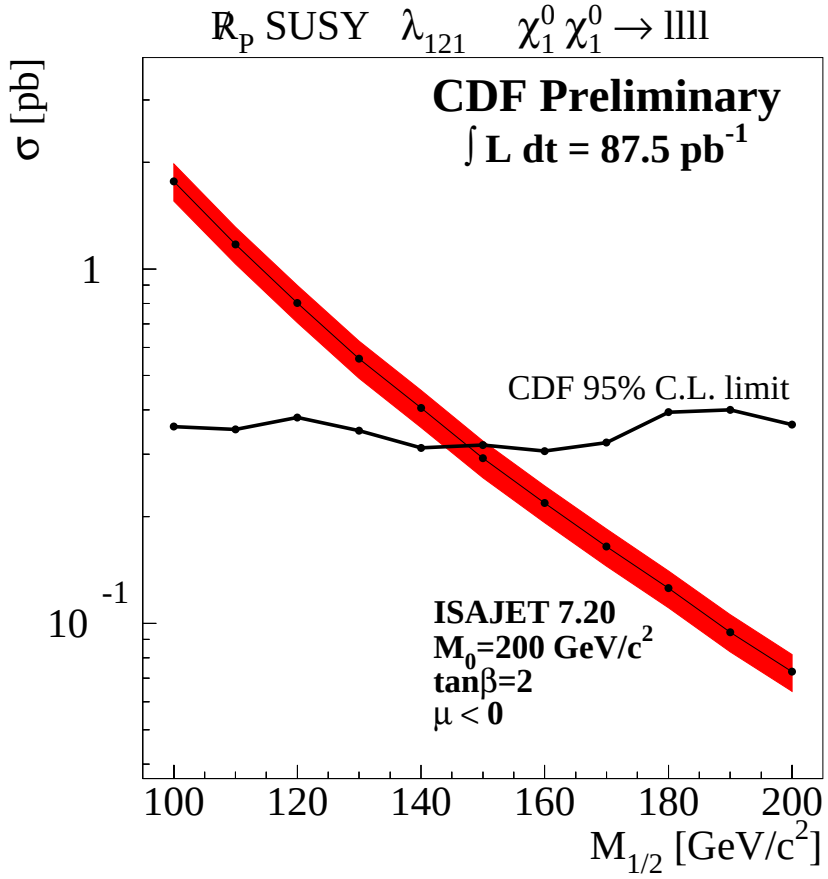

Abbildung 12.1: *Cross section times branching ratio as a function of $M_{1/2}$ for M_0=200 GeV. The band marks the theoretical error on the cross section. The solid black line is the CDF 95% confidence level limit. The dots mark the points for which we have run MC simulations.*

be applied in order to suppress the background strongly. Although it is not possible to apply the limits obtained in the present analysis directly to other studies the comparison shows that the analysis has a much higher reach than searches in R_P–SUSY.

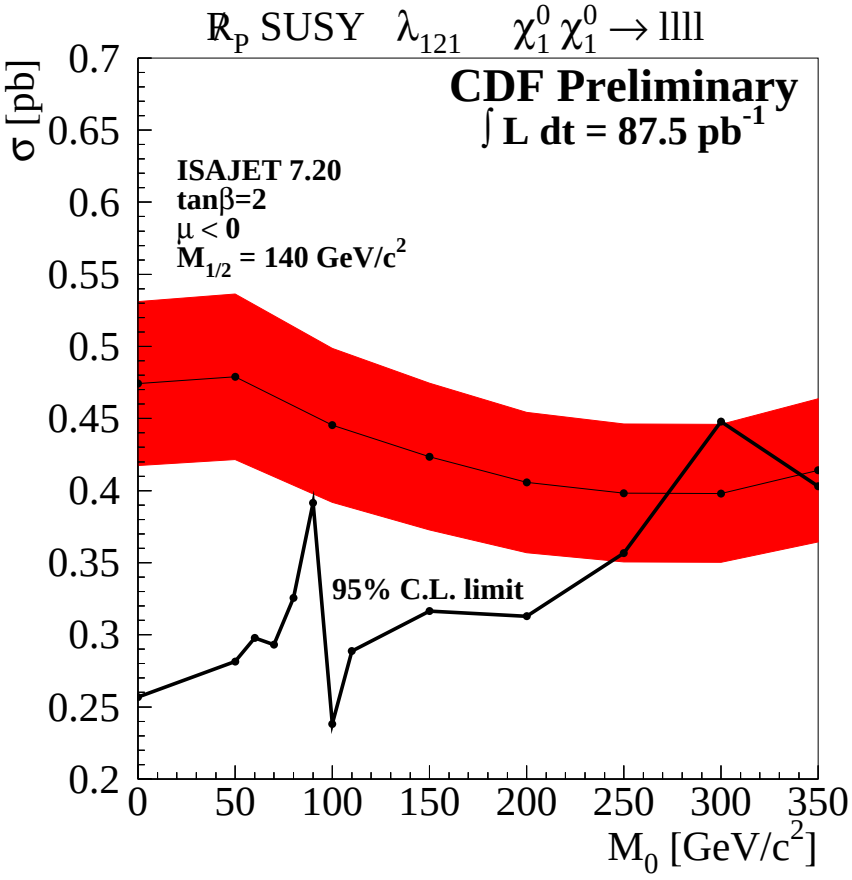

Abbildung 12.2: *Cross section times branching ratio as a function of M_0 for $M_{1/2}$=140 GeV. The band marks the theoretical error on the cross section.The solid black line is the CDF 95% confidence level limit. The dots mark the points for which we have run MC simulations.*

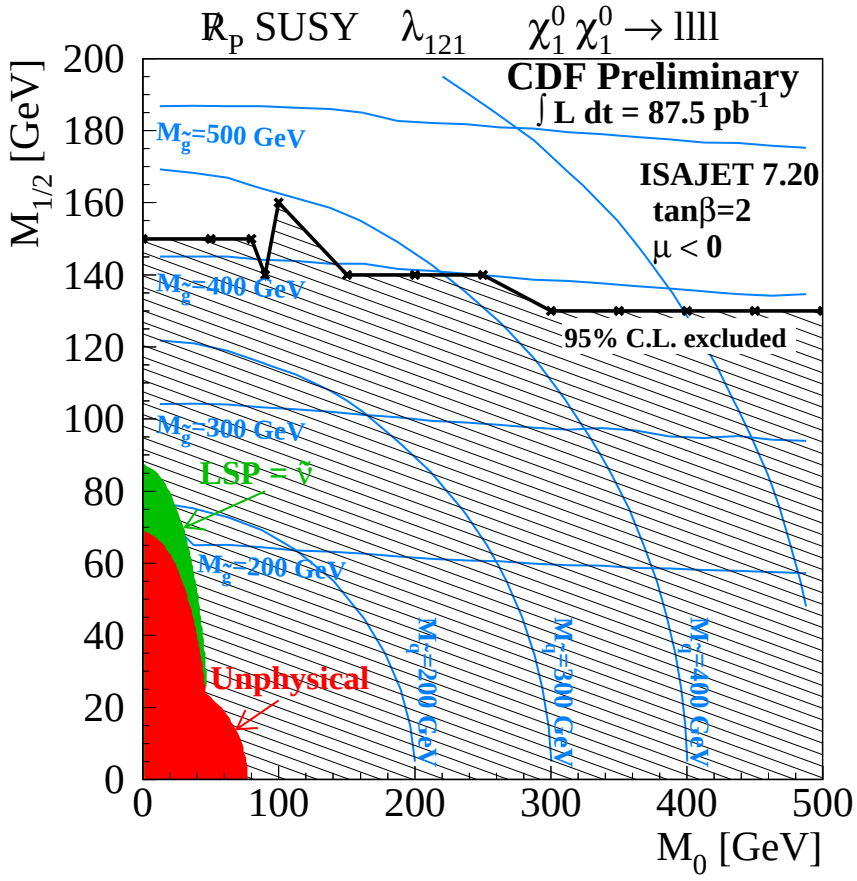

Abbildung 12.3: *Excluded region in the $M_{1/2}$–M_0 plane. The gluino and squark-masses are shown as contours. The dark region in the lower left yields unphysical behaviour like no electroweak symmetry breaking or tachionic particles. In the lighter region the LSP is the sneutrino, which would give a different signature. The excluded points with the highest values of $M_{1/2}$ are marked with crosses.*

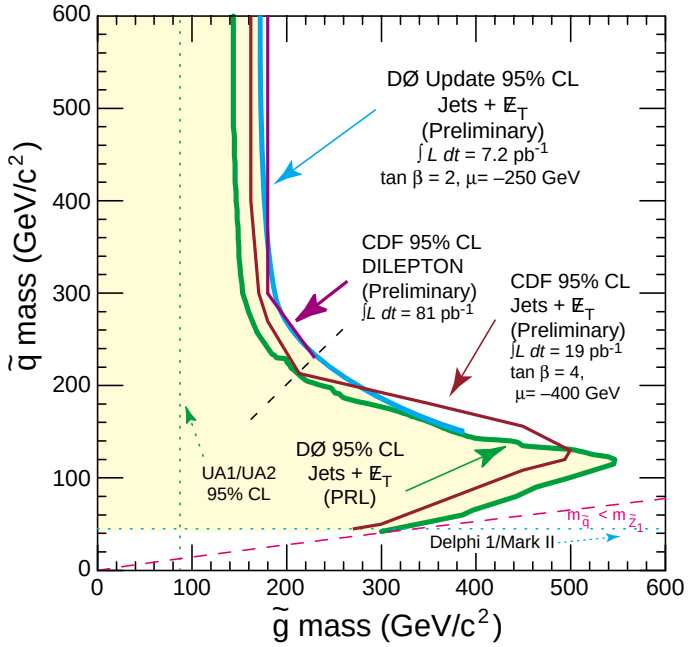

Abbildung 12.4: *Summary plot of the squark and gluino masses excluded by R_P-SUSY searches at the Tevatron.*

Conclusion and Outlook

In this thesis the first ever search for R_P–violating SUSY in the four lepton channel at hadron colliders was presented. In 87.5 pb^{-1} of data one candidate event was found. The structure of the event indicates that it is in fact a $b\bar{b}$ event. This is supported by the fact that $b\bar{b}$ production is the dominant SM background both for events with four leal leptons and for events containing three real leptons and one jet which is misidentified as a lepton. Assuming that the event is signal a conservative limit on the parameters of mSUGRA is set. For $\tan(\beta) = 2$, $\mu < 0$ and $A_0 = 0$ scenarios with $M_{1/2} < 130$ GeV are excluded for values of $M_0 > 300$ GeV. For lower values of M_0 the limit is stronger. The excluded parameter space corresponds to masses of the lightest neutralino less than 56 GeV/c^2 and masses of the lightest chargino and second neutralino of 118 GeV/c^2 independent of the value of M_0. The masses of the squarks and gluinos excluded are in the area of 350 GeV/c^2 for low M_0 and rise with M_0. The lowest limits for the masses of sleptons are on the order of 100 GeV/c^2 and also rise with M_0.

Run II of the Tevatron will start in late 2000 or early 2001. The center of mass energy of the accelerator will be increased to a total of 2 TeV for this run. The Tevatron is expected to deliver an integrated luminosity of at least 2 fb^{-1}, which is about a factor of twenty more than what was recorded during Run I. Currently it is planned to continue the run further and accumulate as much luminosity as possible. With these two improvements and an upgraded detector, new regions of the parameter space can be explored. With the expected luminosity it will be possible to probe scenarios with values of $M_{1/2}$ up to more than 200 GeV. If the one event seen proves to be the first signal event a small increase in luminosity will be enough to give an evidence for the existence of SUSY and open an interesting new area of physics.

APPENDIX

A The Parameters of the RGEs

A.1 Gauge Couplings

The parameters b_i describe the first order contributions to the gauge couplings. They are given by the sum of contributions from the particles with masses below the running mass sale q plus a constant term. The numerical values of the parameters are calculated using the numbers given in table A.1. Each number has to be multiplied by the number of particles below the running mass. The values for the SM leptons and quarks except for the top quarks have been calculated using three generations, because they will always contribute. E.g. for $Q \sim M_{\mathrm{GUT}}$ all particles contribute. Using three generations, two Higgs doublets and a W doublet one obtains:

$$b = \begin{pmatrix} 0 \\ -22/3 \\ -11 \end{pmatrix} + \begin{pmatrix} 23/10 \\ 5/2 \\ 2 \end{pmatrix} + 3 \begin{pmatrix} 37/30 \\ 7/6 \\ 4/3 \end{pmatrix} + 2 \begin{pmatrix} 3/10 \\ 1/2 \\ 0 \end{pmatrix} + \begin{pmatrix} 0 \\ 4/3 \\ 2 \end{pmatrix} = \begin{pmatrix} 33/5 \\ 1 \\ -3 \end{pmatrix}$$

Particle	b_1	b_2	b_3
Constant	0	-22/3	-11
down+leptons	23/10	5/2	2
up	17/30	1/2	2/3
Squarks	11/30	1/2	2/3
sleptons	3/10	1/6	0
higgsinos	1/5	1/3	0
higgs	1/10	1/6	0
W	0	4/3	0
gluino	0	0	2

Tabelle A.1 *: The contributions of the different particles to the coefficients b_i in SUSY models.*

A.2 Yukawa Couplings

For running masses above M_{SUSY} the coefficients c_i are given by

$$c_i^\tau = \begin{pmatrix} 9/5 \\ 3 \\ 0 \end{pmatrix}, \qquad c_i^b = \begin{pmatrix} 7/15 \\ 3 \\ 16/3 \end{pmatrix}, \qquad c_i^t = \begin{pmatrix} 13/15 \\ 3 \\ 16/3 \end{pmatrix}.$$

For running masses below M_{SUSY} the coefficients are changed to

$$c_i^\tau = \begin{pmatrix} 9/4 \\ 9/4 \\ 0 \end{pmatrix}, \qquad c_i^b = \begin{pmatrix} 1/4 \\ 9/4 \\ 8 \end{pmatrix}, \qquad c_i^t = \begin{pmatrix} 17/20 \\ 9/4 \\ 8 \end{pmatrix}.$$

Literatur

[1] F. Halzen, A. Martin, "Quarks and Leptons: An Introductory Course in Modern Physics",John Wiley & Son, New York (1984).

[2] C.S. Wu, E. Ambler, R.W. Hayward, D.D. Hoppes and R.P. Hudson, "Experimental Test Of Parity Conservation In Beta Decay," Phys. Rev. **105**, 1413 (1957).

[3] J.N. Bahcall, P.I. Krastev and A.Y. Smirnov, "Where do we stand with solar neutrino oscillations?," Phys. Rev. **D58**, 096016 (1998) hep-ph/9807216.

[4] C. Athanassopoulos *et al.* [LSND Collaboration], "Evidence for anti-nu/mu –> anti-nu/e oscillation from the LSND experiment at the Los Alamos Meson Physics Facility," Phys. Rev. Lett. **77**, 3082 (1996) nucl-ex/9605003.

[5] B. Zeitnitz *et al.*, "Neutrino oscillation results from KARMEN," Prog. Part. Nucl. Phys. **40**, 169 (1998).

[6] The Super-Kamiokande Collaboration and Y. Fukuda and others, "Measurement of a small atmospheric ν_μ/ν_e ratio", Phys. Lett. B433 9-18 (1998).

[7] C. Caso *et al.*, "Review of particle physics," Eur. Phys. J. **C3**, 1 (1998).

[8] H. Kalka, G. Soff, "Supersymmetry",B.G. Teubner Verlag (1997).

[9] S.P. Martin, "A supersymmetry primer," hep-ph/9709356.

[10] H. E. Haber, G. L. Kane, The Search for Supersymmetry: Probing Physics Beyond the Standard Model", Phys. Rep. 117 (1985) 75.

[11] A. H. Chamseddine *et al.*, Phys. Rev. Lett. **49**, 970 (1982); R. Barbieri *et al.*, Phys. Lett. B**119**, 343 (1982); L. Hall *et al.*, Phys. Rev. D**27**, 2359 (1983). For a review, see R. Arnowitt and P. Nath, "Supersymmetry and Supergravity," VIIth Swieca Summer School, Campos de Jordao, Brazil, (World Scientific, Singapore, 1994).

[12] P. John and B.R. Kim, "Nonlinear local supersymmetric SU(5)-model," Z. Phys. **C73**, 169 (1996). .V. Volkov and V.P. Akulov, "Is The Neutrino A Goldstone Particle ?," Phys. Lett. **B46**, 109 (1973). H. Genten, B.R. Kim, S.W. Ham and S.K. Oh, "Nonlinear supersymmetric standard model and its phenomenology," Z. Phys. **C76**, 117 (1997).

[13] V. Barger, M.S. Berger and P. Ohmann, "Supersymmetric grand unified theories: Two loop evolution of gauge and Yukawa couplings," Phys. Rev. **D47**, 1093 (1993) hep-ph/9209232.

[14] F. Paige and S. Protopopescu, ÏSAJET", in *SupercolliderPhysics,* p. 41, ed. D.Soper (World Scientific, 1986).

[15] K. Inoue, A. Kakuto, H. Komatsu and S. Takeshita, Prog. Theor. Phys. **68** (1982) 927. and **71** (1984) 413.

[16] G. R. Farrar, P. Fayet, Phenomenology of the Production, Decay, and Detection of New Hadronic States Associated with Supersymmetry.", Phys. Lett. B76 575 (1978).

[17] H.E. Haber and G.L. Kane, "The Search For Supersymmetry: Probing Physics Beyond The Standard Model," Phys. Rept. **117**, 75 (1985).

[18] For a review to R-parity violation see e.g., H. Dreiner, "An Introduction to Explicit R-parity Violation", hep-ph/9707435 v2. Published in "Perspectives on Supersymmetry", G. L. Kane, editor, World Scientific (1998).

[19] St. Weinberg, SSupersymmetry at Ordinary Energies. 1. Masses and Conservation Laws.", PRD 26 (1982) 287; N. Sakai, T. Yanagida, Proton Decay in a Class of Supersymmetric Grand Unified Models", Nucl. Phys. B197 355 (1984).

[20] L. J. Hall, M. Suzuki, Ëxplicit R Parity Breaking in Supersymmetric Models.", Nucl. Phys. B231 419 (1984).

[21] The H1 Collaboration, Öbservation of Events at Very High Q**2 in e p Collisions at HERA.", ZPhys C74, 191 (1997); The ZEUS Collaboration, Comparison of ZEUS Data with Standard Model Predictions for e+ p —¿ e+ X Scattering at High X and Q**2.", ZPhys C74, 207 (1997).

[22] M. Chertok, J.P. Done, and T. Kamon, "Search for R Parity Violating Squark Decay in LS Dielectron + Multijet Events", CDF Note 4185 (1998); "Search for Lepton Number Violating Neutralino Decay in LS Dielectron + Multijet Events", CDF Note 4229 (1998);M. Chertok, J.P. Done, and T. Kamon for the CDF Collaboration, "Search for R Parity Violating Supersymmetry using Like-sign Dielectrons in $p\bar{p}$ Collisions at $\sqrt{s} = 1.8$ TeV", CDF Note 4704 and Fermilab-Pub-98/374-E, Phys. Rev. Lett. **83**, 2133 (1999).

[23] Particle Data Group, Phys. Rev. D**54**, 1 (1996).

[24] V. Barger, G. F. Guidice and T. Han, "Some new aspects of supersymmetry R-parity violating interactions", Phys. Rev. D**40**, 2987 (1989).

[25] P.R. Harrison and C.H. Llewellyn Smith, "Hadroproduction Of Supersymmetric Particles," Nucl. Phys. **B213**, 223 (1983). G.L. Kane and J.P. Leveille, "Experimental Constraints On Gluino Masses And Supersymmetric Theories," Phys. Lett. **112B**, 227 (1982). H. Baer and X. Tata, "Component Formulae For Hadroproduction Of Lefthanded And Righthanded Squarks," Phys. Lett. **160B**, 159 (1985). S. Dawson,

E. Eichten and C. Quigg, "Search For Supersymmetric Particles In Hadron - Hadron Collisions," Phys. Rev. **D31**, 1581 (1985). Next to leading order was calculated by: W. Beenakker, R. Hopker, M. Spira and P.M. Zerwas, "Squark production at the Tevatron," Phys. Rev. Lett. **74**, 2905 (1995) hep-ph/9412272. W. Beenakker, R. Hopker, M. Spira and P.M. Zerwas, "Squark and gluino production at hadron colliders," Nucl. Phys. **B492**, 51 (1997) hep-ph/9610490.

[26] S. Abachi et al., Nucl. Instr. Meth. **A338**, 185 (1994).

[27] F.Abe et al., Nucl. Instr. Meth. **A271**, 387 (1988).

[28] Baer et al PRD 51,2180 (hep-ph/9410283) (1995).

[29] J.P. Done et al., SSUSY Dilepton Selection for Run I", CDF Note 4446 (1998).

[30] F. Abe *et al.* [CDF Collaboration], "A Measurement of the ratio sigma x B (p anti-p $\rightarrow$ W $\rightarrow$ e neutrino) / sigma x B (p anti-p $\rightarrow$ Z0 $\rightarrow$ e e) in p anti-p collisions at s**(1/2) = 1800-GeV," Phys. Rev. **D52**, 2624 (1995).

[31] S. Kopp, C. Grosso-Pilcher, "A Good Run List for the 1992-1993 CDF Run", CDF Note 1992 (1993).

[32] H. Dreiner, Private communications.

[33] D. Cronin-Hennessy, A. Beretvas, "Luminosity at CDF", CDF Note 4721 (1998).

[34] J. P. Done *et al.*, "Study of the Run 1B Lepton Identification Efficiencies for SUSY Searches", CDF Note 4218 (1997).

[35] http://www-cdf.fnal.gov/internal/physics/exotic/susy/info/mc_run_1b.html

[36] B. Tannenbaum, "A Search for Chargino-Neutralino Production at the Fermilab Tevatron Collider", CDF Note 4571 (1998).

[37] S. Tether, "The Fake Lepton Rate for the Run 1B SUSY Trilepton Analysis", CDF Note 3566 (1996).

[38] S. Rolli, B. Drucker, "THE CDF VECBOS MANUAL",CDF Note 3185 (1995). http://b0ig05.fnal.gov:8001/vecbos_note.ps

[39] M. Worcester, D. Saltzberg, J. Nachtman, "Development of New Isolation Variables and Estimation of Fake Rates in Dilepton SUSY Searches at CDF", CDF Note 5081, (1999)

[40] B. Tannenbaum *et al.*, "Update to the Run 1A + 1B Chargino-Neutralino Search Using Trilepton Events", CDF Note 4188 (1997)

[41] F. Abe *et al.* [CDF Collaboration], "Upsilon production in p anti-p collisions at s**(1/2) = 1.8-TeV," Phys. Rev. Lett. **75**, 4358 (1995).

[42] See e.g. D0 Collaboration, "SUGRA-GUT Motivated SUSY Search in the Dielectron Channel at D0", Fermilab Conf-96/254-E (1996)

[43] J. Conway K. Maeshima, "Poisson Upper Limits Incorporating Uncertainties in Acceptance and Background", CDF Note 4476 (1998).

Acknowledgements

Most of the work leading to this thesis has been done in collaboration with the CDF SUSY working group. I thank all members of this group for the good and relaxed atmosphere. I expecially thank Dr. James P. Done, Dr. Stephan Lammel and Prof. Dr. Regina Demina for useful discussions and helpful hints.

During the time of my graduate study I was financially supported by the Land Baden Württemberg and the Graduiertenkolleg "Elementarteilchenphysik an Beschleunigern" of the faculty of physics.

I thank Prof. Dr. Thomas Müller for giving me the opportunity to do this analysis in the field of Supersymmetry and the freedom he gave me in choosing the topic of this work. I also thank him for the possibility to work in the US for a year and the support for presenting the results of this work.

I thank Prof. Dr. Jay Hauser for being "Korefferent" and for inviting me to work in his group at UCLA for some time. I would like to thank the people I worked with at that time for the good atmosphere and the friendly reception.

I thank Hans–Jakob Grimm for discussions about SUSY and for reading the more theoretical part of the manuscript.

I thank Dr. Michael Lindgren, Dr. Stephan Lammel and Dr. Dirk Neuberger for introducing me to CDF and to the the US in general.

I thank the members of the IEKP software group for the good an relaxed working atmosphere. Special thanks go to Hans–Jakob Grimm, Markus Moch and Thomas Allmendinger for reliably indicating the beginning and the end of the lunch breaks and to Fritz Vollmer for sharing my enthusiasm about Karlsruhe.

I specially thank Dr. Ralf Ehret, Dr. Ulrich Schwickerath and Patrick Schemitz for the excellent teamwork while managing the IEKP computer cluster. The same holds for the work with Burkhard Zittel, now manager of the faculty computers. Working together with them has been a pleasure.

Finally I thank Coco and my parents for their support during the time it took to finish this work and for their trust in me.